

# **SECURE WATERMARKING OF DIGITAL DATA FOR COPYRIGHT PROTECTION**

A DISSERTATION

SUBMITTED IN PARTIAL FULFILLMENT OF THE REQUIREMENTS

FOR THE AWARD OF DEGREE

OF

MASTER OF TECHNOLOGY

IN

**SIGNAL PROCESSING AND DIGITAL DESIGN**

Submitted by:

**ASHISH SINHA**

**2K20/SPD/02**

Under the supervision of:

**PROF. JEEBANANDA PANDA**



**DEPARTMENT OF ELECTRONICS AND COMMUNICATION ENGINEERING**

**DELHI TECHNOLOGICAL UNIVERSITY**

(Formerly Delhi College of Engineering)

Bawana Road, New Delhi – 110042

**MAY 2022**

DELHI TECHNOLOGICAL UNIVERSITY

(Formerly Delhi College of Engineering)

Bawana Road, New Delhi – 110042

**CANDIDATE'S DECLARATION**

I, Ashish Sinha, Roll No. 2K20/SPD/02, student of M.Tech (Signal Processing and Digital Design), hereby declare that the project dissertation titled “Secure Watermarking of Digital Data for Copyright Protection” which is submitted by me to the Department of Electronics and Communication Engineering, Delhi Technological University, Delhi in partial fulfilment of the requirements for the award of degree of Master of Technology in Signal Processing and Digital Design, is original and not copied from any source without citation. This work has not previously formed the basis for the award of any Degree, Diploma Associateship, Fellowship or other similar title or recognition.



Place: Delhi

ASHISH SINHA

Date: 27 May 2022

**DEPARTMENT OF ELECTRONICS AND COMMUNICATION ENGINEERING**

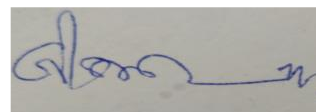
DELHI TECHNOLOGICAL UNIVERSITY

(Formerly Delhi College of Engineering)

Bawana Road, New Delhi – 110042

**CERTIFICATE**

I hereby certify that the project dissertation titled “Secure Watermarking of Digital Data for Copyright Protection”, which is submitted by Ashish Sinha, Roll No. 2K20/SPD/02, Department of Electronics and Communication Engineering, Delhi Technological University, Delhi in partial fulfilment of the requirements for the award of degree of Master of Technology in Signal Processing and Digital Design is a record of the project work carried out by the student under my supervision. To the best of my knowledge this work has not been submitted in part or full for any Degree or Diploma to this university or elsewhere.



Place: Delhi

Date: 27 May 2022

JEEBANANDA PANDA

SUPERVISOR

PROFESSOR

(Department of Electronics and  
Communication Engineering)

Delhi Technological University

Bawana Road, Delhi – 110042

## ABSTRACT

The exponential growth of technologies, media to access the same and simplification of the related processes has spurred an unprecedented growth in this domain. When the digital media is generated, transmitted and distributed over multiple devices and interconnecting networks, maintenance of its authenticity and ensuring the intellectual rights of the owners and authorized users is of utmost significance. With the progressive evolution in technology and distribution networks, prevention of widespread dissemination of sensitive and private information is an arduous challenge. The attacks on the secured information are designed so as to enable unscrupulous users to gain illegitimate access to the secured data, who may tamper with its contents and/or undermine the associated intellectual property rights of the owner and authorized users.

To effectively deal with problems of such kind, we need to ensure that the content of the data being transmitted is minimally modified, if not left unchanged, on exposure to such attacks. Further, the identity of the owner and her intellectual rights should be protected from infringement. The above requirements are pivotal for maintaining the authenticity of the data, protection of the content from undesirable alterations during transmission and assertion of the copyright of its rightful owners and users.

As a solution to counter this menace, digital watermarking of the cover work has been proposed in this field. It serves the different purpose highlighted above by embedding secret data (watermark) in the cover work, through minimal modification of its content. The immediate advantage of this approach is the level of imperceptibility of the

embedded watermark can be suitably modulated. Further, depending upon the kind of anticipated attacks in the channels of distribution and transmission, the scheme can be configured to provide the required level of robustness and security. Embedding the data in this manner also leads to better security too as the location and content of the watermark within the cover work are difficult to ascertain. Some schemes have also been designed to offer good capacity in terms of the quantum of watermarking data which can be embedded, thus boosting the robustness and security of the methodology.

While watermarking of a multitude of media including text, video, printed circuits etc. have been undertaken, all of them are based on the fundamental challenges seen in the watermarking of 1-D and 2-D data. To this extent, the initial works in the domain revolved around addressing the different shortcomings in the techniques related to the watermarking of audio and images. This was crucial as addressing these problems provided more clarity on similar problems faced in watermarking of cover work with higher data volume and complexity.

First, we discuss about watermarking of 1-D data. Watermarking of audio signals is considered as a pertinent challenge owing to the feature of non-degradation of audio quality post insertion of the watermark, for ensuring non-distinguishability from the original cover work, while maintaining the watermark imperceptibility. Further, the watermark should also continue to serve its purpose of copyright protection of the intellectual property and maintain robustness a variety of signal processing and distortive attacks. In fulfilment of the above key requirements and other vital characteristics of a good watermarking scheme viz. security and payload capacity, this dissertation outlines an effective methodology for watermarking of the audio signal in the time-frequency

domain through the use of linear canonical transform (LCT). The embedded watermark was found to be survive wide range of attacks ranging from signal processing to audio quality distortive. Further, the technique provides good security and offers an appreciable payload capacity up to 15% of the audio signal length.

Next, we shift our focus to 2-D and 3-D data. Here, we consider both grayscale and colour RGB images. For images specified in grayscale, strong watermarking decreases the invisibility. Contrary to this, weaker watermarking improves imperceptibility but reduces the robustness. For embedding the watermark, we deploy the image partitioning approach based on the psycho-visual redundancy. Watermark scrambling using Arnold Transform and subsequent embedding in the lowest frequency DWT sub-band of the image leads to improved security, robustness as well as the imperceptibility as compared to contemporary schemes.

For 3-D colour (RGB) images, we adopt 2 approaches. As many image moments suffer from limited reconstruction ability, errors during numerical approximation, low stability and diminished feature integrity, this work provides a novel two-tiered zero watermarking framework for color images using Fractional Order Generic Polar Complex Exponential Transform (FrGPCET). Initially, the watermark is scrambled using quasi-affine transform. The stable fractional order moments are calculated in a fast and accurate manner, using higher order interpolators and Gaussian numerical integration. Through incrementally iterative pseudo-random selection and Otsu thresholding, an augmented moment feature vector is formed which is in-turn used for embedding the watermark. The second tier is focused towards increasing the imperceptibility by removing any background artifacts, and reducing information redundancy. It involves the

sequential use of Discrete Cosine Transform and Huffman coding. Comparison with the state-of-the-art methodologies has shown that the proposed technique surpasses them in terms of watermark's imperceptibility and robustness to different attacks. It is also inherently secure, offers good payload capacity, and can be implemented efficiently with nominal computational resources.

Our second approach relies on increasing the similarity between the power spectra of the host and watermark images. We wish to minimize the severity of the attacks based on estimation of the MMSE. This leads to an energy efficient watermarking scheme offering contemporary imperceptibility and robustness against state-of-the-art watermarking techniques. The principles leveraged include inter alia graph signal processing, spectral graph wavelet, variational mode decomposition and local dominant orientation feature extraction. Each of them serves to enhance the strength of the watermarking in terms of imperceptibility, robustness, security, payload capacity and energy efficiency.

## ACKNOWLEDGEMENT

I, Ashish Sinha, Roll No. 2K20/SPD/02, student of M.Tech (Signal Processing and Digital Design), hereby thank and express my sincere gratitude to my supervisor, Prof. Jeebananda Panda, with whose continuous support and insightful guidance, this project titled “Secure Watermarking of Digital Data for Copyright Protection” was successfully undertaken by me.

A handwritten signature in blue ink that reads "Ashish Sinha". The signature is written in a cursive style and is underlined with a single horizontal stroke.

Place: Delhi

ASHISH SINHA

Date: 27 May 2022



## CONTENTS

CANDIDATE’S DECLARATION .....	ii
CERTIFICATE .....	iii
ACKNOWLEDGEMENT .....	viii
CONTENTS.....	ix
LIST OF TABLES .....	xii
LIST OF FIGURES .....	xiii
LIST OF SYMBOLS, ABBREVIATIONS AND NOMENCLATURE .....	xv
<b>CHAPTER 1 .....</b>	<b>16</b>
1.1.    GENERAL .....	16
1.2.    DIGITAL WATERMARKING .....	17
1.3.    HISTORY OF WATERMARKING .....	19
1.4.    CHARACTERISTICS AND APPLICATIONS.....	20
1.5.    AUDIO WATERMARKING.....	21
1.6.    IMAGE WATERMARKING.....	24
1.7.    PROPOSED SCHEMES .....	25
1.7.1.    AUDIO WATERMARKING IN TRANSFORM DOMAIN .....	25
1.7.2.    IMAGE WATERMARKING IN FREQUENCY DOMAIN.....	26
1.7.3.    MOMENT BASED IMAGE WATERMARKING .....	27
1.7.4.    IMAGE WATERMARKING USING GRAPH SIGNAL PROCESSING AND LOCAL DOMINANT FEATURES .....	27
1.8.    ORGANIZATION OF DISSERTATION .....	29
<b>CHAPTER 2 .....</b>	<b>30</b>
2.1.    GENERAL .....	30
2.2.    LITERATURE REVIEW.....	33
<b>CHAPTER 3 .....</b>	<b>46</b>
3.1. THE FRACTIONAL FOURIER TRANSFORM .....	46
3.2. THE LINEAR CANONICAL TRANSFORM .....	47
3.2.1.    CONTINUOUS LINEAR CANONICAL TRANSFORM.....	47

3.2.2.	PROPERTIES OF LINEAR CANONICAL TRANSFORM .....	48
3.2.3.	DISCRETE LINEAR CANONICAL TRANSFORM.....	50
CHAPTER 4	.....	51
4.1.	DISCRETE WAVELET TRANSFORM.....	51
4.2.	ARNOLD TRANSFORM .....	52
CHAPTER 5	.....	53
5.1.	OVERVIEW OF WATERMARKING TECHNIQUES BASED ON MODIFICATION OF IMAGE MOMENTS .....	53
5.2.	ORTHOGONAL MOMENTS.....	55
5.3.	IMAGE MOMENTS.....	57
5.4.	ORTHOGONAL MOMENTS .....	60
5.5.	FRACTIONAL ORDER EXPONENTIAL (ORTHOGONAL) MOMENTS .....	70
5.6.	RESISTANCE TO GEOMETRIC TRANSFORMATIONS .....	71
5.6.1.	INVARIANCE TO ROTATION.....	71
5.6.2.	INVARIANCE TO SCALING.....	72
5.6.3.	INVARIANCE TO TRANSLATION .....	73
5.7.	ACCURATE CALCULATION OF ORTHOGONAL MOMENTS.....	74
5.8.	DITHER MODULATION .....	76
5.9.	HUFFMAN CODING.....	78
CHAPTER 6	.....	80
6.1.	GRAPH SIGNAL PROCESSING .....	80
6.2.	SPECTRAL GRAPH WAVELET.....	81
6.3.	VARIATIONAL MODE DECOMPOSITION (VMD).....	82
6.4.	LOCAL DOMINANT ORIENTATION FEATURE EXTRACTION (LDOF) .....	84
CHAPTER 7	.....	86
7.1.	AUDIO WATERMARKING.....	86
7.1.1.	WATERMARK EMBEDDING STAGE .....	86
7.1.2.	WATERMARK DETECTION STAGE.....	88
7.2.	IMAGE WATERMARKING IN FREQUENCY DOMAIN .....	90
7.2.1.	WATERMARK EMBEDDING STAGE .....	92
7.2.2.	WATERMARK EXTRACTION STAGE.....	93
7.3.	MOMENT BASED IMAGE WATERMARKING .....	96
7.3.1.	WATERMARK EMBEDDING (TIER I) .....	96
7.3.2.	WATERMARK EMBEDDING (TIER II).....	101
7.3.3.	WATERMARK EXTRACTION.....	102

7.4.	IMAGE WATERMARKING USING GRAPH SIGNAL PROCESSING AND LOCAL DOMINANT FEATURES .....	104
7.4.1.	WATERMARK EMBEDDING .....	104
7.4.2.	WATERMARK EXTRACTION.....	105
CHAPTER 8	.....	109
8.1.	AUDIO WATERMARKING.....	109
8.1.1.	AUDIO SIGNAL RECORDING / SAMPLING .....	109
8.1.2.	WATERMARK EMBEDDING .....	110
8.1.3.	WATERMARK DETECTION.....	110
8.1.4.	SIGNAL PROCESSING AND FEATURE DISTORTIVE ATTACKS .....	111
8.2.	IMAGE WATERMARKING IN FREQUENCY DOMAIN .....	112
8.3.	MOMENT BASED IMAGE WATERMARKING .....	112
8.4.	IMAGE WATERMARKING USING GRAPH SIGNAL PROCESSING AND LOCAL DOMINANT FEATURES .....	112
CHAPTER 9	.....	113
9.1.	AUDIO WATERMARKING.....	113
9.1.1.	TEST OF IMPERCEPTIBILITY .....	114
9.1.2.	TEST OF ROBUSTNESS .....	115
9.1.3.	TEST OF SECURITY AND LCT PARAMETER SENSITIVITY .....	119
9.2.	IMAGE WATERMARKING IN FREQUENCY DOMAIN .....	122
9.3.	MOMENT BASED IMAGE WATERMARKING .....	125
9.4.	IMAGE WATERMARKING USING GRAPH SIGNAL PROCESSING AND LOCAL DOMINANT FEATURES .....	137
CHAPTER 10	.....	141
REFERENCES	.....	144
APPENDIX A (LIST OF PUBLICATIONS)	.....	150
APPENDIX B (PLAGIARISM REPORT)	.....	153

## LIST OF TABLES

Table 9.1. Signal Processing Attacks of Maximal Strength/Degree (Contd.) .....	116
Table 9.2: Figures of Merit for the Watermarking Scheme for Different Attacks of Varying Strength/Degree .....	119
Table 9.3: Figure of Merit of the Watermarking Scheme.....	124
Table 9.4: Extracted Watermark under Different Attacks .....	130
Table 9.5: BER Of the Watermark Retrieved under Different Attacks.....	132
Table 9.6: NC of the watermark retrieved under different attacks .....	133
Table 9.7: PSNR of Cover Image and Watermark and NC of Watermark.....	139

## LIST OF FIGURES

Figure 4.1: 2 Level Discrete Wavelet Transform .....	52
Figure 4.2: Image Moments.....	58
Figure 5.1: Mapping from Cartesian to Polar coordinate system .....	74
Figure 7.1: Watermark Embedding Process for Audio Data .....	88
Figure 7.2: Watermark Detection Process for Audio Data.....	90
Figure 7.3: Flowchart for Watermark Embedding Process for Audio Data .....	94
Figure 7.4: Flowchart for Watermark Extraction Process for Audio Data .....	95
Figure 7.5: Watermark Embedding Process .....	100
Figure 7.6: Watermark Extraction Process .....	104
Figure 7.7: Watermark Embedding Process .....	107
Figure 7.8: Watermark Extraction Process .....	108
Figure 9.1: Comparison between the Original and Watermarked Audio Signal .....	114
Figure 9.2 Difference between the Original and Watermarked Audio Signal.....	115
Figure 9.3: Watermark Detection under AWGN Attack .....	116
Figure 9.4: Watermark Detection under LPF Attack.....	117
Figure 9.5: Watermark Detection under HPF Attack .....	117
Figure 9.6: Watermark Detection under Decimation (Cropping) Attack .....	118
Figure 9.7: Watermark Detection under MP3 Compression Attack.....	118
Figure 9.8: Detection Parameter Values for Different $\lambda$ .....	120
Figure 9.9: Detection Parameter Values for Different $\tau$ .....	120
Figure 9.10: Detection Parameter Values for Different $\zeta$ .....	120
Figure 9.11: Original and Watermarked Cover Images.....	123

Figure 9.12: Extracted Watermark after different geometric/image processing attacks of maximum strength .....	123
Figure 9.13: Different Cover Images and Watermark .....	125
Figure 9.14: Variation of Radial Function $E(\rho, \beta)$ with $\beta$ in $0 < \rho < 1$ .....	126
Figure 9.15: Average PSNR v/s Quantization Step $\Delta$ .....	127
Figure 9.16: Attacked Watermarked Images .....	128
Figure 9.17: BER for Rotation, Scaling, Translation and JPEG compression attacks .....	135
Figure 9.18: NC for Rotation, Scaling, Translation and JPEG compression attacks .....	136
Figure 9.19: Original Cover Work and Watermark .....	138
Figure 9.20: Original vs Watermarked Cover Work .....	138
Figure 9.21: Watermark Retrieved under Different Attacks of Maximum Strength/Degree .....	139

## **LIST OF SYMBOLS, ABBREVIATIONS AND NOMENCLATURE**

1. **DCT** – Discrete Cosine Transform
2. **DWT** – Discrete Wavelet Transform
3. **DFT** – Discrete Fourier Transform
4. **LCT** – Linear Canonical Transform
5. **DLCT** – Discrete Linear Canonical Transform
6. **IDLCT** – Inverse Discrete Linear Canonical Transform
7. **FRFT** – Fractional Fourier Transform
8. **PHT** – Polar Harmonic Transform
9. **FrGPCET** – Fractional Generic Polar Complex Exponential Transform
10. **DM** – Dither Modulation
11. **GSP** – Graph Signal Processing
12. **VMD** – Variational Mode decomposition
13. **LDOF** – Local Dominant Orientation Features
14. **MMSE** – Minimum Mean Square Error
15. **AWGN** – Additive White Gaussian Noise
16. **LPF** – Low Pass Filter
17. **HPF** – High Pass Filter
18. **NC** – Normalized Cross-Correlation
19. **SIM** – Similarity Index
20. **SNR** – Signal-to-Noise Ratio

## **CHAPTER 1**

### **INTRODUCTION**

#### **1.1. GENERAL**

Recent exponential proliferation of digital technologies and associated media and products have been driven by more economical and accessible technologies. However, due to the unchecked growth and lack of suitable access and distribution control protocols, the technologies and platforms have very often been mis-utilized with mala fide intentions of committing copyright infringements and gaining unauthorized access to the original cover work, for illegal commercial, piracy and espionage operations. Multimedia piracy therefore poses a magnanimous challenge for the creators and distributors of the digital media as not only does it constitute violation of intellectual property rights, it leads to unaccounted financial losses and poses threat to verification and authentication [1,2]. Roughly speaking with reference to a global perspective, it has been estimated that over 95% of media downloaded in the audio format, over the internet is illegal and amounts to losses to the tune of billions of dollars [3]. Further, cybercrime related to image manipulation and counterfeiting has grown at unprecedented rates since the genesis of the Internet [4]. This dissertation has also proposed the development of tools and frameworks for the regulation of this menace of counterfeiting, unauthorized digital media manipulation, illegal downloads and piracy. Driven by the appurtenant demand from the industry and the need for development of approaches to tackle the issue of copyright violation in digital media, the theme of secure digital watermarking has been broached upon in this dissertation, for audio and image data.



## 1.2. DIGITAL WATERMARKING

In this, we insert a digital instrument of ownership in the digital media (watermark). This information could be in the form of a copyright notice, owner's identity, and is decipherable only by the authorized personnel [5]. The digital media is preconditioned prior to watermarking, and is known as the cover signal. Insertion of the watermark or "embedding", leads to the generation of the transformed "watermarked" signal. Extraction or detection is attributed to the process of watermark retrieval. Together, they comprise of the fundamental steps in the watermarking.

The terms watermarking, cryptography and steganography may appear similar in usage and application but they can easily be distinguished on the basis of fundamental principle of concealing the information. While cryptography deals with encoding the data stream using a cipher key which is accessible to only the authorized users, steganography involves concealing of unrelated information within a set of data, with the latter only serving the purpose of the obfuscation of the hidden information. It should be noted that through cryptography, security is only ensured during the transmission. Once decrypted, the data is prone to mis-utilization by the malicious elements, who may take control of the ownership of the data in itself. In contrast to both the foregoing techniques, watermarking entails embedding of unrelated secret information in the digital media by modification of its very content in a suitable manner. This renders the embedded information ("the watermark") imperceptible, in separable and co-transformable. This means that watermark is invisible to the human eye, cannot be separated from the digital media and undergoes the same transformation as the media. This is central to the behaviour and nature of the watermark [4,5].

Different types of watermarking schemes are defined based on the nature of the cover signal, type of embedded watermark, and watermark insertion process. Watermarking is classified into visible and invisible types based on the perceptibility of the inserted watermark. It may also be categorized into robust, semi-fragile and fragile when we consider robustness as the criteria. It may also be divided into blind, semi-blind and non-blind, based on the use of cover signal for watermark extraction. Generally, schemes used for watermarking offering custom levels of imperceptibility and robustness are designed based on the requirement of a particular application. It is also governed by the kind of anticipated attacks on the copyright material. Details corresponding to the different characteristics and applications of watermarking follow later in this chapter.

### 1.3. HISTORY OF WATERMARKING

Steganography has been used from time immemorial for the purposes of relaying secret information in a hostile environment undetected. Predominantly, it was used for spying and espionage related activities, wherein communication of private and secret information was to be conducted in an environment known to pose risks to the safe transmission and delivery of the data. More recently, it has been used in tandem with the explosion in the growth of digital technologies, especially the Internet, wherein the security and encryption of the data is put to test in a much more extensive and rigorous manner.

Digital watermarking developed from the pertinent requirement of concealment of information related to the owner identity and authenticity within an object. In the initial days, a watermark served this purpose when it was embedded within objects of monetary and intellectual significance such as paper money (bills), books etc. Later, with the advancement in data generation and communication media and channels, its use grew to other forms of information. Post the World War II epoch, watermarking found its way for use in anti-counterfeiting initiatives of music industry. Towards the 1970s, researchers proposed applications of watermarking for the protection of owner identity and copyright information in the data present in the document format. The interest in this domain, however witnessed an upward spiral in the 1990s, where watermarking applications were expanded to a broad category of cover work. This allowed the community to explore multiple techniques by leveraging the existing ones and improvising upon them through active research in the related areas. Audio and image watermarking are two of the most widely explored areas in the arena of digital watermarking and have formed the basis of research undertaken in this domain with respect to other types of cover work [5].

## 1.4. CHARACTERISTICS AND APPLICATIONS

The use watermarking spans across a wide variety of applications. Generally speaking, watermarks possess the following fundamental traits: they are imperceptible, they are inseparable from the cover work in which they are embedded and they undergo the same transformations as the cover work. In particular, the performance of a given watermarking scheme can be assessed basis a finite set of properties like robustness, fidelity and so forth. Their significance is contingent on the application for which they are designed for [4,5].

A brief overview of the different applications of watermarking is presented below

- a. Broadcast monitoring: This is used for the detection of the content broadcast on public networks via the watermark embedded within it.
- b. Owner identification: This is used for assertion of the identity of the owner of the digital data.
- c. Transaction tracking: This is used to identify and regulate the illegal distribution of copyrighted material which may have been initially sought through ethical means.
- d. Content authentication: This is used for the purposes of verification of the sanctity of the data after it has been subjected to certain signal processing attacks.
- e. Distribution control: Watermark may be programmed to convey information to the processing unit to prevent the copying/duplication of the data while in use. Also, specific technologies/equipment may be designed to generate desired response to the stimulus communicated via the embedded watermark.
- f. Other Applications: Watermarking has been used for a variety of applications which do not have direct relation to the security and authenticity aspect associated with it. For example, it has been successfully deployed in eliminating the delay between AV transmissions on television through compressed embedding of audio data into the

latter, synchronization of lyrics with the song by directly embedding it within the audio etc.

Some parameters which are instrumental in the characterization of a watermarking scheme are listed below

- a. Fidelity: The imperceptibility of the cover work post insertion of the watermark
- b. Payload Capacity: The quantity of watermarking information that can be embedded in the cover work.
- c. Detection Capability: Blind (Does not require the cover work for watermark extraction) vs. Non-Blind (Cover work necessary for watermark extraction)
- d. False positive rate: The expected frequency for detection of watermark in non-watermarked content
- e. Robustness: The ability of the watermark to resist common processing attacks
- f. Security: The degree of resilience of the watermark to hostile attacks
- g. Cost: The computational cost associated with watermark embedding and extraction.

## **1.5. AUDIO WATERMARKING**

Audio watermarking has been proposed in the literature as a means to enforce the copyright protection digitally and ensure the non-infringement of the intellectual property rights associated with the audio cover work. The scheme mainly involves concealing the watermark in the original audio signal imperceptibly, without affecting its principal characteristic viz. tone composition, frequency content, pitch variations, loudness [6]. For the purposes of authentication and detection of copyright infringement, authorized personnel may extract the watermark, using a sequence of predefined steps, in order to identify the

source of attack and trace the history of unauthorized access and tampering of the original cover work.

Robustness, security, imperceptibility and high payload capacity [6] are some key characteristics of a good watermarking scheme. Imperceptibility of the watermark in the audio domain is of the utmost significance as it has been observed that embedding the watermark in the acoustic data often leads to undesirable distortions in the audio signal characteristics, which can be used to easily identify the presence of the watermark. Further, watermarking schemes based on the principle of blind extraction are preferred as they do not necessitate the transmission of the original audio signal, thus improving the efficiency and security of the scheme. They are broadly classified into time domain, spread spectrum based, echo hiding, patch work based, and frequency domain [7,8]. Keeping in mind the criteria of imperceptibility, security, and robustness against signal processing and feature distortive attacks, the frequency domain (transform domain) methods have been found to offer a simple and effective approach for watermarking of the digital audio data. The simplified watermark embedding and extraction is also strengthened by the security of the watermarking scheme. Additionally, many of the proposed schemes in the frequency domain are blind in nature. Interestingly, the frequency domain methods offer comparable robustness to signal processing attacks vis-à-vis other methods, and hence has been chosen for implementation of the proposed scheme.

The frequency/transform domain methods for audio watermark embedding are pre-dominantly based on the transformation of the audio signal into the frequency domain using the Discrete Cosine Transform (DCT), Discrete Wavelet Transform (DWT), Discrete Fourier Transform (DFT). The scheme takes advantage of the human auditory perception mechanism and its traits related to recognition and sensitivity to certain frequency bands, to offer an optimal and effective watermarking scheme which meets the standard criterion of

robustness and imperceptibility. The watermarking technique involves subjecting the incoming audio signal to the transformation and modification of the transform coefficients, in a selective manner, in accordance with the contents of the watermark. Further, in order to detect the presence or extract the watermark, the signal is subjected to inverse transformation, followed by identification of the watermarked transform coefficients and extraction of watermark therefrom.

The key idea behind selection of the frequency domain watermarking over other schemes has been illustrated here. Due to audio signals exhibiting resilience against changes to a variety of structural and functional attributes, different gateways for watermarking are made available, with the option to preserve the audio quality and its fundamental perceptual characteristics. However, this is always undertaken with due regards to the requirements of robustness and imperceptibility of the embedded watermark. Different strategies have been formulated for watermarking in the frequency domain, with a simplified yet robust approach [9,10]. The detected robustness of such schemes was maximum for various signal processing and feature distortive attacks. This is due to the modulation of the spectral coefficients instead of the samples in time domain, which ensures a strong defense against such attacks. Further, necessary degree of imperceptibility is maintained, which is essential for keeping the perceptual characteristics of the audio signal intact. The principal consideration for the maintenance of imperceptibility is the location of embedding the watermark, which is chosen diligently so as to affect the audio signal in the minimalistic manner. Other methodologies are based on the principles of echo coding, which embeds the watermark through variation of echo between the original audio signal and its echo and the patch work scheme, which is based on the creation of patches for the purpose of embedding the watermark. However, despite of the relative ease of implementation watermarking methods based on them, they fall short in providing the desired levels of robustness against the signal processing and feature distortive attacks. Further, they are not suitable for audio signals with sparse frequency distribution [6]. In contrast, the spectral domain methods provide good robustness and ensure imperceptibility of the embedded watermark, as outlined above.

## 1.6. IMAGE WATERMARKING

Image watermarking basically involves hiding the watermark information within the original cover image, invisibly, and without influencing the principal characteristics related to the visual appearance of the image like chromatic distribution, saturation and contrast, thus maintaining high image fidelity [11]. For the purposes of authentication and detection of copyright infringement during the transmission of the digital media a set of predefined steps are used for watermark detection/extraction, so as to ascertain the source of attack and its history.

The two principal and contradictory requirements of any digital watermarking algorithm for images are imperceptibility and robustness. It has been found that for images specified in grayscale, strong watermarking decreases the invisibility. Contrary to this, weaker watermarking improves imperceptibility but reduces the robustness. Thus, they should be balanced through a feasible trade-off, without affecting the security. During watermarking, the innate visual attributes of the image must be preserved. This can be achieved through higher correlation between the cover image and watermarked image, by designing the algorithm in such a way so as to affect the original visual attributes of the image minimally, or by utilizing the psycho-visual redundancy to segregate it into visually similar components and undertaking selective watermarking. While the former technique sequentially implements all the watermarking stages, it may lead to greater computational and processing load, if a statistical methodology is implemented for the preservation of the qualities of the image. Further, it has the risk of losing robustness at the cost of imperceptibility.



## 1.7. PROPOSED SCHEMES

Basis the foregoing introduction, we propose a total of four different watermarking schemes in this dissertation for audio and image data. Their principles, implementation scheme, experiments and outcomes are documented as below

### 1.7.1. AUDIO WATERMARKING IN TRANSFORM DOMAIN

This dissertation illustrates a simple yet effective scheme for watermarking of audio signals in the Linear Canonical Transform domain. The watermark kernel is selected as a set of complex data, drawn from a normal distribution, with zero mean and  $\sigma^2/2$  variance. For the purpose of embedding this sequence of complex numbers into the cover work, the Discrete Linear Canonical Transform (DLCT) of the original audio signal is computed, using a given set of LCT parameters. The DLCT thus obtained is sorted in non-increasing order, so as to identify the transform coefficients belonging to the mid-frequency region. Embedding the watermark in the middle of the spectrum has a two-fold advantage: if embedded in the low-frequency region, the watermark is vulnerable to spurious noise and if embedded in the high frequency region, the imperceptibility of the watermark is reduced significantly. After selection of the mid frequency region, the transform coefficients are modulated using the watermark sequence and replace the originally obtained DLCT coefficients. Thereafter, the DLCT coefficient are re-arranged as before, prior to the computation of the Inverse Discrete Linear Canonical Transform. This is followed by the computation of the IDLCT using the inverse of the LCT parameters used while embedding, to obtain the watermarked audio signal. Extraction of the watermark is done in a manner so as to establish the effectiveness of the method in identifying the originally embedded watermark uniquely. We find the DLCT of the watermarked audio data using the same LCT parameters. This is followed by sorting the transform coefficients in non-increasing manner so as to select the middle frequency components where the watermark was embedded. These coefficients are then utilized for computation of the detection parameter  $d$ , which is formed by the sum of the products of the transform coefficients and the watermark. Here, for the

detection of the originally embedded watermark from amongst a random set of watermarks, the value of the detection parameter is calculated for all the watermarks. It is found that the response, in the form of the detection parameter, is the strongest (highest) in the case of the originally embedded watermark, thus confirming the presence of the watermark in the audio signal.

The proposed technique postulates a secure and efficient technique for embedding the watermark in the frequency domain. Security is reinforced due to the fact that the detection of the watermark is only possible if one is in possession of the exact LCT matrix parameters used while embedding. Further, the scheme is able to withstand attacks of the signal processing and feature distortion kinds, both in the time and frequency domain. The imperceptibility of the watermarking technique is also a major highlight of the proposed methodology, as it addresses one of the major concerns in the domain of audio watermarking. Moreover, the high payload capacity of the watermarking scheme makes it suitable for candidates with higher sampling rates, multi-channels and longer duration audio tracks.

### **1.7.2. IMAGE WATERMARKING IN FREQUENCY DOMAIN**

This dissertation proposes a novel approach for watermarking using the Image Partitioning approach, leveraging the image's psycho-visual redundancy. Following watermark scrambling via Arnold Transform, the same is embedded in the lowest frequency DWT sub-band of the image. This reinforces the security and increases the imperceptibility. Further, frequency domain embedding leads to greater robustness. For grayscale images, the technique performs well against common and specialized signal processing attacks. This was gauged using Peak Signal to Noise Ratio and Normalized Cross-Correlation figures of merit.

### **1.7.3. MOMENT BASED IMAGE WATERMARKING**

Many image moments suffer from limited reconstruction ability, errors during numerical approximation, low stability and diminished feature integrity. Addressing the above challenges, this work provides a novel two-tiered zero watermarking framework for color images using Fractional Order Generic Polar Complex Exponential Transform (FrGPCET). Initially, the watermark is scrambled using quasi-affine transform. The stable fractional order moments are calculated in a fast and accurate manner, using higher order interpolators and Gaussian numerical integration. Through incrementally iterative pseudo-random selection and computation of Otsu threshold, an augmented moment feature vector is formed which is in-turn used for embedding the watermark. The second tier is focused towards increasing the imperceptibility by removing any background artifacts, and reducing information redundancy. It involves the sequential use of Discrete Cosine Transform and Huffman coding. The encoded bit sequence is embedded in the corresponding channel of the cover image and combined with the other channels to yield the final watermarked image. Comparison with the state-of-the-art methodologies has shown that the proposed technique surpasses them in terms of watermark's imperceptibility and robustness to different attacks. It is also inherently secure, offers good payload capacity, and can be implemented efficiently with nominal computational resources.

### **1.7.4. IMAGE WATERMARKING USING GRAPH SIGNAL PROCESSING AND LOCAL DOMINANT FEATURES**

This novel technique seeks to embed the watermark in an imperceptible manner while maintaining the power spectral compliance with the cover image. Meeting of the latter requirement is crucial for energy efficient watermarking where the ratio of the mean square error of the Wiener estimate of the watermark and the watermark itself and the variance of the watermark signal. Maximization of this ratio can be interpreted as the increase in the fraction of the watermark energy which resists the Minimum Mean Square Estimation (MMSE). An increment in this fraction leads to a corresponding decrease in the energy which

can be estimated and hence removed. This has a direct bearing on the robustness of the watermark.

In this work, we propose a secure watermarking approach based on spectral graph wavelet. Through the use of spectral graph wavelet, we intend to achieve high visual quality by exploiting the inter-pixel correlation. A multi-stage methodology is applied in the watermarking process: (i) Scrambling of the watermark image using Arnold Transform (ii) Graph signal processing (GSP) for the preservation of local image features, which in turn helps in achieving better reconstruction quality of the image (iii) Use of Variational Mode Decomposition (VMD) to fragment the image into constituent modes so as to segregate the mode with the maximum power spectral compliance with the watermark (iv) Identification of the locations corresponding to the most influential features using Local Dominant Orientation Feature extraction strategy (v) Alpha blending of the watermark with the host image at the predesignated spots, and (vi) Recombination with the other modes and synthesis using the GSP module for generation of the watermark image. The performance of the proposed method was tested against a wide-ranging data set of cover and watermark images as well as against multiple signal processing and feature distortive attacks. It was found that the developed scheme offered high robustness against these attacks, maintained good imperceptibility of the embedded watermark in the cover image and provided requisite security against different attacks, owing to the composite cipher key formed by the number of iterations of Arnold Transform, type of wavelet, nodes, filters and modes of graph signal processing 2-channel filter bank and the mask information related to the embedding locations of the watermark.

## **1.8. ORGANIZATION OF DISSERTATION**

Chapter 2 of this dissertation presents a comprehensive survey of some of the relevant works done in the field of audio and image watermarking, critically evaluating the outcomes in each case. Chapter 3 to Chapter 6 comprise of a comprehensive study of the underlying principles of the watermarking schemes proposed in this dissertation viz. the Fractional Fourier Transform, the Linear Canonical Transform, the Discrete wavelet Transform (DWT), the Arnold Transform, Orthogonal Image Moments, Fractional Order Orthogonal Image Moments, Polar Complex Exponential Transform, Dither Modulation, Huffman Coding, Graph Signal Processing, Variational Mode Decomposition and Local Dominant Orientation Features. Chapter 7 contains the step-wise description of the proposed methodologies, divided into watermark embedding and extraction stages. Chapter 8 outlines the experimental configurations and simulation parameters used for conducting the experiments. The results thus obtained are presented in Chapter 9, along with requisite discussion and inferences. Based on the preceding, the dissertation is finally brought to a conclusion in Chapter 10.

## **CHAPTER 2**

### **LITERATURE REVIEW**

#### **2.1. GENERAL**

The audio watermarking is principally categorized into the time domain, spread spectrum based, echo hiding, frequency/transform domain, and patch work-based techniques. However, since the proposed technique is based on transform domain, we present a critical evaluation of some of the previous work done in the same domain. For review of the works undertaken in other domains, the reader may consult [8,12].

Audio watermarking in the transform domain has seen intensive investigation in the scientific community, with different watermarking schemes being proposed with varied levels of robustness, imperceptibility, security and capacity. The techniques mainly focus on computing the transform coefficients of the audio signal followed by certain post-transformation operations with the intent for identification of the coefficients where the watermark is to be embedded. This is usually done after segmentation of the transform coefficients based on their frequency scale. Considerations with respect to robustness and imperceptibility of the watermarking scheme are crucial at this stage as they directly affect the watermarking process. Following the identification and selection of suitable coefficients, the watermark may be embedded in a direct or indirect manner, with reference to the alteration of the transform coefficients, depending upon the

transformation deployed, post-transformation processing and the levels of robustness and imperceptibility desired. A comprehensive review of the audio watermarking literature reveals that some of the popular transforms used for watermarking include the Discrete Cosine Transform (DCT), Discrete Wavelet Transform (DWT), Discrete Fourier Transform (DFT), Fast Fourier Transform (FFT), Singular Value Decomposition (SVD). In conjunction with the above, some of the post-transformation processes include Exponential Operations, Logarithmic Operations, Frequency-dependent Segmentation, Energy-based Segregation. Pertinent contributions to the field of transform domain audio watermarking have been reviewed below.

Review of the pertinent literature shows that watermarking for images is preferred in the frequency domain due to better robustness, imperceptibility and stability factors. Here, watermark is directly embedded into the frequency coefficients of the image. The coefficient choice and the transform order may vary depending on the robustness and fidelity specifications. Discrete Wavelet Transform (DWT) is a well-known transform in this domain. In the following section, we review some pertinent previous contributions related to it.

In this chapter, we also provide a general overview into some of the prominent works which lead to the development and diversification of the applications in the field of moments and their invariants and continuously increased scientific interest in moments and moment invariants, along with outlining the various research avenues in the field. A meticulous examination of the publications related to moments in the literature is presented in the next section.

Conventionally, the orthogonal image moments ascribe to the statistical estimate of the pixel distribution inside an image's space. Theoretically, they constitute the projections of an image to the orthogonal basis of some specific polynomials. From a scientific and analytical perspective, the orthogonal moments represent the similarity between the image and the image pattern formed by the kernel function of the specific moment family. We delve into each of these perspectives, in more detail, through an examination of relevant works in the respective fields.

In this approach, we treat the digital image as graphs by regarding every pixel as node and connecting it with other pixels. In this graphical representation of image, the gray value is considered as the weight of the graph signal. Graph representation of image signal has been implemented in [13,14,15]. The graph is represented as  $G = (v, E)$ , with its nodes lying in set  $v$ . These nodes function as the sources of the data. These nodes are connected by a set of weighted branches, known as the edges of a graph and denoted by  $E$ . In terms of graph signals, the data set formed by the nodes can be considered as a sample set. A preliminary idea for data representation using graphs is provided in [13,16]. The filter is designed by first dividing the original graph into a uniform size finite set of bipartite sub-graphs [13] using the decomposition scheme iteratively described in [13,17]. This will lead to the formation of a two-channel wavelet filter bank for the given cover image, which contains of an analysis and synthesis sections, separated by down-sampling and up-sampling blocks. A detailed literature review of the existing techniques employing this methodology is given in Section 2.2.



## 2.2. LITERATURE REVIEW

Dhar et al [18] proposed a blind audio watermarking scheme in DCT domain based on SVD. Therein, the audio cover work was fragmented into non-overlapping frames followed by DCT calculation on a per frame basis. Post-transformation exponentiation operation was applied on the sub-band with highest power of the DCT coefficients on individual frames. SVD was applied to these exponential coefficients and the watermark was embedded into the largest singular value, as decided by the quantization rule. Simulation results demonstrated that the proposed scheme provided high robustness against different attacks such as noise addition, cropping, re-sampling, re-quantization, and MP3 compression due to watermark being embedded into the largest singular value of the exponential coefficients. Additionally, the technique was characterized by low false positive and false negative error rates.

Ali Al-Haj [2] developed a robust, imperceptible, and semi-blind audio watermarking algorithm by cascading the DWT and SVD. The effect of cascading transcended as complementary but enhanced levels of robustness against watermarking attacks. The underlying technique was based on the distributed formation of the wavelet coefficient matrix and the selection of the off-diagonal positions of the singular value matrix for watermark embedding. This ensures both robustness and imperceptibility of the watermarking scheme. Further, the technique demonstrated high data payload capacity as well.

Dhar et al [9] formulated a robust audio watermarking scheme based on the Fast Fourier Transformation (FFT). The magnitude spectrum of the original audio was segmented and energy of all such segments calculated. Watermark embedding was done

in the most prominent peaks of the highest energy segments, so as to maintain robustness against different attacks viz. noise addition, cropping, resampling, re-quantization, and MP3 compression. Further, the scheme outperformed Cox's in terms of imperceptibility, as evidenced by the Signal-to-Noise Ratio (SNR) values.

Attari et al [7] relied on the spread spectrum in Discrete Wavelet Transform (DWT) domain for designing a robust and blind audio watermarking scheme, wherein the secret data was embedded in low-frequency coefficients, as they are less prone to detection. 6th level approximation coefficients of DWT were modified using the direct sequence spread spectrum (DSSS) technique, for embedding the watermark. Psycho-acoustic imperceptibility enhancement, in conjunction with the use of with Savitsky-Golay filter for better extraction accuracy was undertaken. The experimental results validated robustness against the most common attacks.

Wu et al [1] formulated a blind and watermarking algorithm for audio data by combining the multi-resolution feature of DWT and the energy localization capability of DCT. The segmented audio fragments of the original audio signal were decomposed using DWT and fourth level detail coefficient was selected to be divided into two packets, which were then passed on further for DCT computation, to obtain two sets of transform domain coefficients (TDC) respectively. Watermark was embedded by modifying the average amplitudes of the two sets of TDC based on custom embedding rule. Experimental results confirmed the proposed algorithm's imperceptibility, high payload capacity and robustness in opposition to attacks such as MP3 compression, echo addition, re-sampling, low-pass filtering, re-quantization, amplitude scaling.

Liu et al [19] developed a robust audio watermarking algorithm based on DCT and Vector Quantization (VQ). Post segmentation of the audio signal into frames, DCT transformation was performed and middle frequency coefficients of each frame were used to form a vector. This is followed by vector quantization, as directed by the content of the watermark information. These modified coefficients are replaced and IDCT is computed to obtain the watermarked signal. Experimental results revealed the technique's strong robustness to most of the attacks.

Megias et al [6] undertook a tuning analysis of the frequency domain audio watermarking by deploying MPEG 1 layer 3 compression for watermark embedding to isolate the frequency points for embedding of the watermark. The experiment involved use of some of the audio parameters viz. bit rate ( $R$ ), peak magnitude( $p$ ), relative error( $\epsilon$ ) between magnitudes of original and compressed files, quantum of disturbance in magnitude due to embedding of the watermark( $d$ ) and tolerance percentage for reconstruction of the watermark( $q$ ). Results showed that high bit rate enhanced the capacity at the cost of imperceptibility. Parameter  $d$  affected only robustness and imperceptibility.  $p$  and  $\epsilon$  could be tuned for enhancing the imperceptibility and robustness simultaneously. Other pertinent observations with reference to the capacity enhancement and watermark recovery were also made.

Panda et al [20] leveraged Empirical Mode Decomposition (EMD) for blind watermarking of audio data, which provided robustness against some of the non-blind methodologies and relied on the use of adaptive threshold during watermark extraction. Further, the watermark balked filtering attacks as was made possible from the non-masked Intrinsic Mode Function (IMF). Additionally, since the watermarking bits were

associated with the synchronization codes, the scheme was able to resist cropping attacks as well.

Developing a secure watermarking scheme, Cox et al. [5] devised a watermark as an independent and identically distributed Gaussian random vector. Its insertion took place in a spread spectrum manner into the spectral components of the cover work. With the watermark being spread over a pre-defined range of frequency components forming a small fraction of the total spectral content, the cover image is affected in a minimal manner.

Esgandari et al. [21] proposed an image watermarking technique based on discrete wavelet transform, which involved the use of chaotic map for encoding of the watermark and its subsequent embedding in the centre of the image spectrum. The process accentuated the image continuity and robustness to various image processing attacks.

Su et al. [22] postulated a blind watermarking algorithm using colour space transform and Integer Wavelet Transform, for embedding a colour watermark into a colour host image. By quantization of the wavelet coefficient in adherence with the characteristics of the Human Visual System and subsequent embedding in the IWT domain, the embedded watermark was made invisible and robust against common image processing attacks.

Rui-mei et al. [23] created a blind image watermarking algorithm in wavelet transform domain wherein the disintegration of the original grayscale image into some coefficients in different spatial and frequency sub-bands was undertaken, underpinning on the inter-relationship between the parent and the children nodes. Invisibility and robustness against common image processing attacks was confirmed through experimental results.

Yang et al. [24] proposed a watermarking algorithm for colour image based DCT and DWT, wherein a binary watermark was embedded into green component or blue component of colour image. Apart from common attacks, the method demonstrated its invisibility and resisted JPEG compression, noise addition, low pass filtering and mosaicking attacks.

Liu et al. [22] concentrated on the probability density function of wavelet coefficients. By modelling it using the generalized Gaussian distribution (GGD) and calculation of the decision threshold using the Neyman-Pearson (NP) criterion, watermarking was performed. The process registered robustness to image processing and geometric attacks due to regulated energy selective embedding.

C. –H. Teh et. al [25] analyzed and compared a variety of moments such as the Legendre moments, Zernike moments, pseudo-Zernike moments, rotational moments, and complex moments, insofar their image pattern recognition capability is concerned. Other parameters on which the moments were examined included the image-representation ability, information redundancy, and noise sensitivity. This led to the

identification and characterization of the properties of these moments along with the definition of the inter-relationships between the various moments. This was duly substantiated using relevant theoretical and experimental observations.

Papakostas [26] worked towards the identification of appropriate moment features used to recognize the patterns present therein. The descriptive nature of the features formed a key determining attribute. The proposed works presented some of the, prominent classes of moments along with their characteristics and their suitability with reference to the pattern recognition exercises was discussed. Using two separate features election algorithms, moment features were selected so as to provide better discernibility between facial expressions, captured under different facial pose and illumination conditions. A descriptive experimental analysis using multiple publicly available data sets reported enhancement of recognition performance of moment features, when selected from a predefined set with respect to a particular application.

Kautsky et. al [27] proposed the use of moment invariants for image blurring. Drawing on the pertinent works in the domain, the authors developed a common technique for the construction of blur invariants from random moments without deriving them on a per polynomial basis. The methodology relied on eliminating the dependent terms in blur invariants and demonstrated an orderly implementation of the invariants in orthogonal bases using recurrent relations.

Alghoniemy et al. [28] suggested a novel technique for moment-based image watermarking, wherein the watermark was formed by the mean of several functions of

the second and third order moments invariant to scaling and orthogonal transformations. The watermarked image retained its imperceptibility through combination of the original image and an empirically weighted nonlinear transformation of the original. The watermarking scheme was reversible and extremely robust to all geometric transformations and other signal processing attacks.

Papakostas et al. [29] formulated techniques for the fast computation of the Zernike and Pseudo-Zernike moments. The utility of the algorithm design was leveraged in the use of computed moments as discriminative features in pattern classification applications, where the calculation of higher order single moments is entailed. This is achieved by the substitution of the factorial computations, with recursive fractional terms of the orthogonal polynomials. As a result of the use of the proposed technique, the computational complexity was improved from  $O(n^3)$  to  $O(n^2)$ . This was verified through suitably designed experiments which validated the superiority of the proposed technique.

Hosny [30] devised a mechanism for the computation of the exact Legendre moment for images using a recurrence relationship, by mathematically integrating the Legendre polynomials over the pixels of the image. This method successfully addresses the errors stemming from numerical approximation, which is extensively used in the conventional methods. Acceleration of the moment calculation is proposed using a fast and efficient variant of the algorithm. When compared against other conventional methods, the results evince the advantage of the use of the proposed methodology vis-à-vis the precursory techniques.

Mukundan et al. [31] introduced a new set of orthogonal moment functions based on the discrete Tchebichef polynomials which served as effective means for the characterization of pattern features of two-dimensional images. The moment computation was made error free on account of it being devoid of any numerical approximation. The moments thus derived are better in performance as compared to the conventional orthogonal moments such as Legendre moments and Zernike moments, in terms of retention of analytical properties which form the basis of redundancy in the information set formed by the moments. Further, the different mathematical aspects of Tchebichef moments and their ability of accurate representation of features were proved using the principle of image reconstruction.

Yan-Wang et al. [32] worked on the problem for designing a watermarking scheme robust against desynchronization attacks, which dislocates the watermark position. Using multi-scale Harris detector and wavelet moment theory, the authors formulated a content dependent image watermarking algorithm with low computational complexity, appreciable image quality showing steady resilience against desynchronization attacks. The watermark was associated with the geometrically invariant image features thus enabling detection of watermark in the absence of synchronization error. Experimental results revealed robustness of the scheme against common image processing operations as well as desynchronization attacks, with the operation of the watermarking technique remaining invisible.

Tsougenis et al. [33] devised the first adaptive moment-based color image watermarking by utilizing the rotation invariance, low reconstruction error and high computation accuracy linked to the quaternion radial moments' (QRMs). The performance of the technique was demonstrated through multi-embedding binary watermarks in the quaternion radial moments of the image. The scheme adaptively



adjusts the strength of the watermark by factoring in the cover image's morphology, and ensuring optimal trade-off between robustness and imperceptibility. Simulation results confirmed the technique's ability to resist common signal processing and geometric attacks. The use of adaptive process accentuates the robustness and imperceptibility, which is reflected through the figures of merit computed post watermark extraction.

Papakostas [34] covered the research in the field of moments and their invariants in a comprehensive manner, by highlighting the potential of this domain and the growing interest of the community in the connected areas. The study also presents an in-depth description of the challenges in the consequent improvisations related to the theoretical and practical aspects of the moments. It also summarizes the current challenges, areas of work and future scope of development in the associated fields of moments and moment invariants.

Papakostas et al. [35] designed an optimized image watermarking methodology that enhanced the contribution of the local features and relied on the use of Krawtchouk moments. The technique utilized a basic genetic algorithm to achieve optimization of the parameters influencing the localization of properties while maintaining the overall performance of the watermarking scheme. The use of the technique yielded high quality watermarked images while recording low bit error rates during watermark extraction. The proposed scheme performed desirably under multiple non-geometric attacks and thereby formed a robust and accurate watermarking methodology.

Flusser et al. [36] explained in detail the various image processing applications based on the use of moments as projections of an image's intensity onto a proper polynomial basis. Watermarking and invariant pattern recognition were some of the applications expounded upon, among other prominent ones. An extensive survey of both image analysis and pattern recognition techniques was conducted and new concepts of invariants to linear filtering and implicit invariants were proposed. The manuscript also covered in depth the pertinent aspects related to efficient computational algorithms for discrete domain moment calculation. The authors also illustrate the theory through practical examples, demonstrating moment invariants in real applications across computer vision, remote sensing and medical imaging. Key features: Presents a systematic review of the basic definitions and properties of moments covering geometric moments and complex moments.

Teague [37] defined the two-dimensional image moments calculated using Zernike polynomials and proposed the construction of a large number of independent, algebraic combinations of Zernike moments, invariant against geometric and desynchronization transformations. He further compared this approach with the common method of moments and reviewed the two-dimensional pattern recognition and three-dimensional object recognition using the proposed framework. Unique image reconstruction in time/frequency domain using finite number of moments was also broached upon, followed by discussion of a coding scheme for image storage and retrieval.

Suk et al. [38] developed a new category of affine moment invariants for color images. This was done by calculating additional invariants can be computed, using the same transformation, on a per channel basis. These moments were shown to have lower order and hence were robust against noise. They were also contrasted against

another group of invariants featuring second power of the image function. The properties of the proposed features were verified through numerical experiments on real images.

Xin et al. [39] studied the invariance properties of some ZMs/PZMs and identified the suitable candidates for watermarking applications, from the perspective of achieving good imperceptibility and robustness to geometric distortions. It was showcased later, that the embedded information could be decoded at low error rates and offered string resistance to signal processing and feature distortive attacks.

Shuman et al. [16] described the main challenges associated with the signal processing on graphs which typically involves the combination of harmonic analysis with an integrated system of algebraic and spectral graph concepts. Their work proposed the definitions of graph spectral domains, by treating them analogous to the classical analog frequency domain, with specific thrust on the inclusion of the irregular graph structures. Approaches generalizing the basic operations such as filtering, translation, modulation, dilation, were reviewed and localized, multiscale transforms used for efficient extraction of information from high-dimensional graph data was studied.

Narang et al. [13] developed the two-channel wavelet filter banks for analysis of graph functions linked to the vertices of any given finite weighted undirected graph. Aliasing occurs due to spectral folding observed during down-sampling in bipartite graphs. This led to the construction of critically sampled two-channel filter banks, and quadrature mirror filters (referred to as graph-QMF) for bipartite graph alleviating the aliasing phenomenon and providing perfect reconstruction. Using Chebyshev polynomial

for filter realization, the proposed filter banks offered critical sampling while maintaining orthogonality, nullifying aliasing and providing perfect reconstruction. For a generic graph, a bipartite subgraph decomposition was proposed followed by Graph-QMF design for each bipartite subgraph.

Zhang [17] devised a technique for the design of two channel compactly supported near orthogonal graph wavelet filter banks. Its kernel filter satisfied the condition of a flat spectrum in both the passband and stopband. This was instrumental in the development of the closed-form solution for the maximally flat filters, with specific degrees of flatness at different eigen values. The remainder of the coefficients was used to lower the reconstruction error of filter banks. Experimental results revealed that the proposed graph filter banks proposed proved superior in performance compared to the conventional kernel filters.

Drawing on the results obtained for the use of orthogonal transforms in conjunction with graph data, Narang et al. [15] extrapolated the results previously obtained to more generalized and flexible biorthogonal transforms. Leveraging the same principles, “one-dimensional” two-channel filter banks were initially designed on bipartite graphs, and then extended to “multi-dimensional” separable two-channel filter banks for arbitrary graphs via a bipartite subgraph decomposition. The wavelet filters so designed were completely specified using the sufficient conditions for perfect reconstruction and orthogonality. Due to the inherent drawback of this design being non-hop localized, i.e., the computation at each node is not limited to a finite-hop neighborhood surrounding the node. Therefore, the authors proceeded to make the graph wavelets hop-localized by constraining the condition of orthogonality. A set of biorthogonal pair of graph-wavelets which continued to satisfy the perfect reconstruction conditions were formulated. The design had strong resemblance to the standard Cohen-

Daubechies-Feauveau's (CDF) construction which entailed factorization of a maximally-flat Daubechies half-band filter. The utility of these filters was shown for standard signal processing applications, besides the stochastic graphs defined for certain signals.

Working for the development of wavelet transforms for function defined on vertices of the vertices of an arbitrary finite weighted graph, Hammond et al. [14] proposed a technique which relied on scaling of the spectral decomposition of the discrete graph Laplacian  $L$ , which can be considered as the using the graph analogue of the Fourier domain. Given a wavelet generating kernel and a scale parameter, we define the scaled wavelet operator which was used to generate the spectral graph wavelets through local application of the operator on an indicator function. Under specific constraints, the transform can be made invertible. Additionally, the authors designed a fast Chebyshev polynomial approximation algorithm for undertaking the transformation. Certain possible applications of the transform were explained through various examples of wavelets on graphs.

## CHAPTER 3

### PRINCIPLES OF AUDIO WATERMARKING

#### 3.1. THE FRACTIONAL FOURIER TRANSFORM

The one-dimensional Fractional Fourier Transform (FRFT)  $Y^\alpha$ , of order  $r$  and angle of rotation  $\alpha$ , where  $r \in \mathbb{R}$ , is a linear transformation [40], performed over an integral, and, which maps a given function  $i(t)$  in the following manner

$$Y_\alpha(\mu) = \int_{-\infty}^{\infty} i(t)H_r(\mu, t)dt \quad (3.1)$$

where

$$H_r(\mu, t) = \begin{cases} \sqrt{\frac{1 - jcot\alpha}{2\pi}} e^{j(t^2 + \mu^2) \cot(\frac{\alpha}{2}) - j\mu t \csc\alpha} & , \text{if } \alpha \neq k\pi, k \in \mathbb{I} \\ \delta(t - \mu), & \text{if } \alpha = 2k\pi, k \in \mathbb{I} \\ \delta(t + \mu), & \text{if } \alpha + \pi = 2k\pi, k \in \mathbb{I} \end{cases} \quad (3.2)$$

The FRFT is regarded as the transform which rotates the plane of energy concentration by the specified angle  $\alpha$ . Plainly speaking, it corresponds to the rotation of the signal in the time-frequency/transform domain by the angle  $\alpha$ . The inverse transform is computed by calculating the FRFT of the transformed signal with the angle  $-\alpha$ . Also, due to the additivity property of FRFT, the equivalent FRFT of signal rotated through angle  $\alpha + \beta$  is equivalent to successive FRFT applications with the angles  $\alpha$  and  $\beta$ . It

should also be noted that the FRFT for  $\alpha = \frac{\pi}{2}$  corresponds to the ordinary Fourier Transform.

The discrete time implementation of FRFT (DFRFT) has been defined multiple times. However, the essential principle of calculation of the fractional power of the DFT matrix remains uniform. For further details of the different implementation mechanisms, the reader may refer [40].

## 3.2. THE LINEAR CANONICAL TRANSFORM

### 3.2.1. CONTINUOUS LINEAR CANONICAL TRANSFORM

The one-dimensional continuous linear canonical transform with the real-valued parameter matrix  $X = \begin{pmatrix} a & b \\ c & d \end{pmatrix}$  of a signal  $x(t)$  is given by [41]

$$T_{a,b,c,d}(\mu) = L^{a,b,c,d}(x(t)) = \begin{cases} \int_{-\infty}^{\infty} x(t)R_{a,b,c,d}(t,\mu)dt, & b \neq 0 \\ \sqrt{d}e^{\frac{j(cd)}{2\mu^2}}x(d\mu), & b = 0 \end{cases} \quad (3.3)$$

where the parameter matrix elements satisfy  $ad - bc = 1$ . The LCT transformation kernel, denoted by  $R_{a,b,c,d}(t, \mu)$ , is expressed as

$$R_{a,b,c,d}(t, \mu) = \sqrt{\frac{1}{j2\pi b}} e^{j\left(\frac{d\mu^2}{2b} - \frac{\mu t}{b} + \frac{at^2}{2b}\right)} \quad (3.4)$$

The LCT offers an extra three degree of freedom, as compared to the FRFT with one additional degree of freedom. If  $a = \frac{\zeta}{\tau}$ ,  $b = \frac{1}{\tau}$ ,  $c = -\tau + \frac{\lambda\zeta}{\tau}$  and  $d = \frac{\lambda}{\tau}$ , the LCT may be re-expressed as

$$T_{a,b,c,d}(\mu) = L^{a,b,c,d}(x(t)) = \begin{cases} \int_{-\infty}^{\infty} x(t)R_{a,b,c,d}(t,\mu)dt, & b \neq 0 \\ \sqrt{\lambda/\tau}e^{\frac{j(-\lambda + \frac{\lambda^2\zeta^2}{\tau^2})}{2\mu^2}}x(d\mu), & b = 0 \end{cases} \quad (3.4)$$

The kernel function is given by

$$R_{a,b,c,d}(t,\mu) = \sqrt{\frac{\tau}{j2\pi}}e^{j\left(\frac{\lambda\mu^2}{2} - \mu t\tau + \frac{\zeta t^2}{2}\right)} \quad (3.6)$$

where the LCT parameter matrix is given by

$$X = \begin{pmatrix} a & b \\ c & d \end{pmatrix} = \begin{pmatrix} \frac{\zeta}{\tau} & \frac{1}{\tau} \\ -\tau + \frac{\lambda\zeta}{\tau} & \frac{\lambda}{\tau} \end{pmatrix} \quad (3.7)$$

Some noteworthy features and properties of LCT are provided below.

### 3.2.2. PROPERTIES OF LINEAR CANONICAL TRANSFORM

Some essential properties of linear canonical transform are explained below

#### Property 1: Additivity

$$L_{X_2} [L_{X_1}[x(t)]] = L_{X_3}[x(t)] \quad (3.8)$$



where  $X_i = \begin{pmatrix} a_i & b_i \\ c_i & d_i \end{pmatrix}$ ,  $i = 1, 2, 3$  are real matrices and  $X_3 = X_1 \cdot X_2$ , where ‘ $\cdot$ ’ stands for matrix multiplication. This property holds for complex matrices only if  $Im\left(\frac{a_2}{b_2} + \frac{d_1}{b_1}\right) > 0$ . If  $Im\left(\frac{a_2}{b_2} + \frac{d_1}{b_1}\right) = 0$  then  $b_1, b_2 \in \mathbb{R}$ .

**Property 2: Unitarity**

$$L_{A^{-1}}[L_A[x(t)]] = L_A^H[L_A[x(t)]] = x(t) \quad (3.9)$$

where  $L_{A^{-1}}$  represents the inverse of the LCT and  $L_A^H$  is the expression of unitarity for the LCT operator. This property holds for complex parameters only when  $b_1 \in \mathbb{R}$ .

We shall limit our discussion only to real parameters of the LCT matrix, where both of the above properties hold. It should also be noted that the LCT reduces to FRFT for the parameter matrix  $X = \begin{pmatrix} \cos\theta & \sin\theta \\ -\sin\theta & \cos\theta \end{pmatrix}$ . The FRFT is then given by

$$L_{X_{FRFT}}(x(t)) = \sqrt{e^{-\frac{j\theta}{2}}} T_\theta(\mu) \quad (3.10)$$

where  $T_\theta(\mu)$  denotes the FRFT of the signal  $x(t)$ , at an angle  $\theta$ . If  $\theta = \frac{\pi}{2}$ , the FRFT further reduces to the Fourier Transform and is given by

$$L_{X_{FT}}(x(t)) = \sqrt{-j} T(\mu) \quad (3.11)$$

The corresponding LCT parameter matrix is given by

$$X = \begin{pmatrix} 0 & 1 \\ -1 & 0 \end{pmatrix} \quad (3.12)$$

Relations, properties and their pertinent proofs for LCT can be found at [41,42,43].

### 3.2.3. DISCRETE LINEAR CANONICAL TRANSFORM

Processing of the signals in the digital domain necessitates the implementation of the transformation in the same domain as well. Different techniques have been proposed for the fast implementation of the DLCT. In [42], setting  $\delta_x = \delta_y = (N|\beta|)^{-1/2}$ ,  $x = n\delta_x$ ,  $y = m\delta_y$ ,  $m, n = 0, 1, \dots, N - 1$ , the  $N$ -point DLCT of  $x(n)$  can be defined as [42]

$$x_X(m) = \sum_{n=0}^{N-1} x(n)R_X(m, n) \quad (3.13)$$

where the discrete LCT kernel is given as

$$R_X(m, n) = \frac{\sqrt{\beta}e^{-\frac{j\pi}{4}}}{\sqrt{N|\beta|}} \exp \left[ \frac{j\pi}{N|\beta|} (\lambda m^2 - 2\tau mn + \zeta n^2) \right] \quad (3.14)$$

This discrete approximation of LCT is analogous to the discrete approximation of the Fourier Transform (DFT). Further, the approximation follows the properties of additivity and unitarity of the continuous LCT.

## CHAPTER 4

### PRINCIPLES OF IMAGE WATERMARKING IN FREQUENCY DOMAIN

#### 4.1. DISCRETE WAVELET TRANSFORM

The discrete wavelet transform is visualized as a multilevel enhancement of the fixed resolution Fourier Transform. For this transform, the wavelets form the basis functions and decompose the two-dimensional image into four equal sized sub-images. The low-frequency sub-image can be decomposed continually and the remaining high frequency sub-bands account for the horizontal, vertical and diagonal directions. These are logarithmically distinguished in the spectral domain. The image is first divided into four sub-bands such as LL1, LH1, HL1 and HH1 by cascading horizontal and vertical channels and critically sub-sampled using filter banks. In the next hierarchy level, the sub-band LL1 is further divided into 4 sub-bands, each of which is critically sub-sampled. The process may be repeated to the desired extent. The lowest frequency part, LL1, has limited significant information content as compared to other sub-bands, hence is chosen for watermark embedding.

Different kinds of wavelets including inter alia Haar, Daubechies, Coiflets, Symlets, Morlets, Mexican Hat Meyer and Biorthogonal wavelets may be used. Some of them also permit decomposition using higher order wavelets. For our experiments, Haar (First Order Daubechies) wavelet is used for single level DWT decomposition.

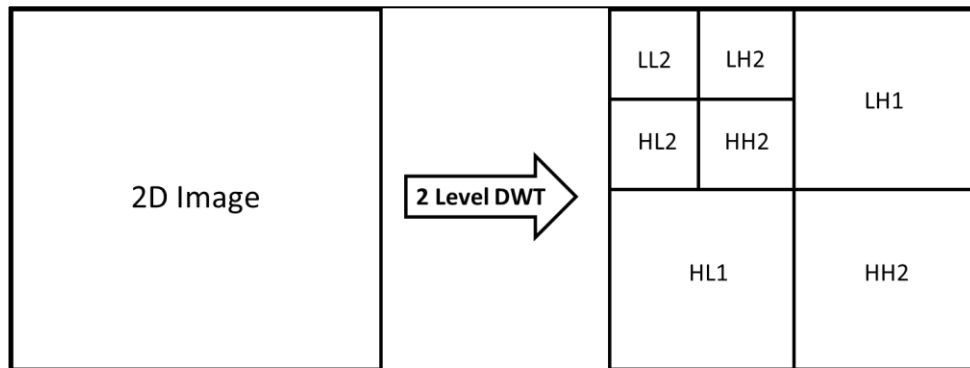


Figure 4.1: 2 Level Discrete Wavelet Transform

## 4.2. ARNOLD TRANSFORM

The Arnold Transform is a chaotic map-based transformation, defined in 2D as

$$\begin{bmatrix} x' \\ y' \end{bmatrix} = \begin{bmatrix} 1 & 1 \\ 1 & 2 \end{bmatrix} \begin{bmatrix} x \\ y \end{bmatrix} \text{mod } 1 \quad (4.1)$$

The inverse transformation is defined as

$$\begin{bmatrix} x \\ y \end{bmatrix} = \begin{bmatrix} 2 & -1 \\ -1 & 1 \end{bmatrix} \begin{bmatrix} x' \\ y' \end{bmatrix} \text{mod } 1 \quad (4.2)$$

which also shows its invertibility.

The above transformations are applicable on a per pixel basis.

## CHAPTER 5

### PRINCIPLES OF IMAGE WATERMARKING IN TRANSFORM DOMAIN

#### 5.1. OVERVIEW OF WATERMARKING TECHNIQUES BASED ON MODIFICATION OF IMAGE MOMENTS

The transform domain watermarking principle is leveraged for watermarking the images using changes made to the moments thereof. The orthogonal moments themselves act as the medium for embedding the watermark. Orthogonal image moments have been exploited extensively in the fields of pattern recognition and trend analysis [44], deep learning and computer vision [26,27,45] and a whole other array of image processing [46] applications. This can be attributed to the compact nature of content descriptors, minimum information redundancy which are instrumental for satisfying the principal conditions of semantic description of an image. The mathematical properties, especially geometric invariance and independence are particularly beneficial in this respect [28]. Different families of moments have been proposed in literature over the past few decades, offering a diverse set of descriptive and image representation capabilities. Some of the popular ones and often frequently deployed for pertinent applications include the Fourier–Mellin [46], Zernike [28], pseudo-Zernike [29], Legendre [30], Tchebichef [31] and Krawtchouk [47] moments.

To achieve the watermarking of digital images by relying on the moments thereof, the watermark is first constituted as mean of several functions of the second and third order moments devised to be immutable against scaling and orthogonal transformations. This also makes the watermark extraction blind. The watermarked image is a formed by a linear combination of the cover image and a suitably scaled transformed image. Watermark detection is as reversible due the nature of the orthogonal moments.

The foregoing forms the foundation of many watermarking techniques based on the modification of the orthogonal moments. Some of these have been enumerated below

- a. Use of normalized orthogonal moments as a vector followed by watermark embedding by modification of the vector coefficients. Such methodologies are normally deployed in the transform domain [48].
- b. Leveraging the uneven invariance property of circularly orthogonal moments, for designing a multi-bit watermark. This is accomplished through the quantization of the selected moment magnitudes using quantization index modulation [49] to encode an array of bits. The manipulation may be done to a desired extent and in a pre-specified manner, so as to achieve watermark robustness to geometric distortions and other transformational attacks.
- c. The use of orthogonal moments can be coupled to image feature extraction techniques belonging to the class of scale-invariant feature transformations. The transformed images thus obtained are used to embed the watermark through modulation of the magnitudes of Tchebichef moments for attaining robustness and the blind detection [50].
- d. Some derivatives of the above technique employ wavelet moment theory in conjunction with Harris-detector based feature extraction, to develop an image watermarking algorithm with low computational complexity and appreciable resistance to various attacks. Post extraction of the features and construction of local feature regions (LFRs), significant regions are identified for embedding the watermark into the LFRs by modifying their wavelet moment invariants. This aids in reduction of synchronization error [32,51].
- e. Extension of the principle from gray-scale images to color images using moment-based watermarking has seen the advent of multiple quaternionic image transformation approaches. The mathematical inter-relations and properties of the quaternions and different polar harmonic transform (PHT) are utilized for achieving geometrically invariant watermarking of color images. Literature is replete with

instances of [52] quaternion radial moments and [33] quaternion exponent moments as an alternative moment domain for color image watermarking with the goal to enhance robustness.

- f. Different variants of the methodology based on quaternions and polar harmonic transforms have been proposed, which emphasize on the localization of moment coefficients. Effectively, they serve to control the embedding location of the watermark through a multitude of optimization algorithms [34,35].

It should be noted that the ability to conceal a piece of information is determined by their magnitudes, polynomial orders and repetitions, parameters of the moment coefficients, which are greatly inter-connected and extremely inter-dependent. Together, they are crucial for maintaining the robustness and imperceptibility of the watermarking scheme.

## **5.2. ORTHOGONAL MOMENTS**

The research undertaken in the period preceding the development of neural networks and in the nascence of artificial intelligence, saw the use of hand-crafted representations and feature engineering in the computer vision, pattern recognition and related applications. Hand-crafted features representation has its own place in the domain of feature extraction as many of its attributes cannot be matched even by the sufficiently advanced versions of deep learning models [53]. Image representation methods can be broadly classified as under [54]:

- Moments and moment invariants – viz. Zernike Moments (ZM), Legendre Moments, and Polar Harmonic Transforms (PHT).
- Frequency transform – based on Fourier Transform, Walsh Hadamard Transform, and Wavelet Transform;

- Dimensionality reduction – employing Principal Component Analysis (PCA), Singular Value Decomposition (SVD), and Locally Linear Embedding (LLE);
- Texture – using Scale Invariant Feature Transform (SIFT), Gradient Location and Orientation Histogram (GLOH), and Local Binary Patterns (LBP);

As the representation of the image entails a semantic analysis, it follows that the following criteria must be satisfied by all image representation techniques, in general [36]:

- Distinguishability – the features identified should clearly reflect the inter-class deviations/separations;
- Robustness – static representation for a single class i.e. intra-class variations do not affect the feature map of an object from a particular class.

Representations relying on frequency transform, texture, and dimensionality reduction have been frequently used in a gamut of applications. However, it has been commonly observed that due to the prevalent semantic inaccuracies between the low-level feature descriptors and high-level visual attributes, the robustness and discriminatory nature of the feature map is often compromised [55]. In opposition to this, moments and moment invariants are able to bridge the semantic gaps due to their inherent mathematical properties:

- Independence – Orthogonal basis functions leads to elimination of information redundancy in the moment data, which in turn is responsible for better discernibility in image representation;
- Geometric invariance – invariance against geometric transformation, i.e. rotation, scaling, translation, and flipping, is extracted from the moment data, which enhances the robustness of image representation.



Moments and moment invariants were first proposed in 1962, with suggestive applications in the field of pattern recognition [56]. A myriad of image representation techniques using orthogonal moments have been proposed in the literature, since then, for a wide range of applications and offering various level of customized image representation through the distinct moment computation techniques. The reconstruction and calculation aspects of the moments have also been explored in depth and have undergone major improvements since first proposed. Efforts have been directed towards fast and accurate calculations of the classical moments. Recently, the work has been extended to 3D object invariant representation [57]. State-of-the-art methods based on unit disk-based orthogonal moments have also been proposed [34,58].

### 5.3. IMAGE MOMENTS

The image moment is defined as the inner product  $\langle u, X_{ab} \rangle$  of the image function  $u$  and the basis function  $X_{ab}$  of  $(a + b)$  order over the domain  $F$  [54]:

$$\langle u | X_{ab} \rangle = \iint X_{ab}^*(i, j) u(i, j) \, di \, dj$$

where the asterisk  $*$  denotes the complex conjugate. The immediate geometric interpretation of moment set  $\langle u, X_{ab} \rangle$  can be understood as the projection of  $u$  onto a subspace formed by a set of basis functions  $\{X_{ab} : (a, b) \in \mathbb{Z}^2\}$  [58]. We select a specific set of basic functions  $X_{ab}$  whose properties in  $\langle u, X_{ab} \rangle$  are compliant with the semantic necessities of image representation. According to the mathematical properties of basic functions, the family of image moments can be divided into different categories, as shown in below figure.

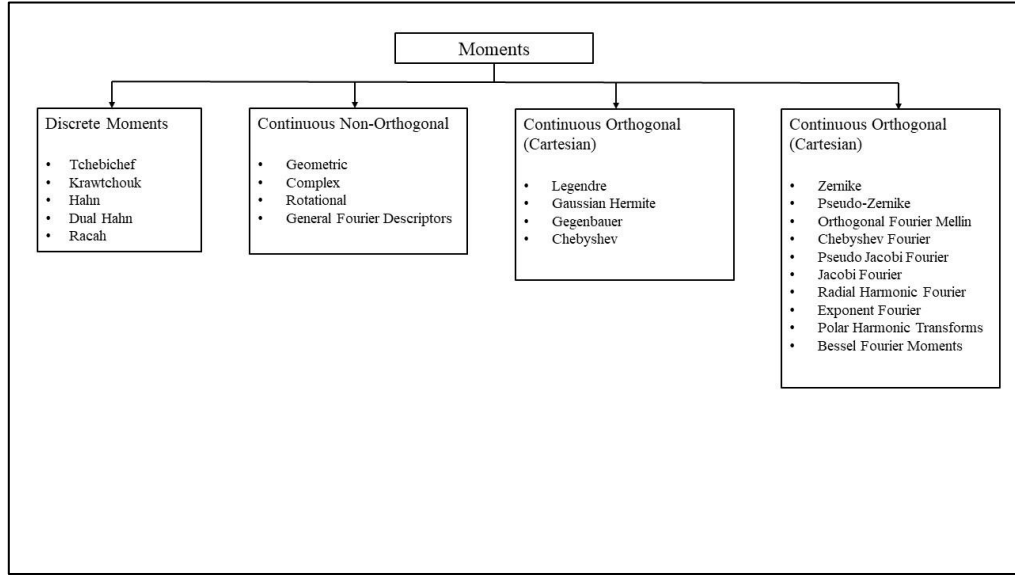


Figure 4.2 Image Moments

On the basis of orthogonality, the image moments can be classified into orthogonal and non-orthogonal moments. The orthogonality implies that any two different basis functions  $X_{ab}$  and  $X_{a'b'}$  from the basis function set are uncorrelated or mutually “perpendicular” in geometric parlance (statistical independence), thus eliminating redundancy in the moment domain. Mathematically,  $X_{ab}$  and  $X_{a'b'}$  are orthogonal when the following condition is satisfied

$$\langle X_{ab} | X_{a'b'} \rangle = \iint X_{ab}(i,j) X_{a'b'}^*(i,j) di dj = \delta'_{ii} \delta'_{jj} \quad (5.1)$$

where  $\delta_{mn}$  is the Kronecker delta function expressed as

$$\delta_{mn} = \begin{cases} 0, & m = n \\ 1, & m \neq n \end{cases} \quad (5.2)$$

Depending on the continuity of the basis function, the image moments can be categorized into continuous and discrete moments. For two-dimensional (2D) images, the basic functions are defined in the 2D real-valued space and the 2D digital image space, i.e.,

the domains  $D \in \mathbb{R}^2$  and  $D \in \mathbb{Z}^2$ , respectively. Continuous moments of a digital image may be calculated using an appropriate discretization approximation of the continuous integral, entailing certain computational errors. On the other hand, discrete moments, such as Hahn and Racah do not involve any approximation errors and hence are more suited for high-precision image processing applications [59,60].

Treating the coordinate system as a parameter for the segregation of the basis functions, image moments can be divided into Cartesian and circular moments. In the case of continuous moments, the basis functions of Cartesian moments are defined in  $M = \{(i, j) : i \in (-\infty, +\infty), j \in (-\infty, +\infty)\}$  or  $M = \{(i, j) : i \in [-1, 1], j \in [-1, 1]\}$ , while the domain for the circular moments is  $M = \{(\rho, \phi) : \rho \in [0, +\infty), \phi \in [0, 2\pi)\}$  or  $M = \{(\rho, \phi) : \rho \in [0, 1], \phi \in [0, 2\pi)\}$  (i.e., the unit circle). Rotation invariance of transformation is achieved when

$$X_{ab}(\rho \cos \phi, \rho \sin \phi) = X_{ab}(\rho, \phi) = \Gamma_a(\rho) K_b(\phi) \quad (5.3)$$

with angular basis function  $K_b(\phi) = \exp(jb\phi)$  and radial basis function  $\Gamma_a(\rho)$  could be of any form [58]. Let  $u'$  be the rotated version of the original image  $u$ . When  $X_{ab}$  conforms to the above equation, there must be a function  $J$  such that

$$J(\{u, X_{ab}\}) = J(\{u' | X_{ab}\}) \quad (5.4)$$

which is indicative of rotational invariance. Therefore, the Cartesian moments, such as Legendre moments [37], Gaussian-Hermite moments [61], Gegenbauer moments [62], Chebyshev moments [63], are incompatible for rotation invariance. For the calculation of circular moments, coordinate transformation is required to translate images specified in Cartesian plane to a rotation-compatible plane, while minimizing the associated error.

The preceding theoretical analysis, provides clarity on the superiority of the circular orthogonal moments than other moments for image representation applications.

#### 5.4. ORTHOGONAL MOMENTS

The continuous orthogonal moments along with their respective mathematical expression are given below

##### a. Jacobi Fourier Moments

The kernel of the Jacobi Fourier Moments ( $X_{ab}(\rho, \theta)$ ) is formed using two independent function sets: Deformed Jacobi Polynomial  $J_a(\gamma, \delta, \rho)$  as the radial basis function and Fourier Exponential Factor  $\exp(jb\theta)$  as the angular basis function. The kernel is hence denoted as

$$X_{ab}(\rho, \theta) = J_a(\gamma, \delta, \rho) \exp(jb\theta) \quad (5.5)$$

where  $a, b$  are integers. The kernel function is orthogonal over the unit circle and this condition is expressed as

$$\int_0^{2\pi} \int_0^1 X_{ab}(\rho, \theta) X_{cd}(\rho, \theta) \rho d\rho d\theta = \delta_{ac} \delta_{bd} \quad (5.6)$$

where  $\delta_{ac}, \delta_{bd}$  are Kronecker delta functions and  $\rho = 1$  is the highest object scale. As  $\exp(jb\theta)$  is orthogonal, the radial basis function is also orthogonal in the interval  $[0,1]$

$$\int_0^1 J_a(\rho, \delta, \theta) J_c(\rho, \delta, \theta) \rho d\rho = \delta_{ac}(\delta, \theta) \quad (5.7)$$

Jacobi Polynomial is given by

$$P_a(\gamma, \theta, \rho) = \frac{a!(\theta-1)!}{(\gamma+a-1)!} \sum_{k=0}^a (-1)^k \frac{(\gamma+a+k-1)!}{(a-k)!k!(\theta+k-1)!} \rho^s \quad (5.8)$$

The above Jacobi polynomial is also orthogonal in  $[0,1]$

$$\int_0^1 P_a(\gamma, \theta, \rho) P_b(\gamma, \theta, \rho) f(\gamma, \theta, \rho) d\rho = c_a(\gamma, \theta) \delta_{ab} \quad (5.9)$$

where  $f(\gamma, \theta, \rho)$  is the weight function and  $c_a(\gamma, \theta)$  is the normalization constant given by

$$c_a = \frac{a! [(\gamma-1)^2] (\gamma-\theta+a)!}{(\theta+a-1)! (\gamma+a-1)! (\gamma+2a)} \quad (5.10)$$

The weight function is expressed as

$$f(\gamma, \theta, \rho) = (1-\rho)^{\delta-\theta} \rho^{\theta-1}, \gamma-\theta > -1, \theta > 0, \gamma, \theta \in \mathbb{R} \quad (5.11)$$

Therefore, the radial basis function becomes

$$J_a(\gamma, \delta, \rho) = \sqrt{\frac{f(\gamma, \theta, \rho)}{c_a \rho}} P_a(\gamma, \delta, \rho) \quad (5.12)$$

An image function can be defined as the sum of its weighted orthogonal moments in the polar coordinate system as below

$$I(\rho, \theta) = \sum_{a=0}^{\infty} \sum_{b=-\infty}^{\infty} \psi_{ab} J_a(\rho) e^{jb\theta} \quad (5.13)$$

Here  $\psi_{ab}$  are the decomposition coefficients and are referred to as the Jacobi Fourier Moments

$$\psi_{ab} = \int_0^{2\pi} \int_0^1 I(\rho, \theta) J_a(\gamma, \theta, \rho) e^{-ja\delta} \rho d\rho d\theta \quad (5.14)$$

### b. Pseudo-Jacobi Fourier Moments

For an image  $X(\rho, \phi)$  with order  $a$  and repetition  $b$ , PJFM over a unit circle is expressed as

$$M_{ab} = \int_0^{2\pi} \int_0^1 J_a(\rho) \exp(-jb\phi) X(\rho, \phi) \rho d\rho d\phi \quad (5.15)$$

where  $J_a(\rho)$  is the real valued Pseudo-Jacobi Fourier polynomial and is expressed as

$$J_a(\rho) = \left[ \frac{2(a+2)(\rho-\rho^2)}{(a+3)(a+1)} \right]^{\frac{1}{2}} \sum_{k=0}^n \frac{(-1)^{a+k} (a+k+3)!}{k! (a-k)! (k+2)!} \rho^k \quad (5.16)$$

### c. Zernike Moments

This was first proposed by Frits Zernike, who developed a kernel having group of complex orthogonal Zernike polynomials which are defined inside a unit circle over the polar coordinate space. If  $I(\rho, \phi)$  represents the image in the polar coordinate system,  $a$  is the order and  $b$  is the repetition type

$$Z_{ab} = \frac{a+1}{\pi} \int_0^{2\pi} \int_0^1 I(\rho, \theta) Y_{ab}^*(\rho, \phi) \rho d\rho d\phi \quad (5.17)$$

where  $Y_{ab}$  is given by

$$Y_{ab}(\rho, \phi) = X_{ab}(\rho) e^{jb\phi}, a \geq 0, 0 \leq |b| \leq a, a - |b| = \text{even}, \phi = \arctan\left(\frac{b}{a}\right) \quad (5.18)$$

Radial polynomials are defined below

$$Y_{ab}(\rho) = \sum_0^{\frac{a-|b|}{2}} (-1)^k \frac{(a-k)!}{k! \left(\frac{a+|b|}{2} - k\right)! \left(\frac{a-|b|}{2} - k\right)!} \rho^{a-2k} \quad (5.19)$$

They also satisfy the condition for orthogonality

$$\int_0^1 Y_{ab}(\rho) Y_{a'b'}(\rho) \rho d\rho = \frac{1}{2a+1} \delta'_{aa} \quad (5.20)$$

where  $\delta_{ij}$  is the Kronecker delta function. These polynomials form a complete orthogonal set over the unit circle

$$\int_0^{2\pi} \int_0^1 Y_{ab}(\rho, \phi) Y_{a'b'}^*(\rho, \phi) \rho d\rho d\phi = \frac{\pi}{a+1} \delta'_{aa} \delta'_{bb} \quad (5.21)$$

#### d. Pseudo Zernike Moments

The kernel forms a complete set orthogonal basis function

$$Y_{ab}(\rho, \phi) = X_{ab}(\rho) e^{jb\phi}, a \geq 0, 0 \leq |b| \leq a \quad (5.22)$$

The radial pseudo Zernike polynomial is hence defined as

$$X_{ab}(\rho) = \sum_{s=0}^{a-|b|} \frac{(-1)^s (2a+1-s)! r^{a-s}}{s! (a-|b|+1-s)! (a-|b|-s)!} \quad (5.23)$$

The Pseudo-Zernike Moments are consequently defined as

$$PZ_{ab} = \frac{a+1}{\pi} \int_0^{2\pi} \int_0^1 I(\rho, \phi) Y_{ab}^*(\rho, \phi) \rho d\rho d\phi \quad (5.24)$$

The orthogonality condition matches that of the Zernike polynomials for  $p = p_m$  making the total number of PZMs as  $(1 + p_m)^2$ .

### e. Legendre Moments

They are derived from Legendre polynomials which are orthogonal in the interval of  $[-1, 1]$ . They are defined on Cartesian coordinate system and can acquire near zero values, thus attaining perfect orthogonality and non-redundancy. The absis function is given by

$$\phi_{ab}(i, j) = P_a(i)P_b(j) \quad (5.25)$$

where  $P_a(i)$  is the  $a$ th order of the Legendre polynomial and  $(a + b)$ th is specified as

$$L_{ab} = \frac{(2a+1)(2b+1)}{4} \int_{-1}^1 \int_{-1}^1 P_a(i)P_b(j)I(i, j) didj \quad (5.26)$$

where  $P_a(i)$  si the  $a$ th iorder of the Legendre polynomial and is given by

$$P_a(i) = \frac{1}{2^n} \sum_{k=0}^{\frac{n}{2}} (-1)^k \frac{(2a-2k)!}{k!(a-k)!(a-2k)!} i^{a-2k} \quad (5.27)$$

### f. Gegenbauer Moments

These are ultraspherical polynomials which are orthogonal in the interval  $[-1, 1]$ . For order  $n$  and scaling parameter  $\beta > -0.5$ , the polynnomyials are defined as



$$G_n^\beta(i) = \frac{(2\beta)_n}{n!} \left[ H_{12} \left( -n, 2\beta + 1 + n; \beta + \frac{1}{2}; \frac{1-x}{2} \right) \right] \quad (5.28)$$

where  $H_{12}$  is the hypergeometric term defined as

$$H_{12}(x, y, z, t) = \sum_{k=0}^{\infty} \frac{x_k y_k t^k}{z_k k!} \quad (5.29)$$

$\beta_k$  is the Pochhammer's symbol and is given by

$$\beta_k = \beta(\beta + 1)(\beta + 2) \dots (\beta + k - 1) \quad (5.30)$$

Gegenbauer polynomial is also defined as

$$G_n^\beta(i) = \sum_{k=0}^{\lfloor \frac{n}{2} \rfloor} C_{n,k}^\beta i^{n-2k} \quad (5.31)$$

where the coefficient matrix is computed as

$$C_{n,k}^\beta = (-1)^k \frac{\Gamma(n - k + \beta) 2^{n-2k}}{k! (n - 2k)! \Gamma(\beta)} \quad (5.32)$$

where  $\Gamma(\cdot)$  is gamma function and other symbols mean the usual. Gegenbauer polynomials are orthogonal in the space formed by  $[-1,1]X[-1,1]$ , satisfying the orthogonality property

$$\int_{-1}^1 G_a^\beta(i) G_b^\gamma(i) c^\beta(i) di = C_a(\beta) \delta_{ab} \quad (5.33)$$

With the weight function being denoted by  $c^\beta(i) = (1 - i^2)^{\frac{\beta}{2}}$  and the normalization constant being given by

$$C_a(\beta) = \frac{2\pi\Gamma(a+2\beta)}{2^{2\beta}a!(a+\beta)[\Gamma(\beta)]^2} \quad (5.34)$$

Using the recursive relation, we derive the approximation of the image

$$G_a^\beta(i+1) = \frac{2a+\beta}{a+\beta}iG_a^\beta(i) - \frac{(a+2\beta-1)}{a+1}G_{a-1}^\beta(i) \quad (5.35)$$

where  $G_0^\beta(i) = 1, G_1^\beta(i) = 2\beta i, n \geq 1$ . This helps in expressing the Gegenbauer moments as

$$\Lambda_{a,b} = \frac{1}{C_a(\beta)C_b(\beta)} \int_{-1}^1 \int_{-1}^1 v(n,m) G_a^\beta(n) G_b^\beta(m) c^\beta(n_i) c^\beta(m_j) dndm \quad (5.36)$$

In discrete form, it is re-expressed as

$$\Lambda_{a,b} = \frac{1}{C_a(\beta)C_b(\beta)} \frac{4}{XY} \sum_{i=1}^M \sum_{j=1}^N v(n,m) G_a^\beta(n) G_b^\beta(m) c^\beta(n_i) c^\beta(m_j) v(n_i, m_j) \quad (5.37)$$

### g. Chebyshev Fourier Moments

CFM of order a and repetition b in polar coordinates for image  $X(\rho, \phi)$  are defined inside the unit circle as

$$F_{ab} = \int_0^{2\pi} \int_0^1 C_a(\rho) \exp(-jb\phi) X(\rho, \phi) \rho d\rho d\phi \quad (5.38)$$

where  $C_a(\rho)$  are real valued Chebyshev Fourier Radial Polynomials and are defined as

$$C_a(\rho) = \left[ \frac{64(1-\rho)}{\pi^2 \rho} \right]^{\frac{1}{4}} \sum_{k=0}^{\frac{a+2}{2}} \frac{(-1)^k (a-k)!}{k! (a-2k)!} (4\rho-2)^{n-2k} \quad (5.39)$$

## h. Orthogonal Fourier Mellin Moments

For an order of  $a$  and repetition of  $b$ , the moments are defined as

$$O_{ab} = \frac{1}{2\pi b_a} \int_0^{2a} \int_0^1 X(\rho, \phi) Q_a(\rho) e^{-jb\phi} \rho d\rho d\phi \quad (5.40)$$

where  $Q_a(\rho) = \sum_{k=0}^a \beta_{ak} \rho^k$  and  $\beta_{ak} = (-1)^{a+k} \frac{(a+k+1)!}{(a-k)!k!(k+1)!}$

Here  $p \geq 0, q \in \mathbb{Z}, 0 \leq \rho \leq 1$ , over which the set  $Q_a(\rho)$  is orthogonal.

## i. Laguerre Moments

Formed from the root Laguerre polynomials, they are expressed as follows

For an image function  $X(i, j)$ , if  $l_p^\beta(i)$  is a set of discrete orthogonal polynomials and  $e^{-i} i^\beta$  is the weight function satisfying the following relation

$$\sum_{i=0}^{N-1} e^{-i} i^\beta L_b(i) L_a(i) = r(a, N) \delta_{ab} \quad (5.41)$$

where  $b \geq 0, a \leq N-1$ , then the coefficient moments  $L_{ab}$  are defined as

$$L_{ab} = \frac{1}{r(b, N)r(a, N)} \sum_{i=0}^{N-1} \sum_{j=0}^{N-1} e^{-i} i^\beta L_x(i) L_y(j) X(i, j), \quad (5.42)$$

$$x, y = 0, 1, 2, \dots, N-1$$

$$r(x, N) = \sum_{i=0}^{N-1} e^{-i} i^i L_x(i)^2 \quad (5.43)$$

The Discrete Laguerre polynomials are given by

$$L_p^\beta(i) = \frac{(\beta + 1)_p}{p!} [F_{11}(-p; \beta + 1; i)] \quad (5.44)$$

where  $\beta > -1$  and  $p, i, j = 0, 1, 2, \dots, N - 1$ .  $F_{11}$  is generalized hypergeometric function and is given by

$$F_{11}(\beta, i, j) = 1 + \sum_{\mu=1}^{\infty} \frac{\beta(\beta + 1) \dots (\beta + \mu - 1)}{\gamma(\gamma - 1) \dots (\gamma + \mu - 1) \mu!} \quad (5.45)$$

#### j. Gaussian Hermite Moments

GHM are derived from Hermite polynomials defined in the range  $(-\infty, \infty)$  and have a degree  $p$  are given by

$$H_p = (-1)^p \exp(i^2) \frac{d^p}{dx^p} \exp(-i^2) \quad (5.46)$$

This also satisfies the recursive relation  $H_p(i) = 2iH_{p-1}(i) - 2(p - 1)H_{p-2}(i)$ ,  $H_0(i) = 1$ ,  $H_1(i) = 2i$ . The polynomial is also orthogonal as

$$\int_{-\infty}^{\infty} \exp(-i^2) H_p(i) H_q(i) di = 2^p p! \sqrt{\pi} \delta_{ab} \quad (5.47)$$

where  $\exp(-i^2)$  is the weight function.

It is evident that the Hermite basis function is neither zero nor has a tapered window. To address this shortcoming, Gaussian Hermite functions were proposed.

$$\widehat{H}_p(i) = \frac{1}{\sqrt{2^p p! \sqrt{\pi}}} e^{-\frac{i^2}{2}} H_p(i) \quad (5.48)$$

$$\text{which gives } \int_{-\infty}^{\infty} \widehat{H}_m(i) \widehat{H}_n(i) di = \delta_{mn}$$

Normalized Hermite polynomials with standard deviation of the Gaussian function are given as

$$\widehat{H}_p(i/\sigma) = \frac{1}{\sqrt{2^p p! \sqrt{\pi} \sigma}} e^{-\frac{i^2}{2\sigma^2}} H_p\left(\frac{i}{\sigma}\right) \quad (5.49)$$

These functions have a smooth appearance at the edges and are more resilient against noise. For the image function  $X(i, j)$ , the GHM is defined as

$$G_{a,b} = \int_{-\infty}^{\infty} \int_{-\infty}^{\infty} X(i, j) \widehat{H}_a(i/\sigma) \widehat{H}_b(j/\sigma) didj \quad (5.50)$$

whose basis function of degree  $a + b$  is given by

$$\tau_{a,b}(i, j) = \widehat{H}_a(i/\sigma) \widehat{H}_b(j/\sigma) = \frac{1}{\sqrt{2^{(a+b-1)} a! b!}} G(i, j, \sigma) H_a\left(\frac{i}{\sigma}\right) H_b\left(\frac{j}{\sigma}\right) \quad (5.51)$$

### k. Continuous Hahn Moments

These are derived from Hahn polynomials defined as below

$$P_p(i, \gamma, \delta) = j^p \left[ F_{32} \left( \begin{matrix} -p, p + 2\gamma + 2\delta - 1, \delta - ji; 1 \\ \gamma + \delta; 2\delta \end{matrix} \right) \right] \quad (5.52)$$

These polynomials are orthogonal wrt positive absolutely continuous weight function which is given by

$$K(i) = (|\Gamma(\gamma + ji)\Gamma(\delta + ji)|)^2, -\infty < i < \infty, \gamma, \delta > 0 \text{ or } \gamma = \bar{\delta} \text{ and } \text{Re}(\gamma) > 0 \quad (5.53)$$

## 5.5. FRACTIONAL ORDER EXPONENTIAL (ORTHOGONAL) MOMENTS

Exponential moments are circularly orthogonal moments [63] and are expressed as below

$$C_{mn} = \frac{1}{4\pi} \int_0^{2\pi} \int_0^1 g(\rho, \phi) [T_{mn}(\rho, \phi)]^* \rho d\rho d\phi \quad (5.54)$$

where  $m$  and  $n$  are order and repetition respectively and exist in the range  $m, n \in \mathbb{Z}$ . The exponent basis function is defined as  $T_{mn}^\beta(\rho, \phi) = E_m(\rho) e^{-mj\phi}$  with  $E_m(\rho) = \sqrt{\frac{2}{\rho}} e^{-j2\pi m\rho}$ . The exponential basis function is defined in the region where  $\rho \in [0, 1], \phi \in [0, 2\pi]$ .

In terms of fractional variable  $\beta$ , it is expressed as  $B_{mn}^\beta = E_m(\rho, \beta) e^{-jm\phi}$ . Here, the radial basis function is expanded as  $E_m(\rho, \beta) = \rho^{\beta-1} \sqrt{\frac{2}{\rho^\beta}} e^{-j2\pi m\rho^\beta}$ . When compared to the quaternion technique [64], the multi-channel approach is found to be superior, hence the expressions for input color image for different color channels are given by  $f_R(\rho, \phi)$ ,  $f_G(\rho, \phi)$ , and  $f_B(\rho, \phi)$ .

The fractional order moments for these channels, denoted by  $C$ , are consequently computed as

$$FrC_{mn} = \frac{\beta}{4\pi} \int_0^{2\pi} \int_0^1 f_C(\rho, \phi) \rho^{\beta-1} \sqrt{\frac{2}{\rho^\beta}} e^{-j2\pi m \rho^\beta} e^{-jn\phi} \rho d\rho d\phi \quad (5.55)$$

The reconstruction is undertaken as follows

$$f_C^{recon}(\rho, \phi) = \sum_{m=-\infty}^{\infty} \sum_{n=-\infty}^{\infty} FrC_{mn}(f_C) T_{mn}^\beta(\rho, \phi) \quad (5.56)$$

$$\approx \sum_{m=-m_{\max}}^{m_{\max}} \sum_{n=-n_{\max}}^{n_{\max}} FrC_{mn}(f_C) T_{mn}^\beta(\rho, \phi) \quad (5.57)$$

## 5.6. RESISTANCE TO GEOMETRIC TRANSFORMATIONS

### 5.6.1. INVARIANCE TO ROTATION

The original color image  $f_C(\rho, \phi)$  when rotated by an angle  $\theta$  is expressed in terms of the original color image as below

$$f_C^\theta(\rho, \phi) = f_C(\rho, \phi - \theta) \quad (5.56)$$

The FrGPCET of  $f_C^\theta(\rho, \phi)$  is given by

$$\begin{aligned} FrC_{mn}(f_C^\theta) &= \frac{\beta}{4\pi} \int_0^{2\pi} \int_0^1 f_C^\theta(\rho, \phi) [T_{mn}(\rho, \phi)]^* \rho d\rho d\phi \end{aligned} \quad (5.57)$$

$$= \frac{\beta}{4\pi} \int_0^{2\pi} \int_0^1 f_C(\rho, \phi - \theta) E_m(\rho) e^{-mj\phi} \rho d\rho d\phi \quad (5.58)$$

$$= \frac{\beta}{4\pi} \int_0^{2\pi} \int_0^1 f_C^\theta(\rho, \phi) E_m(\rho) e^{-mj(\phi+\theta)} \rho d\rho d\phi \quad (5.59)$$

$$= \frac{\beta}{4\pi} \int_0^{2\pi} \int_0^1 f_C^\theta(\rho, \phi) E_m(\rho) e^{-mj\phi} e^{-mj\theta} \rho d\rho d\phi \quad (5.60)$$

$$= FrC_{mn}(f_C^\theta) e^{-mj\theta} = FrC_{mn}(f_C) e^{-mj\theta}; \mathcal{C} \quad (5.61)$$

$$\in \{R, G, B\}$$

Here,  $FrC_{mn}(f_C^\theta)$  and  $FrC_{mn}(f_C)$  represent the FrGPCET of  $f_C^\theta$  and  $f_C$ , respectively.

Also, since  $|e^{-mj\theta}|$ ,

$$|FrC_{mn}(f_C^\theta(\rho, \phi))| = |FrC_{mn}(f_C(\rho, \phi))| \quad (5.62)$$

which proves the rotational invariance.

### 5.6.2. INVARIANCE TO SCALING

A polar transform is said to be scaling invariant as scaling in the Cartesian system of coordinates is equivalent to variation of the radius vector of the pixel in the circular plane, without change in angle. Since we compute the moments in the polar coordinate system, they are resilient against scaling of the coordinates.



### 5.6.3. INVARIANCE TO TRANSLATION

For translational invariance, the origin of the coordinate system must be shifted to the centroid of the image  $(x', y')$ . Using the definition of geometric moments to calculate the image centroid, we have

$$x' = \frac{(\mu_{10}(f_R) + \mu_{10}(f_G) + \mu_{10}(f_B))}{\mu_{00}} \quad (5.63)$$

$$y' = \frac{(\mu_{01}(f_R) + \mu_{01}(f_G) + \mu_{01}(f_B))}{\mu_{00}} \quad (5.64)$$

$$\mu_{00} = (\mu_{00}(f_R) + \mu_{00}(f_G) + \mu_{00}(f_B)) \quad (5.65)$$

The revised FrGPCET for this coordinate system can be expressed as

$$\overline{FrC_{mn}} = \frac{\beta}{4\pi} \int_0^{2\pi} \int_0^1 f_C(\bar{\rho}, \bar{\phi}) [T_{mn}(\bar{\rho}, \bar{\phi})]^* \bar{\rho} d\bar{\rho} d\bar{\phi} \quad (5.66)$$

$$= \frac{\beta}{4\pi} \int_0^{2\pi} \int_0^1 f_C(\bar{\rho}, \bar{\phi}) E_m(\rho) e^{-mj\phi} \bar{\rho} d\bar{\rho} d\bar{\phi} \quad (5.67)$$

The pixel mapping from Cartesian to Polar coordinate system can be visualized through Fig. 1. Here, a section of the plan is being mapped to an annular region in the polar coordinate system, with the AD and BC edges of the section forming the radii on either side and the interconnecting edge CD transforming to the circular arc in the circular coordinate system. The shaded pixel also shows the corresponding location in the polar coordinate plane.

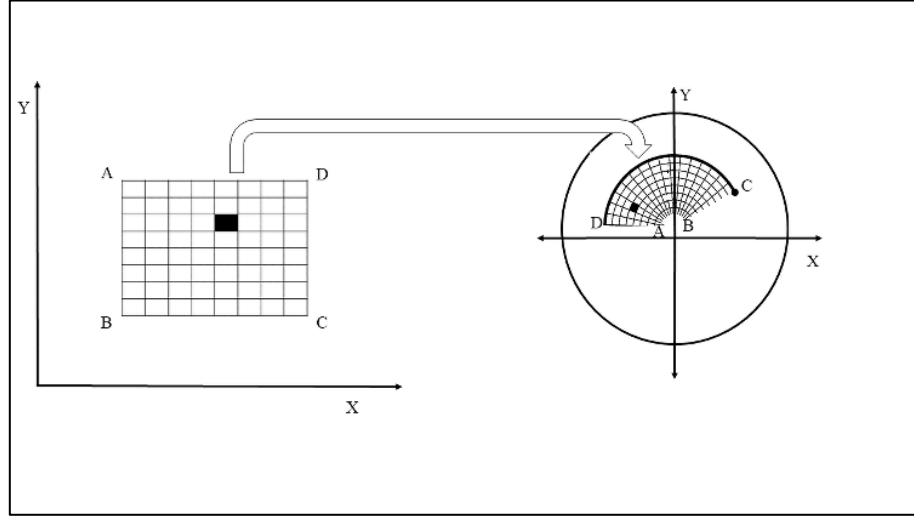


Figure 5.1 Mapping from Cartesian to Polar coordinate system

## 5.7. ACCURATE CALCULATION OF ORTHOGONAL MOMENTS

Accurate moment computation is essential as geometrical aberrations and pixel distortions are introduced during watermarking which diminish the robustness. Here, we leverage the scheme proposed in [65,66] for an exact definition of the FrGPCETs.

$$FrGPCET_{mn} = \frac{\beta}{4\pi} \sum_p \sum_q K_{mn}(\rho_p, \phi_{pq}) \hat{f}_C(\rho_p, \phi_{p,q}) \quad (5.68)$$

where  $K_{mn}(\rho_p, \phi_{pq}) = \Lambda_m(\rho_p) \mathbb{J}_n(\phi_{pq})$ . Further, in accordance with conclusions drawn in [67], computational accuracy is improved using seventh order interpolator to obtain the interpolated color image,  $\hat{f}_C(\rho_p, \phi_{p,q})$ , whose radial and angular kernels are given by

$$\mathbb{J}_n(\phi_{pq}) = \int_{\mathbb{V}_{pq}}^{\mathbb{V}_{p,q+1}} e^{-jn\phi} d\phi \quad (5.69)$$

$$\Lambda_m(\rho_p) = \int_{\mathbb{U}_p}^{\mathbb{U}_{p+1}} T_m(\beta, \rho) \rho d\rho = \int_{\mathbb{U}_p}^{\mathbb{U}_{p+1}} P(\rho) d\rho \quad (5.70)$$

with  $P(\rho) = T_m(\beta, \rho)\rho$ . The limits are expressed as below

$$\mathbb{V}_{p,q+1} = \phi_{p,q} + \frac{\Delta\phi_{p,q}}{2}; \mathbb{V}_{p,q} = \phi_{p,q} - \frac{\Delta\phi_{p,q}}{2} \quad (5.71)$$

$$\mathbb{U}_{p+1} = P_p + \frac{\Delta P_p}{2}; \mathbb{U}_p = P_p - \frac{\Delta P_p}{2} \quad (5.72)$$

Using Calculus,  $\mathbb{J}_n(\phi_{p,q})$  is calculated in the exact form as follows

$$\mathbb{J}_n(\phi_{p,q}) = \left\{ \begin{array}{l} \frac{j}{n} (e^{-n\mathbb{J}\mathbb{V}_{p,q+1}} - e^{-n\mathbb{J}\mathbb{V}_{p,q}}), n \neq 0 \\ \mathbb{V}_{p,q+1} - \mathbb{V}_{p,q}, n = 0 \end{array} \right\} \quad (5.73)$$

Computation of  $\Lambda_m(\rho_p)$  is done using Gaussian Quadrature Numerical Integration in conjunction with orthogonal Legendre polynomials for the calculation of the nodes and coefficients [68,69].

$$\Lambda_m(\rho_p) = \int_{\mathbb{U}_p}^{\mathbb{U}_{p+1}} P(\rho) d\rho \approx \frac{(\mathbb{U}_{p+1} - \mathbb{U}_p)}{2} \sum_{k=0}^{q-1} \omega_k \quad (5.74)$$

$$* P\left(\frac{(\mathbb{U}_{p+1} + \mathbb{U}_p)}{2} + \frac{(\mathbb{U}_{p+1} - \mathbb{U}_p)}{2} \tau_k\right)$$

The weights and positions of the sampling locations are  $\omega_k$  &  $\tau_k, k = 0, 1, 2, \dots, q-1$  and the numerical integration is characterized by the order  $q$ . The values of  $\omega_k$  are constant and  $\sum_{k=0}^{q-1} \omega_k = 2$ . Further,  $\tau_k$  can be defined using  $\mathbb{U}_{p+1}$  &  $\mathbb{U}_p$ . The integral can also be expressed as

$$\Lambda_m(\rho_p) = \int_{\mathbb{U}_p}^{\mathbb{U}_{p+1}} P(\rho) d\rho \approx \frac{(\mathbb{U}_{p+1} - \mathbb{U}_p)}{2} \sum_{k=1}^q \omega_k \quad (5.75)$$

$$* P\left(\frac{(\mathbb{U}_{p+1} + \mathbb{U}_p)}{2} + \frac{(\mathbb{U}_{p+1} - \mathbb{U}_p)}{2} \tau_k\right)$$

For a 2-dimensional function  $P(\rho, \phi)$ , the above relation can be extrapolated to

$$\int_{\mathbb{U}_p}^{\mathbb{U}_{p+1}} \int_{\mathbb{V}_q}^{\mathbb{V}_{q+1}} P(\rho) \Phi(\phi) \rho d\rho d\phi \approx \frac{(\mathbb{U}_{p+1} - \mathbb{U}_p)(\mathbb{V}_{q+1} - \mathbb{V}_q)}{4} \sum_{k=0}^{q-1} \sum_{h=0}^{q-1} \omega_h \omega_k \quad (5.76)$$

$$* \left( P\left(\frac{(\mathbb{U}_{p+1} + \mathbb{U}_p)}{2} + \frac{(\mathbb{U}_{p+1} - \mathbb{U}_p)}{2} \tau_k\right) \right.$$

$$\left. + \Phi\left(\frac{(\mathbb{V}_{q+1} + \mathbb{V}_q)}{2} + \frac{(\mathbb{V}_{q+1} - \mathbb{V}_q)}{2} \tau_h\right) \right)$$

Using the above derivation, the FrGPCET can be accurately calculated.

## 5.8. DITHER MODULATION

We adopt dither modulation for the modification of orthogonal moments. Dither modulation is a special form of quantization index modulation, which was first proposed for data hiding in [70]. With a given base quantizer, the dither modulation function is defined as

$$g_{DM}(y, n) = p(y - \delta(n)) + \delta(n) \quad (5.77)$$

where  $y$  is a scalar variable to be quantized,  $n$  is a message symbol to be embedded in  $y$ , and  $\delta(n)$  is the dither scalar linked to  $n$ . In dither modulation, the quantization units and reconstruction locations of any given quantizer are the shifted versions of these modules of any other quantizer. This enhances the ease of implementation of the dither modulation quantizer. Here, we use binary dither modulation i.e.  $n \in \{0,1\}$ . The base quantizer is a uniform scalar of the type

$$p(y) = \left\lfloor \frac{y}{T} \right\rfloor T \quad (5.78)$$

where  $[\cdot]$  denotes the rounding operation and  $T$  is the quantization step-size.

Assume the watermark  $\Omega$  bit sequence as  $b = (q_1, \dots, q_k), K \leq |\mathcal{X}|$  and  $b_i \in \{0, 1\}$ , to be embedded in an image  $I$ . Moment vector  $\mathbb{M} = (\widehat{\mathbb{M}}_{a_1 b_1}, \dots, \widehat{\mathbb{M}}_{a_K b_K}), \widehat{\mathbb{M}}_{a_i b_i} \in \mathcal{X}$  is securely formed by pseudo-random selection of  $K$  number of moments from  $\mathcal{X}$ . Now, the magnitudes of the moments  $\widehat{\mathbb{M}}_{a_i b_i}, i = 1, \dots, K$  are quantized to form a new vector  $\widetilde{\mathbb{M}} = (\widetilde{\mathbb{M}}_{a_1 b_1}, \dots, \widetilde{\mathbb{M}}_{a_K b_K})$ :

$$|\widetilde{\mathbb{M}}_{a_i b_i}| = \left\lceil \frac{\widehat{\mathbb{M}}_{a_i b_i} - \vartheta_i b_i}{\Delta} \right\rceil \Delta + \vartheta_i(b_i) \quad (5.79)$$

whose dither function,  $\vartheta_i(\cdot)$  is satisfies  $\vartheta_i(1) = \frac{\Delta}{2} + \vartheta_i(0)$ . The constituents of the  $K$ -dimensional dither vector  $(\vartheta_1(0), \dots, \vartheta_K(0))$  are pseudo-randomly generated with another key  $K_2$  and uniformly dispersed over  $[0, \Delta]$ . This enhances the security of the embedded information. The modified orthogonal moments can also be calculated as

$$\widetilde{\mathbb{M}}_{a_i b_i} = \frac{|\widetilde{\mathbb{M}}_{a_i b_i}|}{|\widehat{\mathbb{M}}_{a_i b_i}|} \widehat{\mathbb{M}}_{a_i b_i}, i = 1, 2, \dots, K \quad (5.80)$$

with  $\xi = \widetilde{\mathbb{M}}_{a_i b_i} - \widehat{\mathbb{M}}_{a_i b_i}$ . During quantization, if  $b_i \neq 0$ , the conjugate moment of  $\widehat{\mathbb{M}}_{a_i b_i}$  is quantized, thus warranting similarity in magnitude for generating a real image.

The quantization step size  $\Delta$  is adjusted so as to establish a tradeoff between the watermark's robustness and imperceptibility. An increase in  $\Delta$  improves robustness, but reduces imperceptibility. The converse, is also true. During implementation, the value of  $\Delta$  depends on the quality of the watermarked image required. A metric to quantify the same is the peak signal to noise ratio (PSNR) which is expressed as

$$PSNR(I, \tilde{I}) = 10 \log_{10} \frac{255^2}{\mu_e^2} \quad (5.81)$$

where  $I$  is the original image and  $\tilde{I}$  is its watermarked version. The average square error is given by

$$\mu_e^2 = \frac{1}{K^2} \sum_{i=1}^K \sum_{j=1}^K [\tilde{I}(x_i, y_j) - I(x_i, y_j)]^2 \quad (5.82)$$

## 5.9. HUFFMAN CODING

David Huffman proposed the algorithm for determining minimum cost prefix-free codes in 1951 [71]. The technique deploying such coding schemes came to be known as Huffman coding. The problem statement of minimal redundancy may be formulated as follows: A source alphabet of  $s$  distinct symbols is given, together with a set of symbol weights characterized as  $Y = \langle \gamma_i > 0 | 0 \leq i < s \rangle$ . The weights comprise of real numbers arranged in a non-increasing series.

A binary symbol is generated and designated as the output alphabet. The code is formed by a set of  $s$  positive integers  $X = \langle \chi_i > 0 | 0 \leq i < s \rangle$ , under the assumption that  $i$ th symbol in the source alphabet will be assigned a unique fixed code word of length  $\tau_i$ . Feasibility of the code  $X = \langle \chi_i \rangle$  is confirmed if it satisfies the Kraft Inequality

$$\kappa(X) = \sum_{p=0}^{s-1} 2^{-\chi_p} \leq 1 \quad (5.83)$$

Given the feasibility, a code word of length  $\chi_i$  may be assigned to each symbol in an independent manner, such that no code word is a pre-fix of another code word. This leads to the formation of the “prefix free code.” The cost of a feasible code, denoted  $q(\cdot, \cdot)$ , is linked to the weight associated with each symbol,

$$q(Y, X) = q(\langle \gamma_i \rangle, \langle \chi_i \rangle) = \sum_{i=0}^{s-1} \gamma_i \chi_i \quad (5.84)$$

If the frequency of the symbol  $\gamma_i$  where  $\gamma_i \in \mathbb{Z}$ , then  $\varrho(\cdot, \cdot)$  gives the total number of channel symbols required for transmission. On the other hand, if  $\gamma_i$ 's are symbol occurrence probabilities, then  $\varrho(\cdot, \cdot)$  is the mean per-symbol cost of employing the code as per the probabilities  $\Omega = \langle \omega_i \rangle$ .

Let  $X = \langle \chi_i > 0 | 0 \leq i < s \rangle$  be a viable code. Then  $X$  is a minimum-redundancy code for  $\Upsilon$  if, for every other similar symbol code  $X'$ ,  $\varrho(\Upsilon, X) \leq \varrho(\Upsilon, X')$ . For any sequence  $\Upsilon$  there may exist multiple same least cost minimum-redundancy codes.

It is clear that Huffman code will serve as a minimum redundancy pre-fix code for the purpose of watermarking and thus will be instrumental in enhancing the effective payload capacity of the watermark.

## CHAPTER 6

### IMAGE WATERMARKING USING GRAPH SIGNAL PROCESSING AND LOCAL DOMINANT FEATURES

#### 6.1. GRAPH SIGNAL PROCESSING

A digital image may be represented as a graph where each pixel is treated as vertex and is connected to every other pixel in the image. The gray value of the pixel in the image corresponds to a signal  $T$  in the graphical depiction of an image [13, 14, 72]. Here, we describe the graph as  $\Gamma = (Y, E, \Omega)$ , where  $\Gamma$  is a set of vertices/pixels and  $|v| = N$ . The nodes are interconnected through weighted edges  $E = \{\epsilon_{ij} : v_i, v_j \in Y\}$ .  $\Omega$  comprises of weights  $\omega_{ij}$  of an edge linking vertices  $v_i$  and  $v_j$ . The gray level  $x_i$  is the  $i$ th element of the graph signal  $T$  on vertex  $v_i$ . More details can be found in [13, 16]. The graph is generally shown using adjacency matrix  $M$  where each item is given by  $\omega_{ij}$ , which is the weight of an edge joining the particular set of vertices. The Gaussian weight can be derived from the pixel values using Eq. (6.1). We call a matrix  $\Delta$  as degree matrix if each degree  $\delta_i$  is the addition of all the edges linked to vertex  $v_i$ . On application of the difference operator on graph signal  $T$ , we obtain the Laplacian as shown in Eq. (6.2) and its graph is as defined by Eq. (6.3) [73,74,75].

$$\Omega_{ij} = \begin{cases} e^{-\frac{|x_i - x_j|^2}{\beta}}, & \text{if } |x_i - x_j| < \varepsilon \\ 0, & \text{otherwise} \end{cases} \quad (6.1)$$

Here,  $\beta$  is determined empirically.

$$\Delta x_i = \sum_{v_j: \epsilon_{ij} \in E} \Omega_{ij} [x_i - x_j] \quad (6.2)$$



$$\Lambda = \Delta - \Omega \quad (6.3)$$

where  $\Lambda$  is a partially definite symmetric matrix formed by a discrete set of  $E$  non-negative Eigen values.

## 6.2. SPECTRAL GRAPH WAVELET

We derive the equation for the spectral graph wavelet using the Eigen vectors  $H_k$  of the Laplacian graph formed using  $\Lambda$ . Defining the spectral graph wavelet

$$\chi_{h,n}(m) = \sum_{k=0}^{N-1} \rho(h\mu_k) H_k(n) H_k(m) \quad (6.4)$$

Here, kernel  $\rho$  is a wavelet generating function, at a scale  $h$  and vertex  $n$ .

In our analysis, we employ inter-sine function for the generation of the wavelet and stipulating the scaling function, as required in the Fourier domain. Further, the low frequency of the graph signal is expressed as

$$\rho(\mu) = \begin{cases} \sin\left(\frac{\pi}{2}v\left(\frac{1}{\mu_1}|\mu| - 1\right)\right), & \text{if } \mu_1 \leq \mu < \mu_2 \\ \cos\left(\frac{\pi}{2}v\left(\frac{1}{\mu_2}|\mu| - 1\right)\right), & \text{if } \mu_2 \leq \mu < \mu_3 \\ 0, & \text{otherwise} \end{cases} \quad (6.5)$$

$$\sigma(\mu) = \begin{cases} 1, & \text{if } \mu_1 < \mu \\ \cos\left(\frac{\pi}{2}v\left(\frac{1}{\mu_1}|\mu| - 1\right)\right), & \text{if } \mu_1 \leq \mu < \mu_2 \\ 0, & \text{otherwise} \end{cases} \quad (6.6)$$

$$\vartheta_n(m) = \sum_{k=0}^{N-1} \sigma(h\mu_k) H_k(n) H_k(m) \quad (6.7)$$

where  $(f) = f^4(35 - 84f + 70f^2 - 20f^3)$ ;  $\mu_1 = \frac{2}{3}$ ,  $\mu_2 = 2\mu_1$  and  $\mu_3 = 4\mu_1$ .

### 6.3. VARIATIONAL MODE DECOMPOSITION (VMD)

As a decomposition tool, VMD disintegrates a signal into a discrete set of constituent modes designated as the Intrinsic Mode Function (IMF). These modes are extracted using an optimal iterative approach known as the Alternate Direction Method of Multipliers (ADMM). Each IMF is characterized by in a narrow frequency band, located around a central frequency and having its characteristic center frequencies. These modes are known to offer restricted spatial information. However, they have well defined directional and oscillatory characteristics. Decomposition into the modes brings in the advantage of having continuous variation in the local frequency and amplitudes of the modes. Further, perfect reconstruction is possible using a simple ensemble operation.

The IMF is expressed as the product of slowly varying Amplitude Modulated (AM) function and quickly changing Frequency Modulated (FM) function. Mathematically, it is represented as

$$x_k = \min_{x_k, y_k} \left\{ \sum_k \left\| \left( \left( \delta(t) + \frac{j}{\pi t} \right) x_k(t) \right) e^{-jy_k t} \right\|^2 \right\} \quad (6.8)$$

$$\text{and s. t. } \sum_k x_k = f$$

Here  $f$  is the original signal,  $x$  is the mode,  $k$  represents the number of modes and  $y$  corresponds to the center frequency of the signal.

Extending the concept of 1-D VMD to two dimensions, the VMD operation may be deployed for the degeneration of 2-D matrices (images) into their constituent, bandwidth dependent modes. To undertake the mode extraction in the 2-D case, a special extension of the 1D analytic signal for 2D is used [76]. Considering single sided Fourier spectra, we translate the image frequencies to baseband through heterodyne demodulation. The analytical signal pertaining to the 2-D data is obtained by co-originating the half plane of the center frequency. It is then defined as

$$s. t. \sum_k \hat{x}_{AD,k}(\vec{y}) = \begin{cases} 2\bar{x}_k(\vec{y}), & \text{if } \vec{y}, \bar{y}_k > 0 \\ \bar{x}_k(\vec{y}), & \text{if } \vec{y}, \bar{y}_k = 0 \\ 0, & \text{otherwise} \end{cases} \quad (6.9)$$

Using the principle of constrained mixing and heterodyne modulation, the above equation may be re-expressed as

$$x_{AS,k}(\vec{l}) = x_k(\vec{l}) \left( \delta(\langle \vec{l}, \bar{y}_k \rangle) + \frac{j}{\Pi \langle \vec{l}, \bar{y}_k \rangle} \right) \delta(\langle \vec{l}, \bar{y}_k \rangle) \quad (6.10)$$

Then, the constrained variational mode problem, which is later subjected to optimization, is given by

$$x_k = \min_{x_k, y_k} \left\{ \sum_k \left| |(\nabla[x_{AS,k}(\vec{l})])e^{-j\langle \vec{l}, \bar{y}_k \rangle}| \right|^2 \right\} \quad (6.11)$$

and  $s. t. \sum_k x_k = f$

#### 6.4. LOCAL DOMINANT ORIENTATION FEATURE EXTRACTION (LDOF)

Through the principal component analysis (PCA) based technique of estimation of the local gradient orientation [77], we develop a set of optimal basis vectors to represent the given data and results in the form of minimum mean-square approximation error. PCA is calculated through the Eigen value decomposition of the data covariance matrix or singular value decomposition (SVD) of the data matrix. We choose the SVD approach for our implementation. Specifically, the gradient matrix over a PXP window  $\delta_i$  around the interesting point  $g(x, y)$  of an image is defined as

$$\mathbb{H} = \begin{pmatrix} \dots & \dots \\ \dots & \dots \\ h_x(k) & h_y(k) \\ \dots & \dots \\ \dots & \dots \end{pmatrix}, k \in \delta_i \quad (6.12)$$

where  $h_x(k)$  and  $h_y(k)$  represent the image gradient at point  $(x_k, y_k)$ . The covariance matrix of gradient vectors of points in the window  $\delta_i$  is given by

$$\mathbb{C} = \mathbb{H}^T \mathbb{H} = \begin{bmatrix} \left( \sum_{k \in \delta_i} h_x(k) h_x(k) \right) & \left( \sum_{k \in \delta_i} h_x(k) h_y(k) \right) \\ \left( \sum_{k \in \delta_i} h_y(k) h_x(k) \right) & \left( \sum_{k \in \delta_i} h_y(k) h_y(k) \right) \end{bmatrix} \quad (6.13)$$

Relevant local information can be obtained directly from  $\mathbb{H}$ . The local dominant orientation is calculated from the Singular Value Decomposition of  $\mathbb{H}$ .

$$\mathbb{H} = \mathbb{U} \mathbb{S} \mathbb{V}^T \quad (6.14)$$

where  $\mathbb{U}$  is a pX2 matrix, and  $\mathbb{V}$  is a 2X2 matrix. Further, the column vectors are orthogonal for each matrix.  $\mathbb{S}$  is a diagonal 2X2 singular value matrix which reflects the

energy in the dominant orientation and its perpendicular direction; the first column vector of matrix.  $\mathbb{V}$  ascribes to the dominant orientation of the local gradient field. More details on the subject can be found at [78,79].

We begin with the calculation of local dominant features by performing the SVD of the matrix formed via all gradient vectors in the local patch (overlapped). This is achieved by first calculating the gradient of the entire image and the finding its SVD.  $\mathbb{H}_i$  represents the gradient vector matrix for the  $i$ th local patch. It follows that  $\mathbb{H}_i = \mathbb{U}_i \mathbb{S}_i \mathbb{V}_i^T = \mathbb{U}_i \text{diag}[s_1 \ s_2][v_1 \ v_2]^T$ , where  $v_1 = [v_{1,1}, v_{1,2}]$  is the dominant orientation of the local gradient field, whose angle is defined as

$$\phi_i = \tan^{-1} \left( \frac{v_{1,1}}{v_{1,2}} \right) \quad (6.15)$$

The relative energy  $\xi_i$  of the dominant orientation, in terms of the singular values  $s_1$  and  $s_2$  is given by

$$\xi_i = \frac{s_1 + \theta}{s_2 + \theta}, \theta \geq 0 \quad (6.16)$$

where  $\theta$  is the regularization parameter introduced to restrain the effect of noise and preventing the denominator from falling to zero. Cumulatively, the resulting matrix  $\Theta = [(\theta_1, \xi_1), (\theta_2, \xi_2), \dots, (\theta_N, \xi_n)]^T$  contains the local dominant feature information of the image, where  $N$  is the number of pixels in the image.

## CHAPTER 7

### PROPOSED METHODOLOGY FOR AUDIO AND IMAGE WATERMARKING

The schemes for watermarking of the audio signal and image data in transform domain have been divided into two parts, namely that of watermark embedding and watermark detection. The steps under these, along with relevant assumptions and requisite parameter values, have been sequentially presented below.

#### 7.1. AUDIO WATERMARKING

##### 7.1.1. WATERMARK EMBEDDING STAGE

a. N-dimensional DLCT of audio signal is calculated using eq. 3.13 and 3.14 for a pre-defined set of LCT matrix parameters and the coefficients thus obtained are reordered in decreasing (non-monotonic) series. Let the transform coefficients be represented by  $K_i = L_i + jM_i, |K_i| < |K_{i+1}|, i = 1, 2, \dots, N$

b. The watermark is formed by a set of K complex numbers [80], represented as  $k_i = l_i + jm_i, i = 1, 2, \dots, K$ . The real and imaginary parts of the complex numbers are generated from a normal distribution with zero mean and  $\frac{\sigma^2}{2}$  variance.

c. The middle coefficients are chosen from the re-ordered sequence obtained in a, and clustered together for embedding the watermark. Denoting the location of middle coefficient as  $N_{median}$ , we mark the DLCT coefficients  $K_i$  in the range  $i = N_{median} + 1, N_{median} + 2, \dots, N_{median} + K$  for watermarking. It should be noted at this juncture that selection of the lower order coefficients for watermarking would have rendered the scheme vulnerable to de-noising and signal compression procedures. Further, embedding the

watermark in the higher order coefficients would have compromised the imperceptibility of the watermarking scheme.

d. Based on the principles of direct modulation, the watermark is embedded in the manner

$$K_i^w = K_i + l_i|L_i| + jm_i|M_i|, i = N_{median} + 1, \dots, N_{median} + K \quad (7.1)$$

e. Selective substitution of the DLCT coefficients obtained in d in the series obtained in a.

f. Re-ordering of DLCT coefficients in adherence with the originally computed DLCT in a.

g. Inverse of the LCT matrix used for calculation of DLCT in a is computed, which in turn is used for the computation of IDLCT of the re-ordered watermarked transform coefficients obtained in f using eq. 3.13 and 3.14, thus yielding the watermarked audio signal.

The above steps have been summarized in the flowchart below.

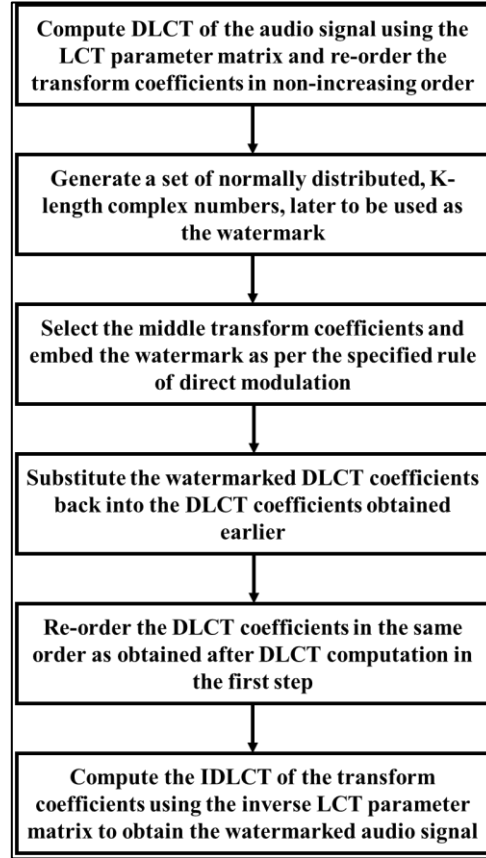


Figure 7.1 Watermark Embedding Process

### 7.1.2. WATERMARK DETECTION STAGE

The watermark detection is primarily based on the principle of detection of the originally embedded watermark in the audio signal, which may have been subjected to different signal processing and feature distortive attacks, from amongst a large set of random watermarks. This involves the calculation of detection parameter, which is used to detect and differentiate the originally embedded watermark. The value of the detection parameter is computed as follows

$$\eta = \sum_{j=N_{median}+1}^{N_{median}+K} (l_i - jm_i)K_i^{attack} \quad (7.2)$$



where  $K_i^{attack}$  comprises of the DLCT transform coefficients used for watermarking. The expectation of  $\eta$  is given by

$$E[\eta] = \frac{\sigma^2}{2} \sum_{j=N_{median}+1}^{N_{median}+K} (|L_i| + |M_i|) \quad (7.3)$$

As is evident from above, there is a requirement of placing a threshold limit on the detection parameter value which will establish a demarcation level for successful detection of the originally embedded watermark. In the absence of such a threshold, there exists a probability of false detection. Initially, it was proposed that the threshold be set as  $\frac{E[\eta]}{2}$ . However, due to the fixed threshold, false positives were reported in the watermark detection process. Using the dynamic scheme proposed in [80], we find the threshold limit for detection parameter, by computation of  $\eta$  for multiple random watermarks and then calculating mean (say  $\rho$ ) and standard deviation (say  $\phi$ ) of the cumulative set of detection parameters thus obtained and setting the threshold as  $\omega = \rho + c\phi$ , where  $c$  is either chosen empirically or selected over the course of numerous experimentations.

The watermark detection methodology, based on the above discussion, is given below

- a. DLCT computation of the received audio signal using eq. 3.13 and 3.14 with the LCT parameters used during embedding.
- b. DLCT coefficient re-arrangement in decreasing(non-monotonic) order and identification of modified transform coefficients  $K_i^{attack}$ .
- c. Creation of a large repository of random watermark sequences (say 1000), using the technique provided in the embedding stage, step b. This also includes the originally embedded watermark.
- d. Calculation of the detection parameter  $\eta$ , using eq. 7.2 for the entire set of watermarks.
- e. Detection parameter threshold calculation as provided for in the entry of this section.

f. Watermark detection using comparison of detection parameter with those obtained in step e.

The above steps have been summarized in the flow chart below.

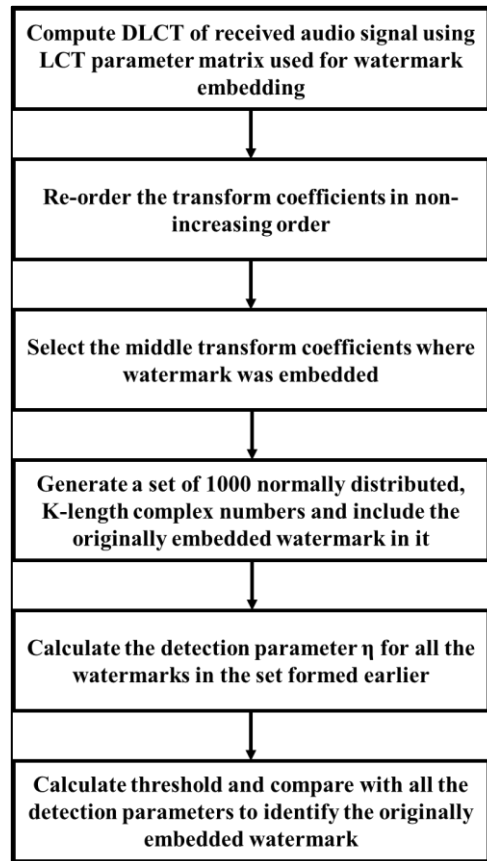


*Figure 7.2 Watermark Detection Process*

## 7.2. IMAGE WATERMARKING IN FREQUENCY DOMAIN

The proposed method is applicable only to equi-dimensional images. Unequal sized images, must undergo suitable resizing as a pre-processing step to watermarking.

### A. Diagonal Image Partitioning

a. The cover image is deconstructed into two sub-images, each consisting of non-zero elements along mutually opposite diagonals. Further, the length and breadth of the images should be marked in even number of pixels.

Suppose a normalized 4X4 grayscale image be represented by

$$X = \begin{pmatrix} 0.63 & 0.65 & 0.69 & 0.62 \\ 0.62 & 0.65 & 0.67 & 0.61 \\ 0.71 & 0.75 & 0.77 & 0.79 \\ 0.69 & 0.70 & 0.76 & 0.78 \end{pmatrix} \quad (7.4)$$

Considering the first image partition along the  $-45^\circ$  diagonal

$$Y = \begin{pmatrix} 0.63 & 0 & 0.69 & 0 \\ 0 & 0.65 & 0 & 0.61 \\ 0.71 & 0 & 0.77 & 0 \\ 0 & 0.70 & 0 & 0.78 \end{pmatrix} \quad (7.5)$$

The second image partition along the  $45^\circ$  diagonal

$$Z = \begin{pmatrix} 0 & 0.65 & 0 & 0.62 \\ 0.62 & 0 & 0.67 & 0 \\ 0 & 0.75 & 0 & 0.79 \\ 0.69 & 0 & 0.76 & 0 \end{pmatrix} \quad (7.6)$$

We find the average of both matrices and select the first one owing to lower variance which is representative of lesser contrast, hence would be more imperceptible.

b. For spatial compression, the rows of sub-image Y in an alternate fashion from top and bottom, as below

$$Y_{compressed} = \begin{pmatrix} 0.63 & 0.70 & 0.69 & 0.78 \\ 0.71 & 0.65 & 0.77 & 0.61 \end{pmatrix} \quad (7.7)$$

c. Reconstruction is possible by keeping every alternate element zero in all the rows, under the assumption that original image size is twice the size of the compressed one.

$$Y = \begin{pmatrix} 0.63 & 0 & 0.69 & 0 \\ 0 & 0.65 & 0 & 0.61 \\ 0.71 & 0 & 0.77 & 0 \\ 0 & 0.70 & 0 & 0.78 \end{pmatrix} \quad (7.8)$$

### B. Watermark Scrambling

As, a chaotic scrambler, the Arnold Transform is defined in 2D as

$$\begin{bmatrix} x' \\ y' \end{bmatrix} = \begin{bmatrix} 1 & 1 \\ 1 & 2 \end{bmatrix} \begin{bmatrix} x \\ y \end{bmatrix} \text{mod } 1 \quad (7.9)$$

The inverse transformation is defined as

$$\begin{bmatrix} x \\ y \end{bmatrix} = \begin{bmatrix} 2 & -1 \\ -1 & 1 \end{bmatrix} \begin{bmatrix} x' \\ y' \end{bmatrix} \text{mod } 1 \quad (7.10)$$

which also shows its invertibility.

The above transformations are applicable on a per pixel basis.

#### 7.2.1. WATERMARK EMBEDDING STAGE

- a. Segregate the cover image using the scheme outlined in A.
- b. Spatially compress the sub-image having lower variance.
- c. On this, compute single level DWT with Haar wavelet.
- d. Choose the lowest DWT sub-band.
- e. Resize the watermark to match the size of the sub-band.
- f. Encrypt the resized watermark using Arnold's transform as described in B.

Due to unequal row and column sizes, the watermark scrambling done in two steps, by dividing the image into two equi-dimensional partitions.

g. Scale the scrambled watermark by an empirical weight and add to the lowest sub-band found in d.

h. Recombine the watermarked sub-band obtained with other high pass sub-bands previously and calculate its IDWT.

- i. Rebuild the watermarked partitioned image using process described in A.
- j. Merge the watermarked partitioned image with its non-watermarked equivalent to obtain the watermarked image.

### **7.2.2. WATERMARK EXTRACTION STAGE**

- a. Segregate the cover image and watermarked image as prescribed in A.
- b. Calculate the spatially compressed images and identify the one with lower variance (cover image) and the one with the higher variance (watermarked image partition).
- c. Apply single level DWT with Haar wavelet on the outputs of step b.
- d. Select the lowest DWT sub-band and subtract from it the lowest sub-band of the cover image's spatially compressed sub-image. This renders the process is non-blind.
- e. Divide by the empirical weight.
- f. Unscramble the watermark using Arnold Transform.

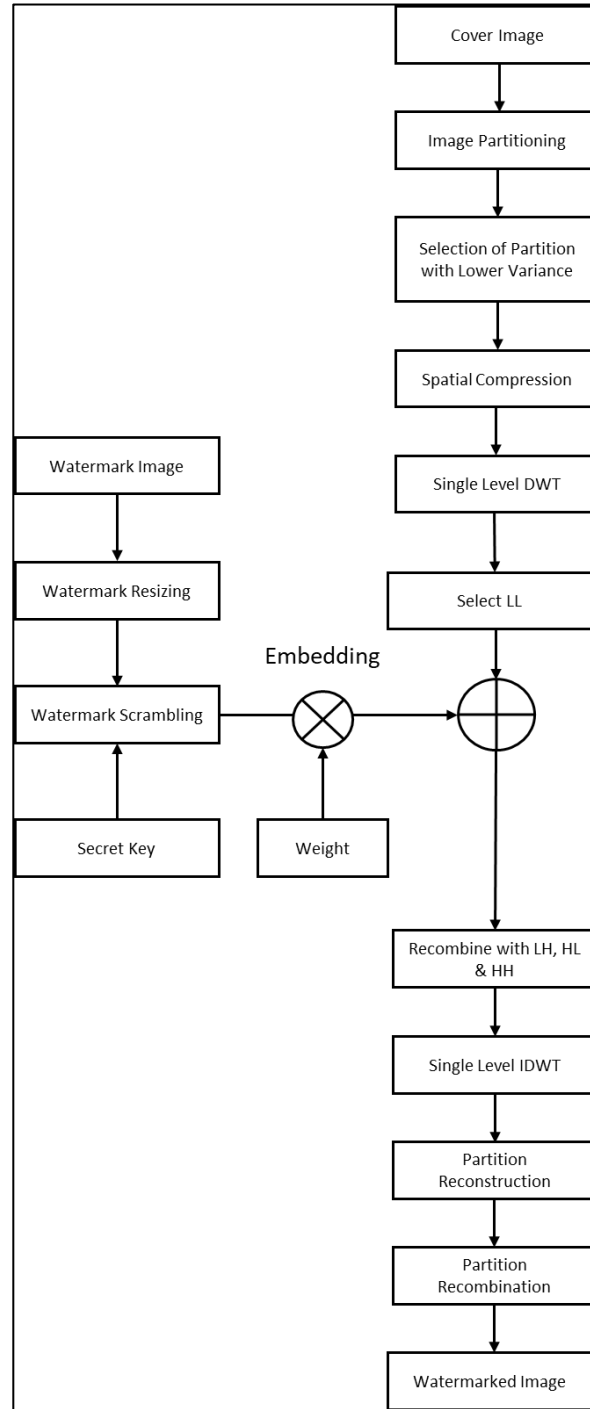


Figure 7.3: Flowchart for Watermark Embedding Process

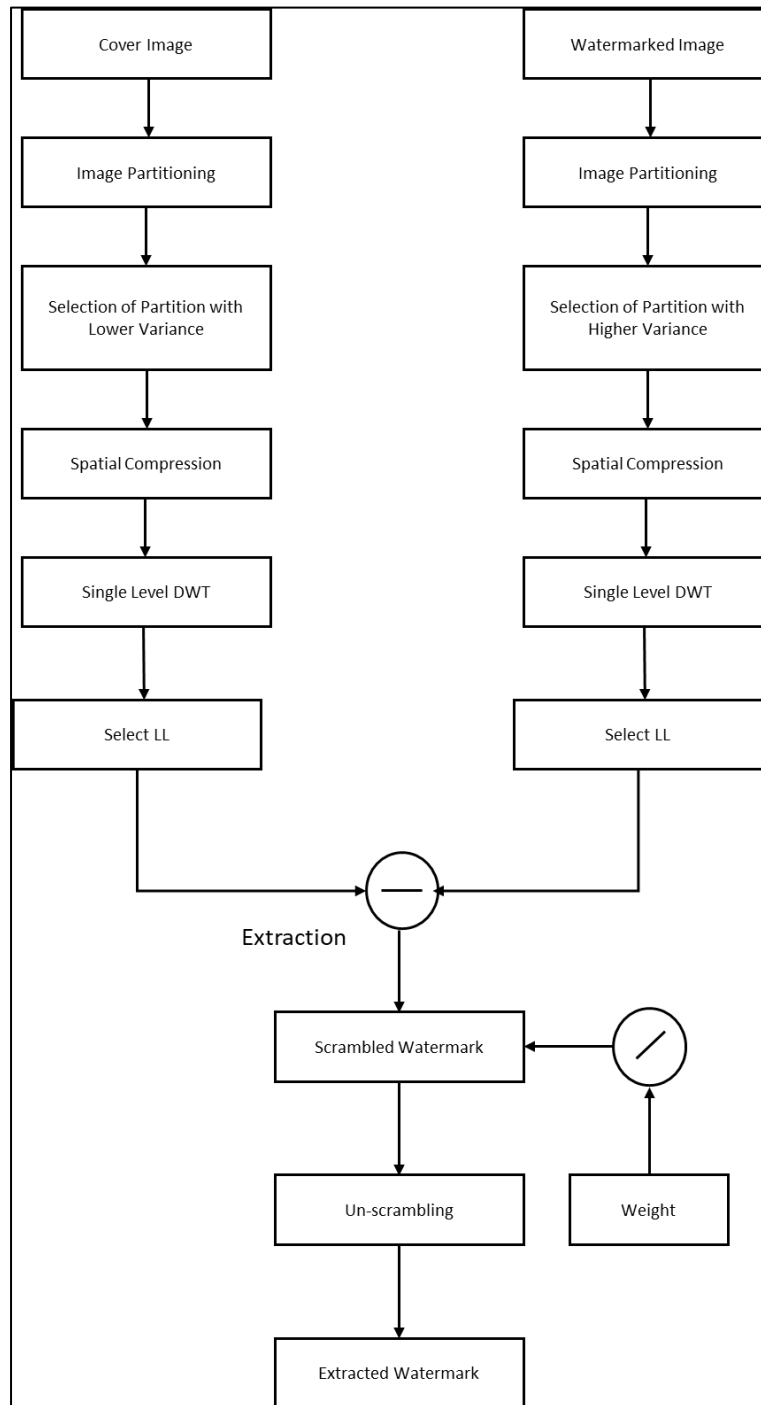


Figure 7.4: Flowchart for Watermark Extraction Process

### 7.3. MOMENT BASED IMAGE WATERMARKING

The methodology is divided into watermark embedding and extraction stages. The following sign convention is adopted for describing the process of watermarking:  $I = \{f(c, d), 0 \leq c < M, 0 \leq d < N\}$  represents the digital color image (cover work), and  $f(c, d)$  is the value of the pixel in gray-scale at the specified location  $(c, d)$ , for a particular channel. The watermark of size  $P \times Q$  is given as  $\Omega = \{\omega(c, d), 0 \leq c < P, 0 \leq d < Q\}$ .

#### 7.3.1. WATERMARK EMBEDDING (TIER I)

The following describes the process of generation and embedding of the watermark in the cover image through the zero-watermarking approach.

##### a. Watermark Scrambling Using Quasi-Affine Transform

The watermark image is scrambled using quasi-affine transform with seed  $\vartheta$ . This is a non-linear transform which is designed for round-off situations and is governed by 6 parameters  $a, b, c, d, e, f$ . It is expressed as below

$$\begin{pmatrix} e' \\ f' \end{pmatrix} = \begin{pmatrix} a & b \\ c & d \end{pmatrix} \begin{pmatrix} e \\ f \end{pmatrix} + \begin{pmatrix} g \\ h \end{pmatrix} \quad (7.11)$$

where  $\begin{vmatrix} a & b \\ c & d \end{vmatrix} = \pm 1$ ,  $(e, f)$  and  $(e', f')$  denote the pixel in the watermark image and its corresponding scrambled version, respectively. The transform is applied on every pixel of the watermark image in order to obtain the scrambled watermark. Additionally, in order to ensure the safety of the scrambling algorithm, the mapping from the unscrambled to scrambled domain should be single-valued and subjective, with respect to the unscrambled domain.

##### b. Isolation of Cover Image Channel



The digital color image  $I$  is read in the RGB format and its blue component is isolated for the insertion of the watermark. This is supported by the argument in [81], which advocates the selection due to the lowest concentration of the cones in the human eye which are receptive to blue color, which makes it fit for embedding the watermark.

### c. Computation of FRGPCET

The fractional order generic polar complex exponential transform is calculated for the isolated cover image channel using the methodology outlined in section 5.5. These are computed in a fast and accurate manner, through the use of seventh order interpolator and Gaussian Quadrature Numerical Integration, as explained in section 5.7.

### d. Robust FRGPCET Coefficient Selection through Pseudo-Random Incrementally Recursive Approach

We adopt an incrementally recursive approach in selection of the FrGPCET coefficients (moments) for watermarking. It starts with the pseudo-random selection of  $10X$  the number of coefficients actually required i.e. we select a total of 10 times the number of pixels in the watermark image. From these coefficients, we eliminate the ones where the order  $q$  of the coefficients is an integer multiple of 4. This is in accordance with conclusions drawn by Xin et al. [82], who had shown that circular orthogonal moments with  $q = 4n, n \in \mathbb{Z}$  should not be used for embedding the watermark bits, so as to inhibit information redundancy. Following this elimination, we also exclude the moments which have magnitude variation smaller than 1%.

$$\mathbb{M} = \{|FrGPCET|, \forall(\Delta|FrGPCET|) < 0.01, q \neq 4n, n \in \mathbb{Z}\} \quad (7.12)$$

Next, we select the required coefficients in an iterative manner – in the first round we select 2 coefficients, in next  $2*4$  coefficients, in the next  $2*4*8$  coefficients and so on, until the total count of the selected coefficients reaches the number of pixels in the watermark image. This approach not only increases the degree of randomization in pixel selection but

also makes the watermarking more stable and resistant to a wider range of attacks. The selected moments are used to form a feature vector, which is later used for insertion of the watermark.

e. Formation of Augmented Feature Vector Mask Using Otsu's Method

The feature vector obtained in previous step is resized to match the size of the watermark. Then, using Otsu's threshold for segmentation [83], we compute the threshold  $\zeta$  for this feature vector 2-D matrix. This in turn is used to create an augmented feature vector mask as below

$$M_{\text{mask}}(c, d) = \begin{cases} 1, & M(c, d) \geq \zeta \\ 0, & M(c, d) < \zeta \end{cases} \quad (7.13)$$

The purpose of this mask is explained as follows – the moments which exceed the threshold correspond to '1' in the mask and will be used for insertion of the same binary value from the watermark i.e. the coefficient for which the threshold is exceeded will be used to embed a binary '1' from the watermark. Similarly, the moment for which the threshold is not met correspond to '0' in the mask and will be used for embedding binary '0' from the watermark. In case of mismatch between the number of '0's and '1's in the mask and that in the watermark, the same is reconciled by giving precedence to the bit value in the watermark and embedding the same at the corresponding location as dictated by the watermark. This conflicting bit location information is also updated on the mask, which is instrumental in watermark extraction.

f. Dither Modulation of the Selected Moments

Using the process described in section 5.8, the selected moments are subjected to dither modulation, based on the bit composition of the watermark and the augmented feature vector mask formed in previous step. Since the image is not altered directly and only its features are used for embedding the watermark information through dither modulation, the proposed scheme qualifies as zero watermarking. Not only this enhances the strength of

watermarking but also increases the imperceptibility as the cover image is minimally impacted by the insertion of the watermark. The modulated moments are embedded back at the respective positions in the moment matrix.

g. Image Reconstruction

Let  $\tilde{I}$  be the reconstructed watermarked image channel post dither modulation,  $I_D$  and  $I_{\tilde{D}}$  are the images formed using the originally obtained moments and those obtained post dither modulation, respectively.

$$\tilde{I}(c_v, d_w) = I(c_v, d_w) - I_D(c_v, d_w) + I_{\tilde{D}}(c_v, d_w) \quad (7.14)$$

$$= I(c_v, d_w) - \sum_{(g,h) \in K'} \hat{\mathbb{M}}_{gh} T_{gh}(c_v, d_w) + \sum_{(g,h) \in K'} \tilde{\mathbb{M}}_{gh} T_{gh}(c_v, d_w) \quad (7.15)$$

$$= I(c_v, d_w) - \sum_{(g,h) \in K'} \hat{\mathbb{M}}_{nl} T_{nl}(c_v, d_w) \quad (7.16)$$

$$+ \sum_{(g,h) \in K'} (\hat{\mathbb{M}}_{nl} + \xi_{gh}) T_{gh}(c_v, d_w) \quad (14)$$

$$= I(c_v, d_w) + \sum_{(g,h) \in K'} \xi_{gh} T_{gh}(c_v, d_w) \quad (7.17)$$

where  $\hat{\mathbb{M}}, \tilde{\mathbb{M}}$  and  $T$  are as per the adopted conventions.

The previous steps were observed to affect the imperceptibility of the embedded watermark due to the presence of some circular artifacts in the background of the watermarked image. This can be assuaged by either reduction of the quantization step  $\Delta$  and mitigating the effect of modification of the moments, especially those located near the origin

on the radial plane. Alternatively, this can be achieved by regulating the  $\beta$  parameter which harmonizes the oscillation of the radial function over the unit circle [84]. In this paper, we leverage the time-frequency representation capability [85] of the fractional order moments to identify in the spectral domain, the moments which have been majorly affected due to watermarking. This is accomplished by computing the Discrete Cosine Transform (DCT) of the reconstructed watermarked image obtained from Step g. Since the computed fractional moments lay specific emphasis on certain regions of the image, we use a prefix free coding scheme in conjunction to reduce the data redundancy in the non-watermarked regions, as well as enhance the overall security. For the foregoing reason, we rely on Huffman coding for compression of the watermarked data. Besides, the use of a coding scheme also enhances the overall security of the watermarking algorithm. Together, the DCT and Huffman coding form the Tier II of the watermark embedding process.

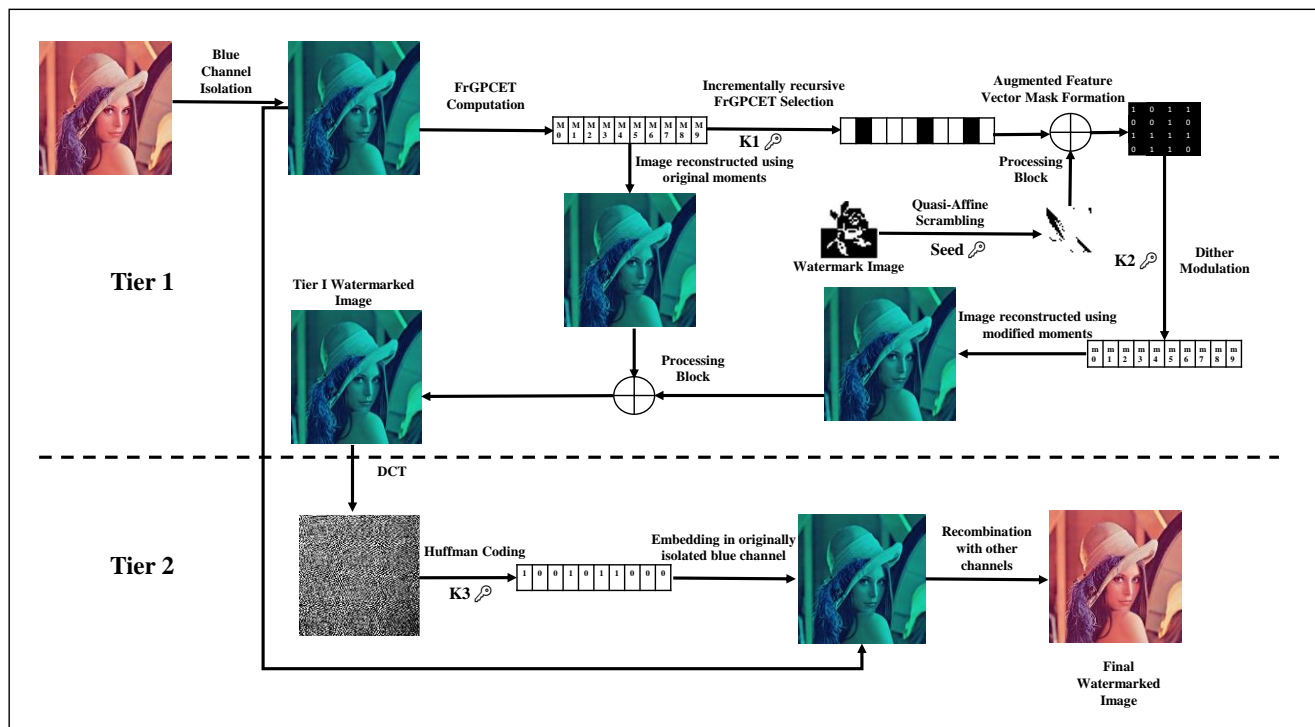


Figure 7.5: Watermark Embedding Process

### 7.3.2. WATERMARK EMBEDDING (TIER II)

#### a. Discrete Cosine Transform

The use of DCT in watermarking of color images has been a common practice. The transform is able to model the correlation between the different color channels. This has been confirmed through various related works [86,87,88,89,90].

The 2D-DCT transforms the pixels from the frequency domain to frequency domain, maintaining the resolution of the image. The transformation results in one DC (low frequency) component and remaining AC (high frequency components). The DCT coefficients form a distinct set of features, where they represent information by their significance to the Human Visual System (HVS). The most important values to human eyes are placed in the top left corner of the coefficients matrix, while the least important values are located in the lower right corner of the coefficients matrix.

The DCT of the watermarked image plane  $\tilde{I}$  is computed using the below relation

$$H(\gamma, \delta) = \frac{2}{\sqrt{MN}} C(\gamma) C(\delta) \sum_{c=0}^{M-1} \sum_{d=0}^{N-1} \tilde{I}(c, d) \cos \left[ \frac{(2c+1)\gamma\pi}{2M} \right] \quad (7.18)$$

$$\cos \left[ \frac{(2d+1)\delta\pi}{2N} \right]; C(\chi) = \begin{cases} \frac{1}{\sqrt{2}}, \chi = 0 \\ 1, \chi > 0 \end{cases}$$

#### b. Huffman Coding

The unique elements of the DCT transformed image  $H(\gamma, \delta)$  are identified through histogram analysis, which are then encoded using Huffman dictionary. The encoded bit stream is subsequently embedded in the blue plane of the cover image at pre-designated

locations identified using key  $K_3$ . Recombination with other channels yields the final watermarked color image.

### 7.3.3. WATERMARK EXTRACTION

The following describes the process of extraction of the embedded watermark from the image. Since the moment computation is reversible, the entire watermarking algorithm is an inverse process. Further, the extraction is blind as the knowledge of the cover image is not a pre-requisite for the extraction of the watermark.

#### a. Isolation of Watermarked Image Channel

First, the blue channel of the watermarked image is separated from the other channels and undergoes bit-plane slicing and pixel-wise concatenation, to obtain the individual gray levels in bits.

#### b. Huffman Decoding

From the channel extracted in step a, the bits corresponding to the locations determined by key  $K_3$  are selected and combined to be fed to the Huffman decoder.

#### c. Inverse Discrete Cosine Transform (IDCT)

The output of the Huffman decoder from the previous step is subjected to inverse Discrete Cosine Transform, to yield back the pixel information in the spatial domain.

#### d. FRGPCET Computation

Using the previously outlined technique in Section 5.5, the FrGPCET of the image retrieved post IDCT is computed.

#### e. Dither Modulation

The selection of the coefficients  $\{\mathbb{m}_{FrGPCET}^*(k), 0 \leq k \leq PXQ\}$  obtained from Step c is done using the secret key  $K_1$  used during embedding. Magnitude extraction is done through quantization, as below

$$|\mathbb{m}_{FrGPCET}^*(k)|_l = \left\lfloor \frac{|\mathbb{m}_{FrGPCET}^*| - \vartheta_k(l)}{\Delta} \right\rfloor \Delta + \vartheta_k(l) \quad (7.19)$$

f. Bit Value Estimation using Otsu's Threshold

The bit sequence obtained from Step e is consolidated and the resulting array reshaped to the original dimensions of the embedded watermark. Then, using Otsu's method, a threshold is computed for the 2D-matrix retrieved from Step d. Based on the threshold and using the similar strategy as in Section 5.8, the bit values for each pixel position are estimated.

g. Unscrambling using Quasi-Affine Transformation

Using the inverse quasi-affine transform and related parameter and seed value as used during embedding in Section 7.3.1, the 2-D matrix from Step e is unscrambled to yield the retrieved watermark.

The process of watermark embedding and extraction have been described in the process flow diagram given in Fig. 7.5 and Fig. 7.6.

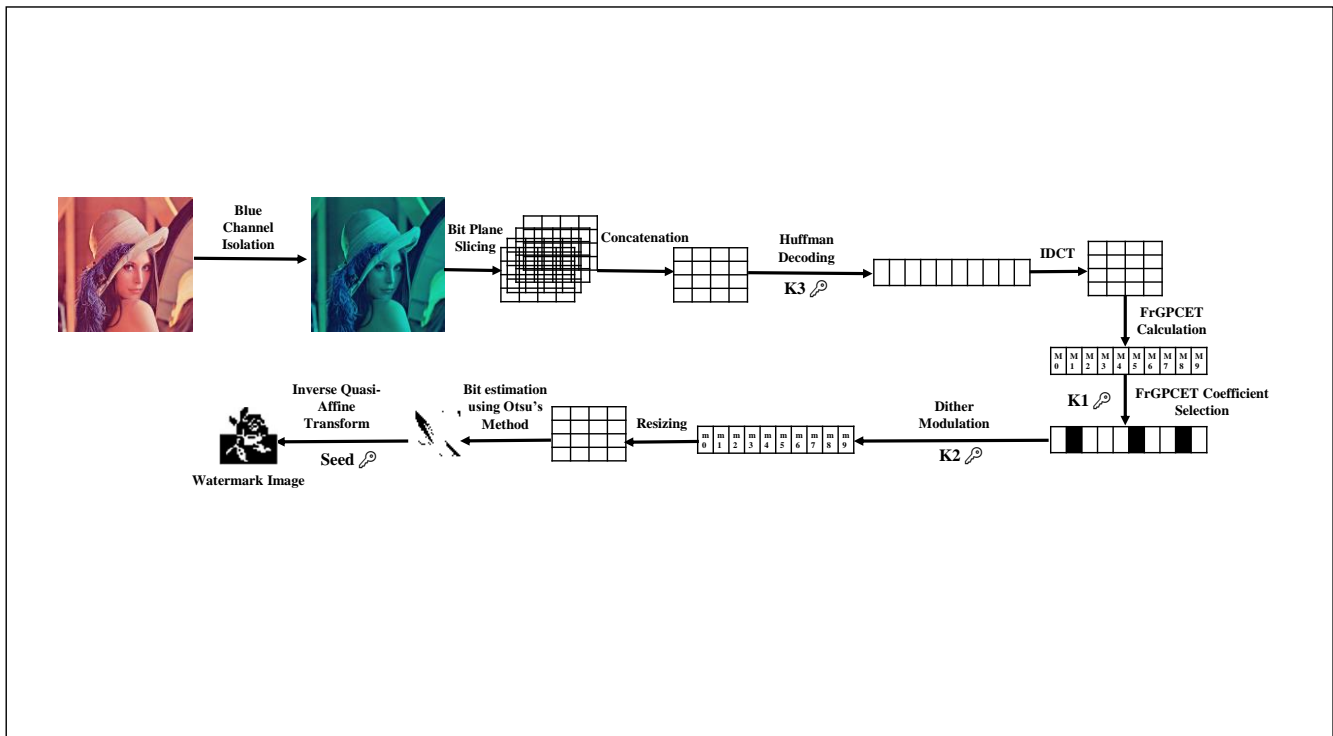


Figure 7.6: Watermark Extraction Process

## 7.4. IMAGE WATERMARKING USING GRAPH SIGNAL PROCESSING AND LOCAL DOMINANT FEATURES

The methodology is divided into watermark embedding and extraction stages and elucidated as below

### 7.4.1. WATERMARK EMBEDDING

- a. The cover image  $C$  and Secret Image  $S$  are read.
- b. Resizing of secret image to the desired dimensions is undertaken.
- c. Arnold transformation of the secret image, using a predefined set of iterations, to compute the scrambled image  $S_{arnold}$ .
- d. Next, a two-dimensional grid graph structure  $G$  with  $N \times N$  nodes is designed. In our case,  $N = 16$ . Then we estimate the maximum Laplacian Eigen value in each case.



e. With the number of filters specified as 2, we construct an Intersine wavelet function.

f. The wavelet constructed in step e is used to form the analysis section of the 2-channel filter bank for both the cover and secret images.

g. We used Variational Mode Decomposition (VMD) to disassociate the analyzed input over image into its constituent modes. This is done to identify the mode with maximum power spectral compliance, as the same will be used for embedding the watermark.

h. We find the normalized power spectra of the scrambled analyzed watermark obtained from step f and that of all the VMD decomposed modes. Then, the degree of closeness of the power spectra so obtained is ascertained for all the modes, by calculating the matrix norm between them.

i. With the minimum distance mode isolated in step h above, we calculate the local dominant orientation feature vector using the technique prescribed in Section 6.4.

j. We sort the LDOF matrix obtained in previous step in descending order and segregate the top 2 rows. The positions of these elements in the original LDOF matrix is also noted.

k. Using the identified positions, we perform alpha-blending operation, wherein the pixel values of the IMF with minimum power spectral distance from the watermark's analysed version are modified in accordance with the analysed scrambled watermark.

l. The modulated analysed image IMF thus obtained is reshaped suitably and recombined with other IMFs.

m. The modulated image is then passed through the synthesis block for the generation of the watermarked image.

#### **7.4.2. WATERMARK EXTRACTION**

a. Proceeding reversibly, we first subject the watermarked image to the analysis section of the GSP filter bank designed using the same parameters as used during watermark embedding.

b. The IMFs and residual matrices are subtracted from the output of step a so as to obtain the matrix for further processing.

c. Using the concept of alpha blending, the watermark pixel value estimates are extracted corresponding the locations where the watermark was embedded.

d. After suitably reshaping the matrix obtained in Step c above, synthesis filter is applied on it to generate the final output of the GSP filter bank.

e. Inverse Arnold Transform is undertaken the output of previous step using the same number of iterations as during watermark embedding to generate the final extracted watermark.

The watermark embedding and extraction stages are presented in the form flow charts in Fig. 7.7 and 7.8, respectively.

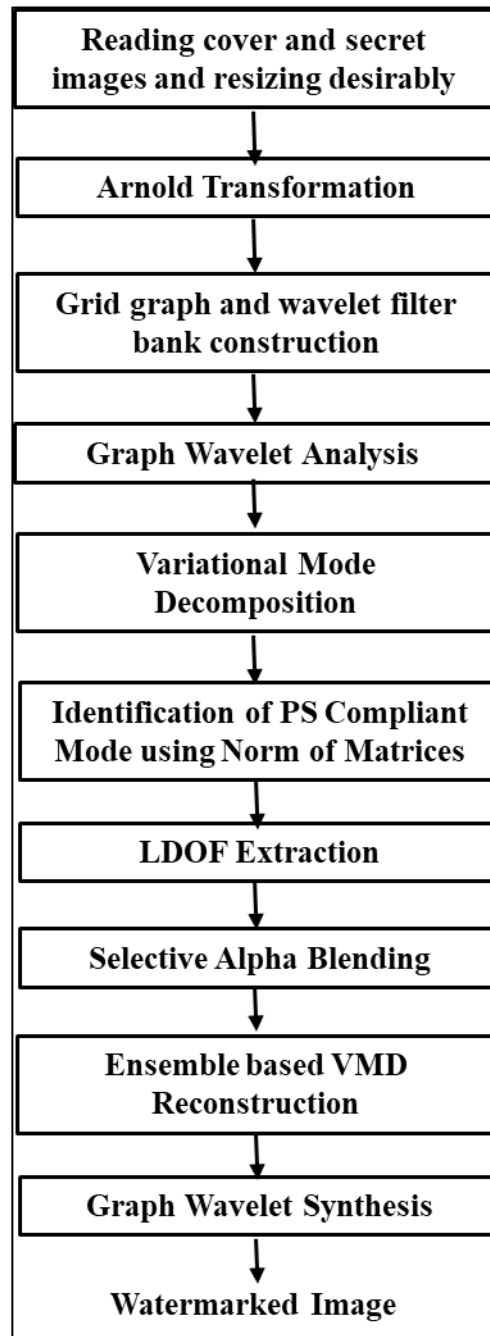


*Figure 7.7: Watermark Embedding Process*

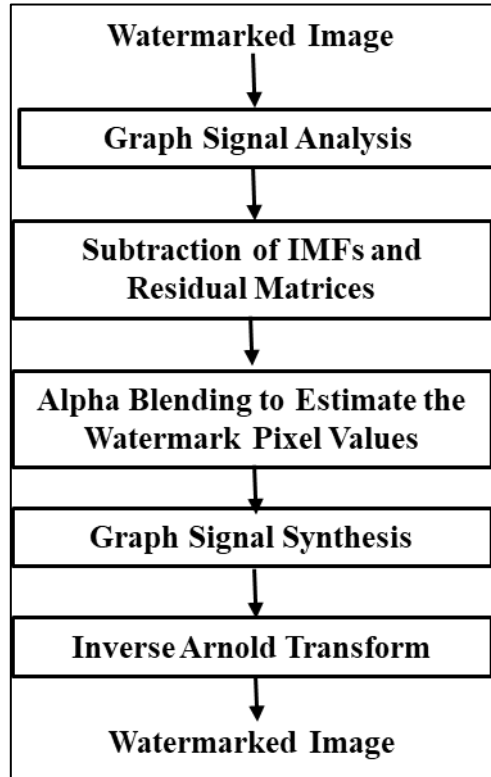


*Figure 7.8: Watermark Extraction Process*

## **CHAPTER 8**

### **EXPERIMENTAL CONFIGURATION AND SIMULATION PARAMETERS**

The watermarking techniques developed here were implemented on MATLAB®R2018a running on Intel® Core™ i3 7<sup>th</sup> generation processor operating at 3.90 GHz. Other parameters used for used prior to watermark embedding and during the watermark insertion and detection have been provided below.

#### **8.1. AUDIO WATERMARKING**

##### **8.1.1. AUDIO SIGNAL RECORDING / SAMPLING**

The audio signal is recorded on a single channel, for 2 seconds, at a sampling frequency of 4 KHz and where, each sample is digitally encoded into 16 bits. The sampling frequency has been chosen while keeping in mind that the significant components of the audio signal are band-limited to 2 KHz, thus the sampling frequency is selected in adherence to the Nyquist criterion for sampling. The technique was by sampling the pre-recorded audio signals.

### 8.1.2. WATERMARK EMBEDDING

a. For embedding the watermark, the LCT parameter matrix chosen for computation of DLCT is given as  $X = \begin{pmatrix} \frac{1}{6} & \frac{5}{6} \\ -\frac{17}{30} & \frac{1}{3} \end{pmatrix}$ . Further, in order to obtain the

watermarked audio signal, the IDLCT is computed using the inverse of the above matrix.

b. The standard deviation for the normally distributed complex watermark sequence generator is selected as 50.

c. Watermark is embedded starting from the median sample position (50<sup>th</sup> percentile location) to nearly up to 65<sup>th</sup> percentile sample of the audio signal. This is in accordance with the requirements of robustness and imperceptibility of the watermark, as explained in Chapter 5.

d. The length of the complex watermark sequence is adaptively set as the difference between the initial position for watermark embedding and the sampling frequency. In the present case, its value is 1120.

### 8.1.3. WATERMARK DETECTION

a. Number of randomly generated and normally distributed complex watermark sequences is kept as 1000.

b. The constant  $c$ , in the threshold for the detection parameter is initially set as 3, based on the outcome of experiments conducted for  $c \in [1,10]$ .

c. For extraction of the embedded watermark, the LCT parameter matrix is the same as the one used during embedding, and is given by  $X = \begin{pmatrix} \frac{1}{6} & \frac{5}{6} \\ -\frac{17}{30} & \frac{1}{3} \end{pmatrix}$ .

#### **8.1.4. SIGNAL PROCESSING AND FEATURE DISTORTIVE ATTACKS**

The following attacks were carried out on the audio signal, in order to simulate the actual audio signal transmission, manipulation and storage scenarios.

a. Additive White Gaussian Noise (AWGN) attack, with a maximum strength of 100 dB. This simulates the commonly added noise during signal transmission and manipulation.

b. Low pass filtering attack, with the passband frequency set at 50 Hz (Minimum audible frequency limit) and stop band frequency defined as 200 Hz. This attack resembles the tone modulation controls exercised for limiting the audible bandwidth of the signal and change its harmonic characteristics.

c. High pass filtering attack, using with the passband frequency set at 100 Hz and stop band frequency fixed as 400 Hz (Maximum frequency ordinarily found in the common audio signals). This attack reproduces the conditions where an audio signal may be manipulated to isolate the different sources of sounds and/or remove plosives (caused due to the vibration of the microphone diaphragm).

d. Decimation (Cropping) attack, by randomly removing a maximum of 10% of the audio signal samples from randomly selected positions, centered around the median sample position, where the watermark is embedded. This operation mimics the condition where an audio signal may be shortened in length due to inadequate sampling rate, deliberate cropping or loss of samples during transmission.

e. MPEG3 compression attack, with sampling rate set as 44.1 KHz. This attack is representative of data compression during downloading/uploading or storage operations which may be performed during handling of the digital audio file.

## 8.2. IMAGE WATERMARKING IN FREQUENCY DOMAIN

Grayscale image of Lena of dimension 512X512 was selected as the cover image. Additionally, the large watermark size demonstrates the good payload capacity of the scheme.

## 8.3. MOMENT BASED IMAGE WATERMARKING

The proposed zero-watermarking scheme was tested on twelve images from the popularly used USC-SIPI image database [4], each of dimensions 512 x 512 x 24 bit, as shown in Fig. 4, and referred to as “Aerial”, “Sailboat on lake”, “Peppers”, “Airplane”, “House”, “Mandrill”, “Splash”, “Female”, “Jelly beans”, “Girl”, “Female from Bell Labs” and “Couple, respectively. A binary watermark of size 64 x 64 bits, shown in the same Fig. 4, was used as the watermark image. The quantization step size was set as  $\Delta = 0.1$ . The value of the fractional parameter  $\beta$  was selected as 1.8, due to homogeneous variation of the radial function  $E_m(\rho, \beta)$  in the interval  $0 < \rho < 1$ , and as compared in Fig. 5 with different values of  $\beta$ . Further, the PSNR (Peak Signal-to-Noise Ratio) is used as a metric to estimate the visual quality of the image as well as to gauge the imperceptibility of the embedded watermark. Maximum order was kept as 100. Also, the experimental results are compared with schemes proposed in [84,92,93,65,91].

## 8.4. IMAGE WATERMARKING USING GRAPH SIGNAL PROCESSING AND LOCAL DOMINANT FEATURES

The proposed watermarking scheme was tested on gray-scale cameraman image of size 256X256. The size of the binary watermark used was 64X64. For Arnold scrambling, number of iterations were fixed at 5. Further, for the Graph Signal Processing unit, number of nodes and filters were selected as 16 and 2 respectively. Also, the number of modes for decomposition of signal using VMD was kept as 8.



## CHAPTER 9

### RESULTS AND DISCUSSION

#### 9.1. AUDIO WATERMARKING

The audio watermarking algorithm proposed above has been evaluated based on the figures of merit of similarity index, the signal to noise ratio and normalized cross-correlation. These are mathematically expressed as

$$\begin{aligned}
 & \text{Normalized Cross Correlation (NC)} \\
 &= \frac{\sum_{j=1}^K W(j) \cdot W(j)^*}{\sqrt{\sum_{j=1}^K W(j)^2} \sqrt{\sum_{j=1}^K W^*(j)^2}} \quad (9.1)
 \end{aligned}$$

$$\text{Similarity Index (SIM)} = \frac{\sum_{j=1}^K W(j) \cdot W^*(j)}{\sqrt{\sum_{j=1}^K W^*(j)^2}} \quad (9.2)$$

where  $W$  and  $W^*$  denote the embedded and extracted watermarks, respectively and  $K$  is the length of the watermark sequence.

$$\text{Signal to Noise Ratio (SNR)} = 10 \log_{10} \left( \frac{\sum_{j=1}^N x(j)^2}{\sum_{j=1}^N (x(j) - x^*(j))^2} \right) \quad (9.3)$$

where  $x$  and  $x^*$  denote the original and retrieved audio signal, respectively and  $N$  is the length of the audio signal.

### 9.1.1. TEST OF IMPERCEPTIBILITY

The below figures graphically illustrate the comparison between the original audio signal and the watermarked audio signal. Further the difference between the two signals has also been plotted.

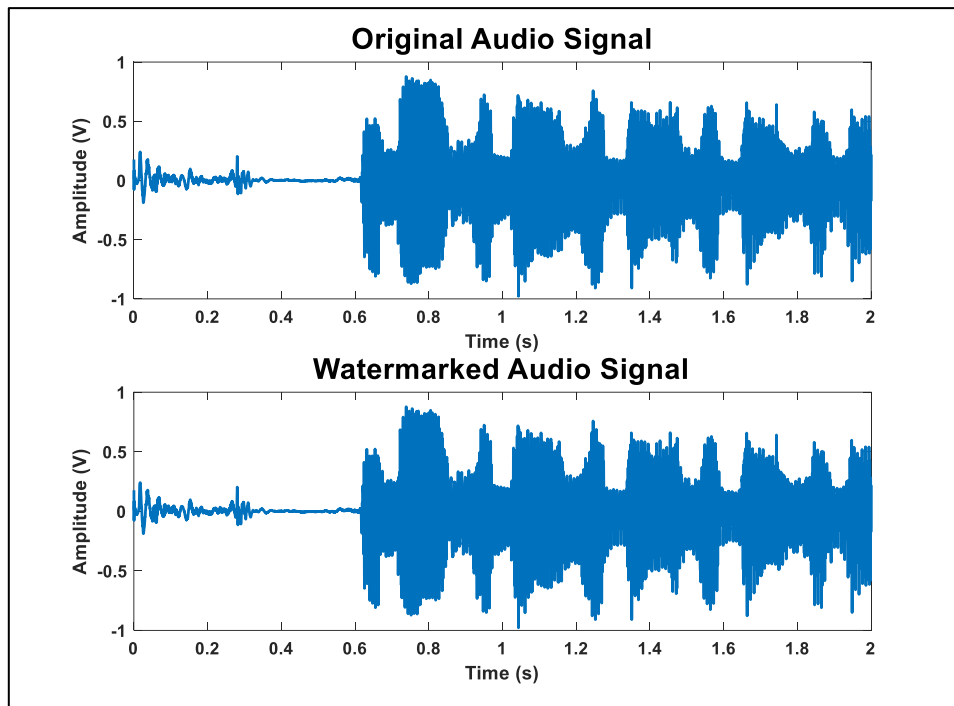


*Figure 9.1: Comparison between the Original and Watermarked Audio Signal*

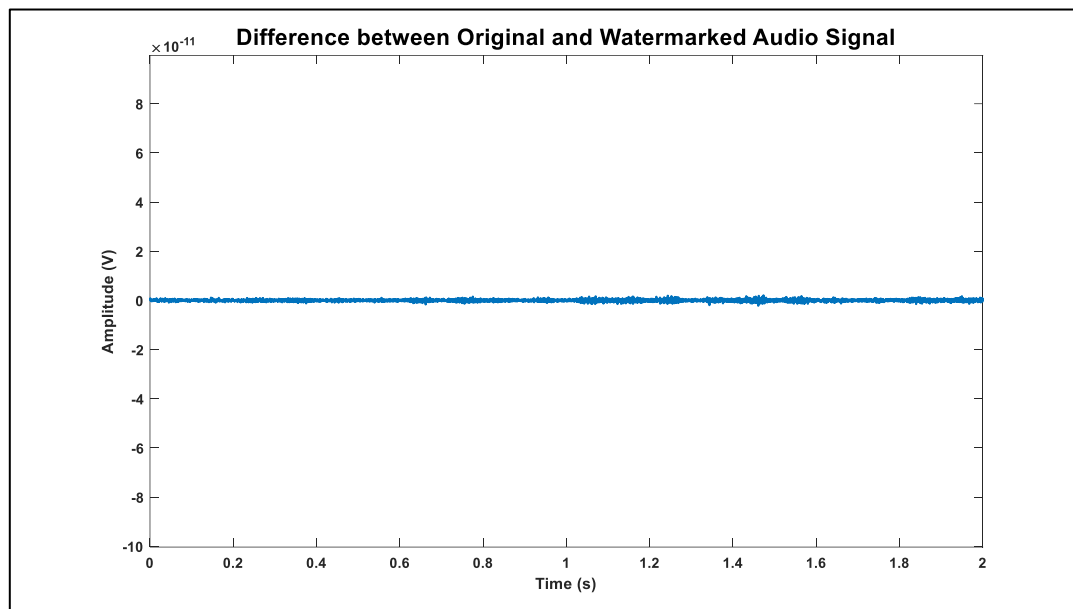


*Figure 9.2 Difference between the Original and Watermarked Audio Signal*

It is seen that the difference between the original audio signal and the watermarked audio signal is of the order of  $10^{-13} \sim 10^{-14}$ , which is negligible. This demonstrates the level of imperceptibility of the proposed watermarking scheme.

### **9.1.2. TEST OF ROBUSTNESS**

Signal processing and feature distortive attacks, described in Chapter 6 are performed on the watermarked audio signal to gauge the robustness of the proposed technique. The below set of Fig. 9.3-9.7 validate the detection of the originally embedded watermark, amongst a group of 1000 random watermarks, at the maximum strength/degree of attacks, as outlined in Table 9.1. The originally embedded watermark is kept at 501<sup>st</sup> position amongst the set of the watermarks used for calculating the detection parameter values.

Table 9.1. Signal Processing Attacks of Maximal Strength/Degree (Contd.)

Type of Attack	Strength/Degree
Additive White Gaussian Noise (AWGN)	100 dB
Low Pass Filtering (Cutoff Frequency - Passband)	50 Hz
High Pass Filtering (Cutoff Frequency - Passband)	400 Hz
Decimation (%age of Samples Removed)	10%
MP3 Compression (Sampling Rate)	44.1 KHz

The red dashed line in the figures indicates the threshold in each case.

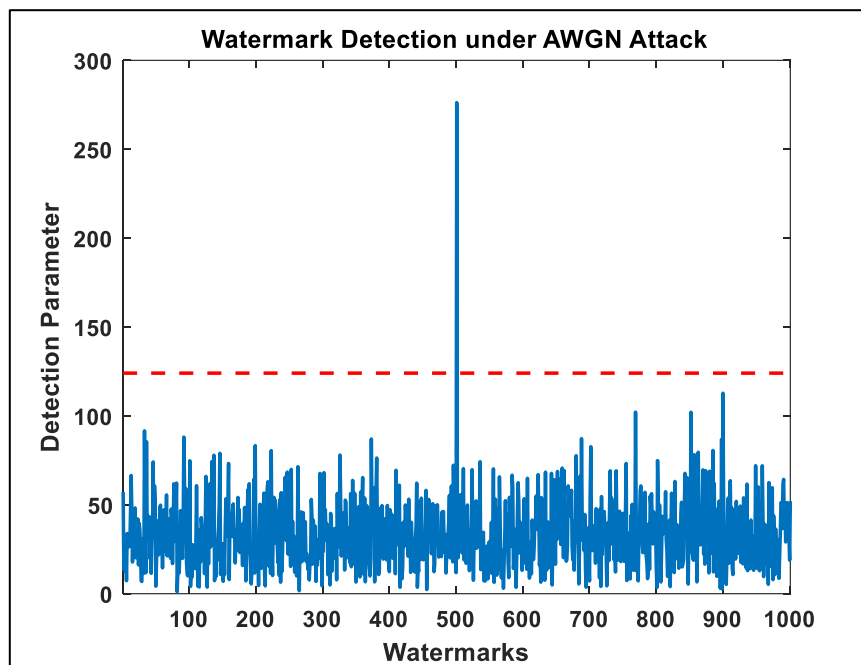


Figure 9.3: Watermark Detection under AWGN Attack

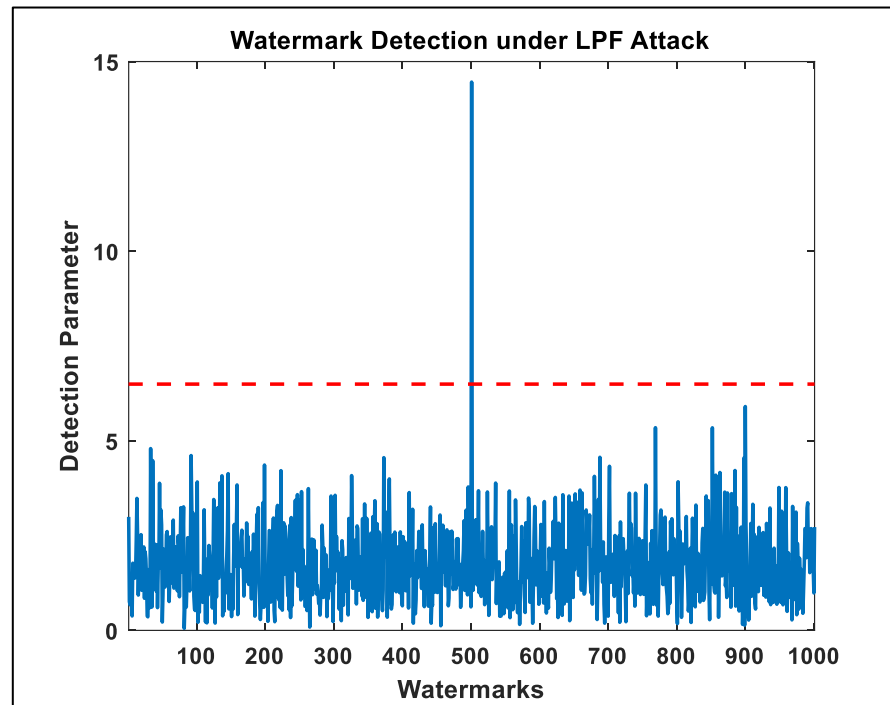


Figure 9.4: Watermark Detection under LPF Attack

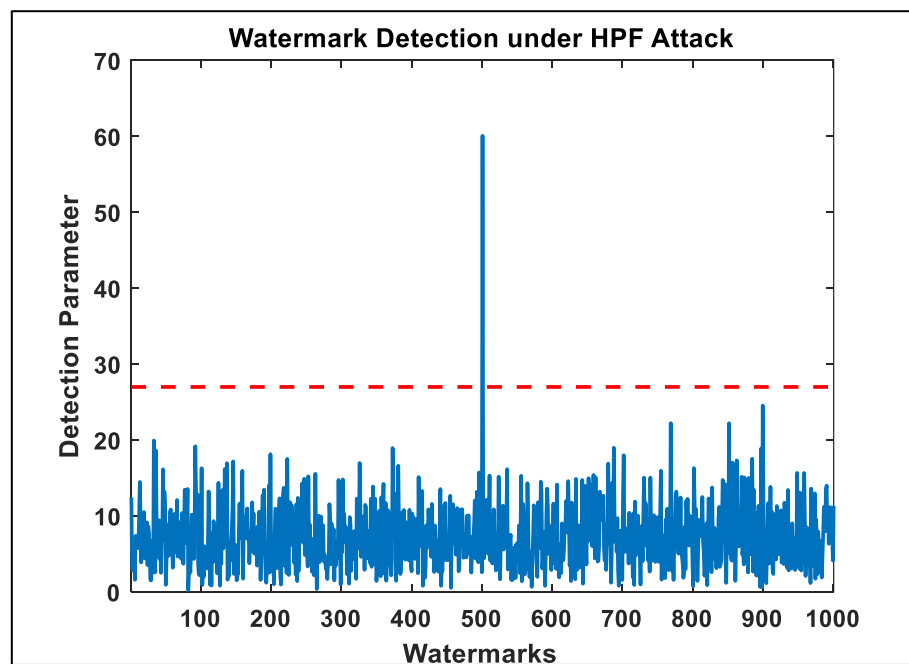


Figure 9.5: Watermark Detection under HPF Attack

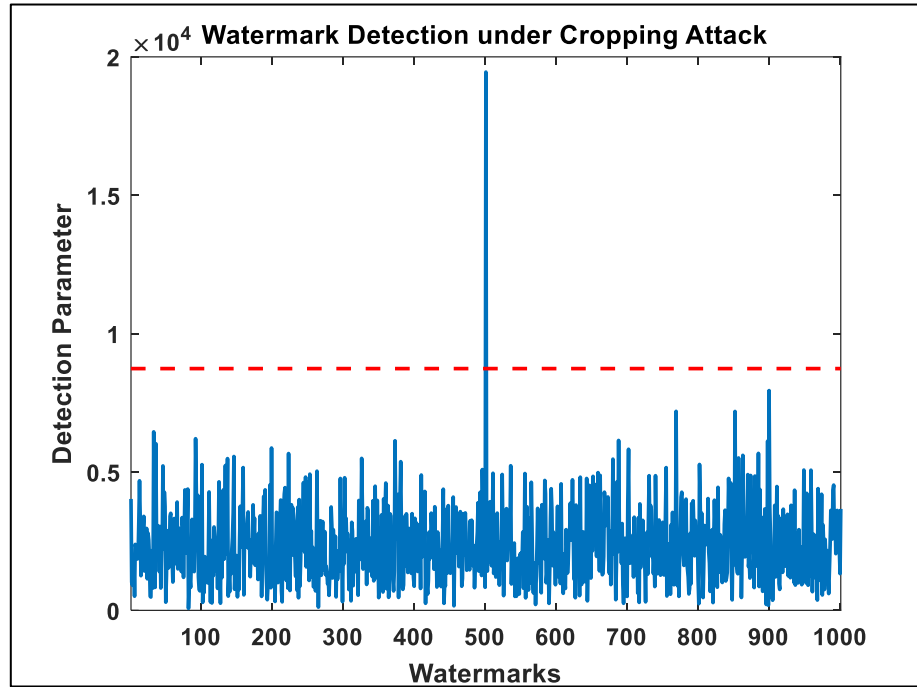


Figure 9.6: Watermark Detection under Decimation (Cropping) Attack

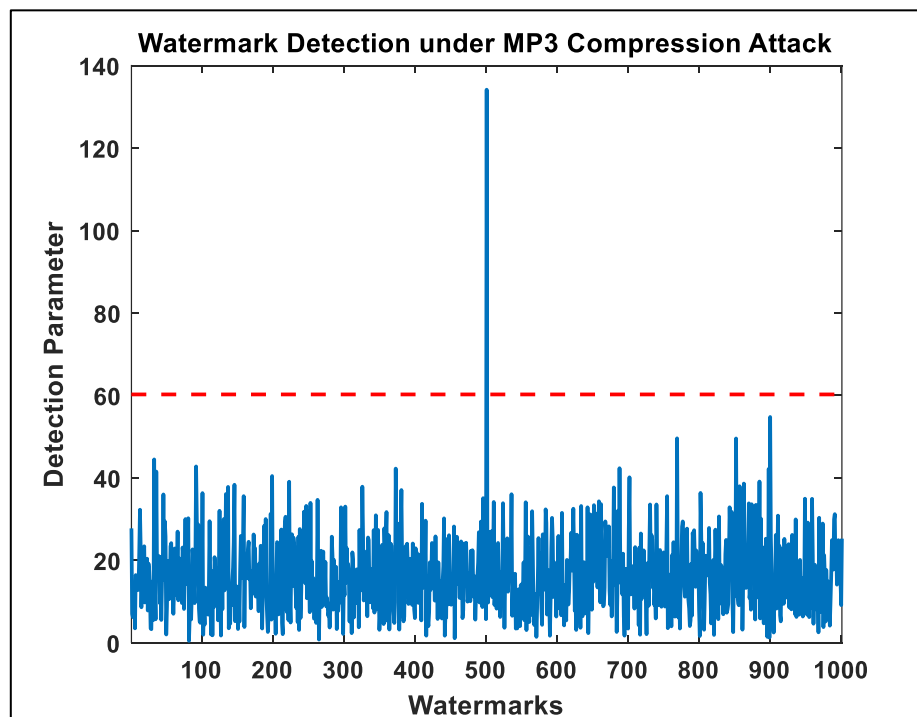


Figure 9.7: Watermark Detection under MP3 Compression Attack

Table 9.2 below lists the values of the figures of merit defined earlier in this chapter, computed for various strength/degree of the signal processing and feature distortive attacks.

*Table 9.2: Figures of Merit for the Watermarking Scheme for Different Attacks of Varying Strength/Degree*

<b>Type of Attack</b>	<b>Strength/Degree</b>	<b>Similarity Index (SIM)</b>	<b>Normalized Cross-Correlation (NC)</b>	<b>Signal to Noise Ratio (SNR) dB</b>
Additive White Gaussian Noise (Strength of Noise in dB)	25	0.8781	0.6332	95.3002
	50	0.8628	0.7705	95.8859
	75	0.9313	0.6243	95.9028
	100	0.8659	0.6978	95.5513
Low Pass Filtering (Passband Cutoff Frequency in Hz)	10	0.5594	0.9936	99.8594
	20	0.8761	0.9919	99.5708
	30	0.9448	0.9672	99.5756
	50	0.8919	0.9915	99.3354
High Pass Filtering (Passband Cutoff Frequency in Hz)	100	0.6822	0.6853	96.5952
	150	0.8267	0.7212	97.1797
	200	0.7750	0.7335	97.7530
	300	0.7355	0.6584	97.1428
Decimation (Percentage of samples cropped out)	2	0.7204	0.9973	83.3639
	5	0.8265	0.9977	73.2754
	7	0.5489	0.9983	67.0179
	10	0.9025	0.9990	60.7395
MP3 Compression (Sampling Rate in KHz)	4	0.7199	0.7280	94.3109
	8	0.7419	0.5350	94.2596
	16	0.9094	0.6000	94.2612
	44.1	0.8221	0.7531	96.1731

### 9.1.3. TEST OF SECURITY AND LCT PARAMETER SENSITIVITY

Figures 9.8 through 9.10 depict the value of the detection parameter obtained when each of the degree of freedom in the LCT parameter matrix is varied between  $[0.1,1]$ .

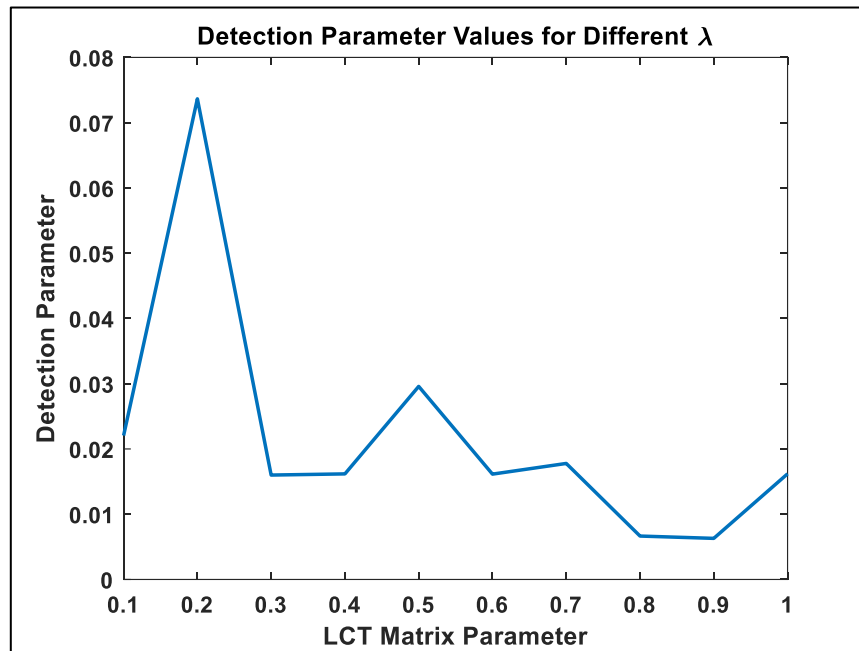


Figure 9.8: Detection Parameter Values for Different  $\lambda$

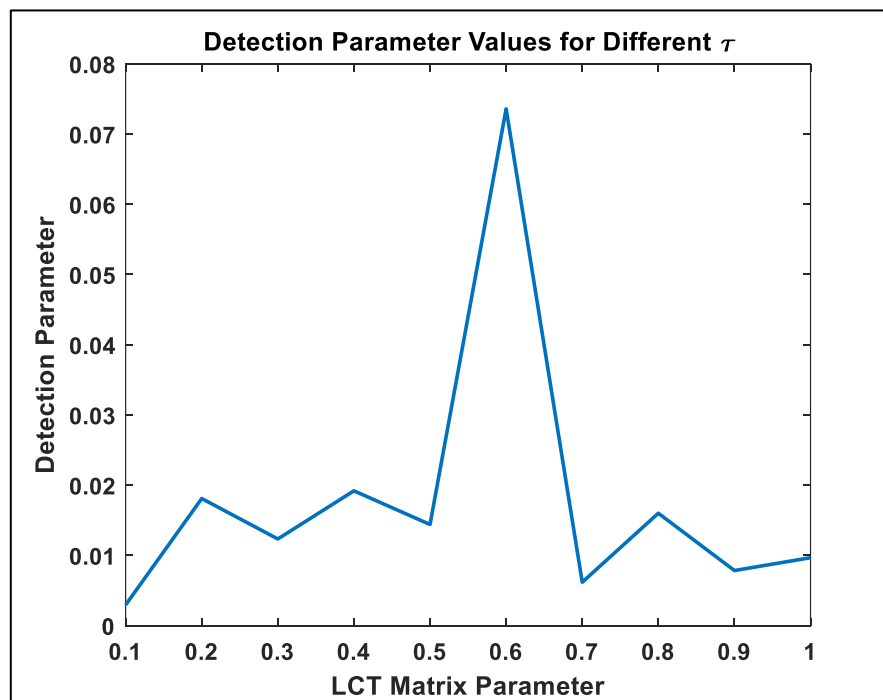


Figure 9.9: Detection Parameter Values for Different  $\tau$



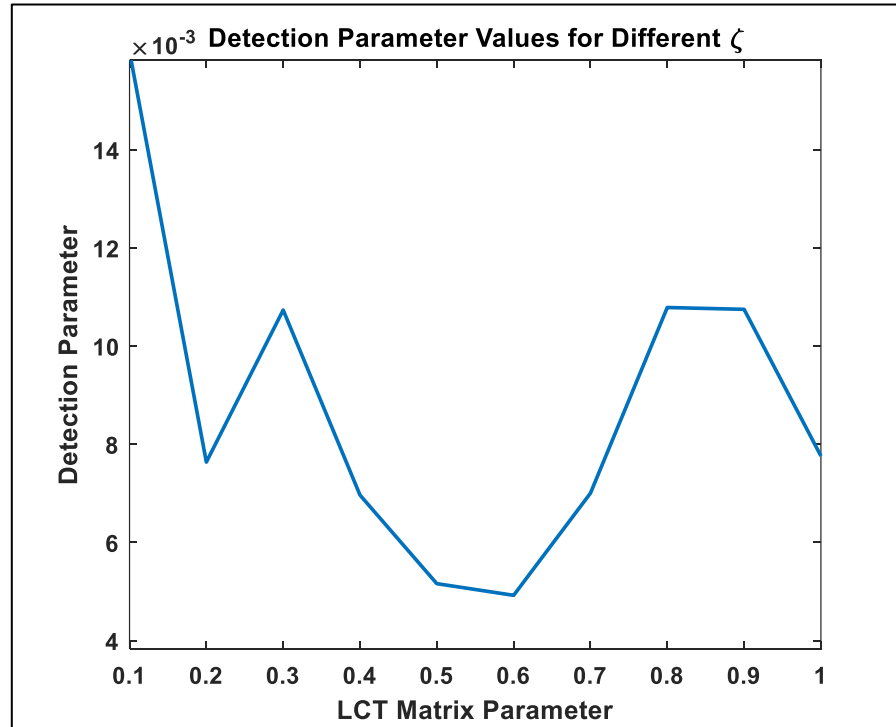


Figure 9.10: Detection Parameter Values for Different  $\zeta$

As evidenced from the table above, the watermarking scheme is blind the original audio cover signal is not required for the detection/extraction of the watermark. Further, the robustness of the scheme against the signal processing and feature distortive attacks is verified from the figures of merit obtained for attacks of different strength/degree on the watermarked audio signal, as provided in Table 9.2. The stability of can be verified from the observation that the values of the detection parameters for the random watermarks used during detection is lower than the stipulated threshold and the value of the detection parameter for the originally embedded watermark exceeds the threshold by over two times, on average. The proposed watermarking scheme is also imperceptible; thus, presence of the watermark cannot be ascertained during auditory perception. The security of the watermark is reinforced as the detection/extraction of the watermark is not possible as DLCT computed using wrong set of LCT matrix parameters will be invalid. This is evinced from the detection parameter calculated for the given set of LCT parameters used while embedding ( $\lambda = 0.2, \tau = 0.6, \zeta = 0.1$ ), which achieves

the highest values only with the original set of LCT parameters (as noticed from Fig. 9.8-9.10). Also, the proposed scheme also offers good payload capacity approximately 15% of that of the original audio signal. Its significance can be understood from the fact that maintenance of imperceptibility and robustness in watermarking are mutually exclusive.

## 9.2. IMAGE WATERMARKING IN FREQUENCY DOMAIN

The efficiency of the technique is assessed by the following criteria, namely the mean squared error (MSE), peak signal to noise ratio (PSNR) and the normalized cross-correlation (NC), which interrelated as follows

$$MSE = \frac{1}{XY} \sum_{u,v} (K(u,v) - L(u,v))^2 \quad (9.4)$$

where  $X$  and  $Y$  are the length and breadth of the original image  $K$  and recovered/transformed image  $L$ .

$$PSNR = 10 \log_{10} \left( \frac{255^2}{MSE} \right) \quad (9.5)$$

The above formula has been specified for 8-bit pixel representation.

$$NC = \frac{\sum_u \sum_v W \cdot W^*}{\sqrt{\sum_u \sum_v W^2 \sum_u \sum_v W^{*2}}} \quad (9.6)$$

where  $W$  and  $W^*$  denote the embedded and extracted watermarks respectively.

We present below the comparison between the original cover and watermarked images and the watermark samples retrieved under different attacks of

maximum strength/degree. Fig. 9.10 provides proof for the imperceptibility and robustness of the embedded watermark via the PNSR and NC figures of merit.



Figure 9.11: Original and Watermarked Cover Images

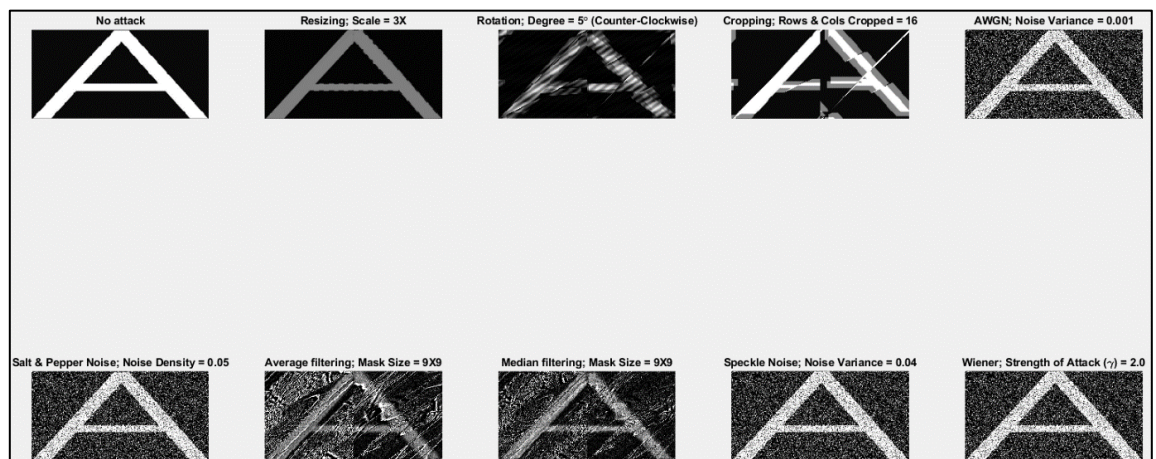


Figure 9.12: Extracted Watermark after different geometric/image processing attacks of maximum strength

Table 9.3: Figure of Merit of the Watermarking Scheme

S.No.	Type of Attack	Strength of Attack/Degree	PSNR of Cover Image (dB)	PSNR of Watermark (dB)	Normalized Cross-Correlation of Watermark
1	Resize (Fraction of the original size)	0.5	73.9100	38.5178	0.9935
		0.6	73.1125	38.5132	0.9815
		2	67.8894	38.5273	0.9904
		3	66.1284	38.5278	0.9825
2	Rotate (Degree in counter-clockwise direction)	0.5	70.9699	37.7033	0.8386
		1	71.0404	38.1968	0.8499
		2	71.1730	38.5027	0.8243
		5	71.4123	38.0223	0.7298
3	Cropping (Number of pixel rows/columns cropped)	4	70.9164	61.2108	0.9110
		8	70.9358	61.3730	0.8110
		12	70.9580	54.4265	0.7141
		16	70.9823	50.3144	0.6548
4	AWGN (Noise Variance)	0.0001	70.8806	72.1548	0.9201
		0.0002	70.7426	66.1481	0.8582
		0.0005	70.9034	64.8152	0.7246
		0.001	70.8313	60.1891	0.6007
5	Salt and Pepper (Noise Density)	0.005	70.4692	62.3712	0.6038
		0.01	70.9669	62.7389	0.5978
		0.02	69.8654	61.1450	0.5962
		0.05	69.6976	64.0218	0.6031
6	Averaging Filtering (Mask Size)	3x3	70.9120	39.4858	0.5598
		5x5	70.9521	38.7595	0.3112
		7x7	70.9332	38.4680	0.2267
		9x9	70.6814	38.2593	0.1874
7	Median Filtering (Mask Size)	3x3	72.1244	39.0164	0.6405
		5x5	74.1697	36.5256	0.3549
		7x7	75.6398	35.0586	0.2345
		9x9	73.6786	34.6463	0.1932
8	Speckle (Noise Variance)	0.005	71.0219	73.8053	0.5319
		0.01	71.0969	57.0549	0.4042
		0.02	70.9747	54.0407	0.2932
		0.04	72.8834	49.8277	0.2130
9		1.1	47.2339	47.3270	0.4927

Wiener Attack (Strength of Attack)	1.5	33.3520	27.6610	0.5596
	1.8	29.2693	16.3457	0.5574
	2.0	27.3307	14.0220	0.5562

We see that the scheme deters a large variety of geometric and signal processing attacks, as evidenced from Fig. 9.12. Further, the invisible method provides good levels of watermark imperceptibility. The watermarking is secured using Arnold Transform. Also, the watermarking scheme offers good payload capacity as watermark.

### 9.3. MOMENT BASED IMAGE WATERMARKING

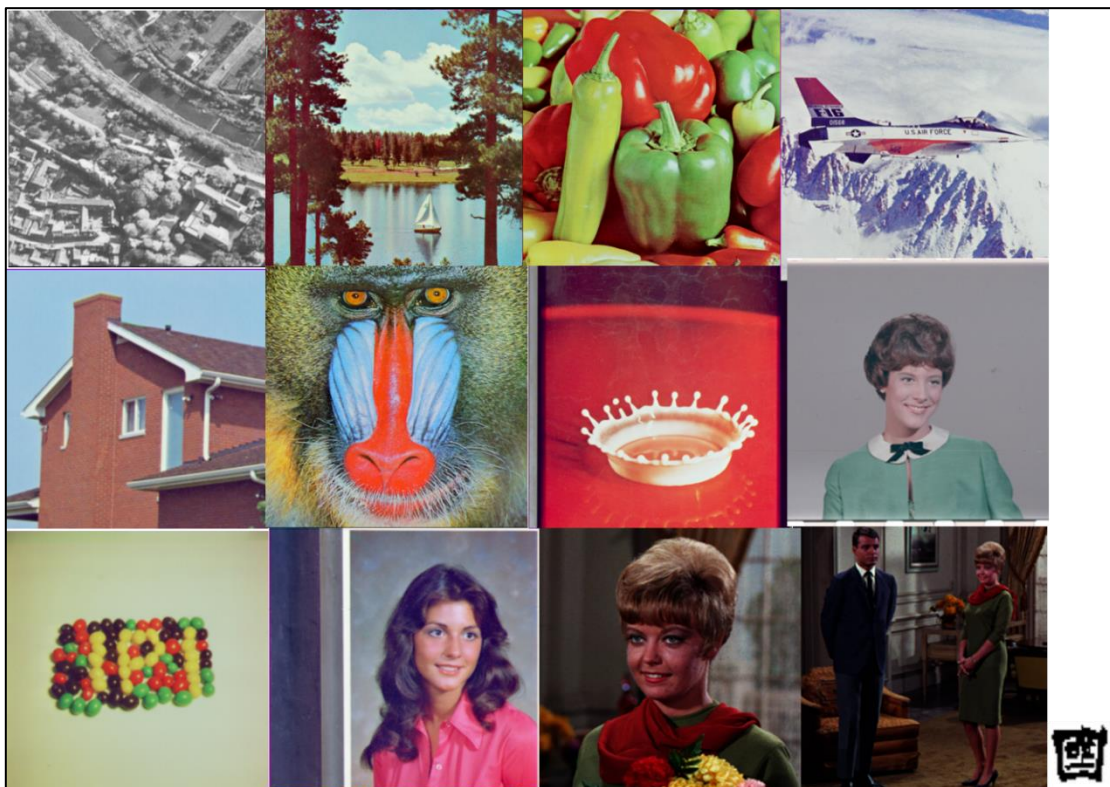


Figure 9.13: Different Cover Images and Watermark

The proposed zero-watermarking scheme was tested on twelve images from the popularly used USC-SIPI image database [4], each of dimensions 512 x 512 x 24 bit, as shown in Fig. 9.13, and referred to as “Aerial”, “Sailboat on lake”, “Peppers”, “Airplane”, “House”, “Mandrill”, “Splash”, “Female”, “Jelly beans”, “Girl”, “Female from Bell Labs” and “Couple, respectively. A binary watermark of size 64 X 64 bits, shown in the same Fig. 9.13, was used as the watermark image. The quantization step size was set as  $\Delta = 0.1$ . The value of the fractional parameter  $\beta$  was selected as 1.8, due to homogeneous variation of the radial function  $E_m(\rho, \beta)$  in the interval  $0 < \rho < 1$ , and as compared in Fig. 9.14 with different values of  $\beta$ . Further, the PSNR (Peak Signal-to-Noise Ratio) is used as a metric to estimate the visual quality of the image as well as to gauge the imperceptibility of the embedded watermark. Maximum order was kept as 100. Also, the experimental results are compared with schemes proposed in [84,92,93,65,91].

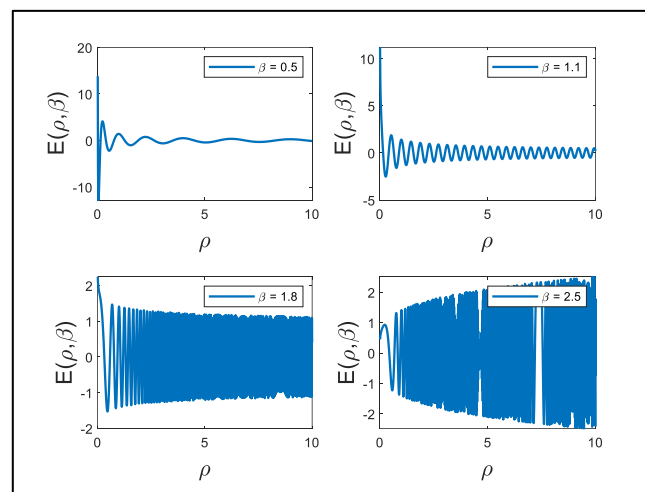


Figure 9.14: Variation of Radial Function  $E(\rho, \beta)$  with  $\beta$  in  $0 < \rho < 1$

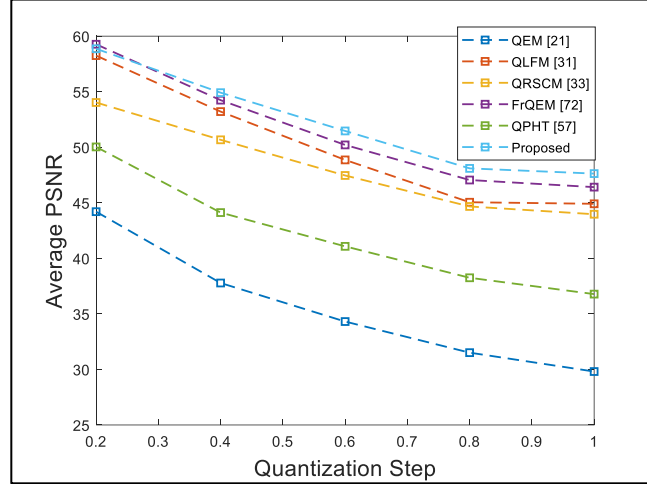


Figure 9.15: Average PSNR v/s Quantization Step  $\Delta$

### A. WATERMARK INVISIBILITY

As a figure of merit to estimate the imperceptibility of the embedded watermark, we use the Peak Signal-to-Noise Ratio (PSNR), which is expressed through the below relation

$$PSNR(I^w, I) = 10 \log_{10} \frac{255^2}{MSE} \quad (9.7)$$

where  $I^w$  and  $I$  represent the watermarked and the original images, respectively and

$$MSE = \frac{1}{M * N} \left( \sum_{c=1}^M \sum_{d=1}^N [I^w(c, d) - I(c, d)]^2 \right) \quad (9.8)$$

From Fig. 9.15, we observe that the PSNR falls (invisibility reduces) when quantization step size is increased. This is consistent with the theoretical definition and significance of the PSNR. We also see that the proposed scheme offers superior performance in respect of the invisibility than the state-of-the-art schemes based on orthogonal polar moments, QEMs and Fractional QEMs.

## B. WATERMARKING CAPACITY

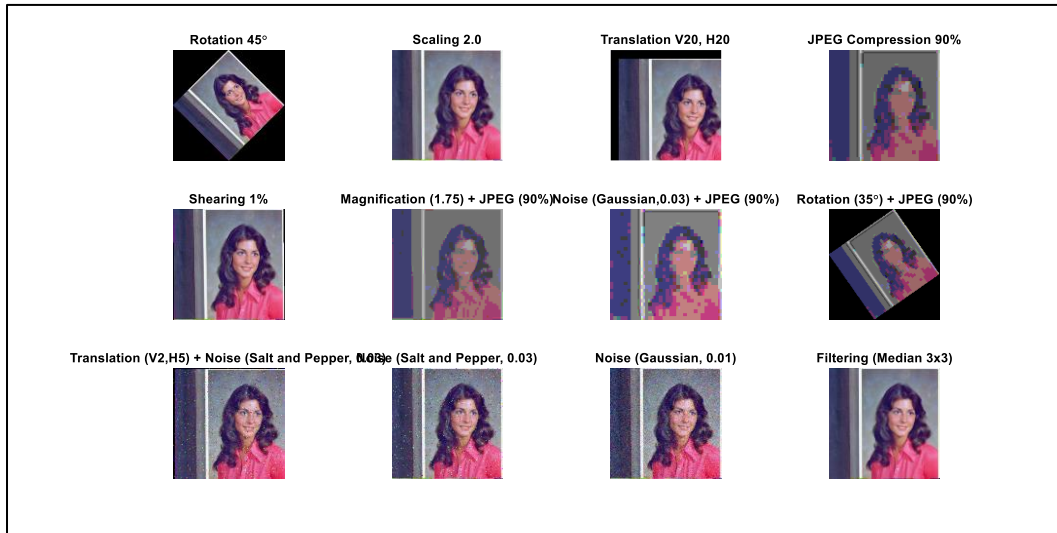


Figure 9.16: Attacked Watermarked Images

Capacity of the watermark is inferred from the number of FrGPCET moments which can be used for watermarking. These are in turn affected by the resolution of the cover image and the order of the FrGPCET. Increasing the order and resolution of the cover image, thereby enhances the robustness as well as increases the payload capacity. For the proposed zero watermarking scheme based on FrGPCET, it was found that the capacity of embedding the watermark nearly uniformly, for a cover image of 512 x 512 x 24 bits, grows with the increment in the order of the moments. Thus, the scheme exhibits good payload capacity.



### C. WATERMARKING ROBUSTNESS

The Bit Error Rate (BER) and Normalized Correlation (NC) are the two metrics used to quantify the robustness of the watermark. They should ideally be 0 and 1, respectively.

$$BER = \frac{1}{PXQ} \left( \sum_{c=1}^P \sum_{d=1}^Q [w(c, d) - \tilde{w}(c, d)]^2 \right) \quad (9.9)$$

$$NC = \frac{\sum_{c=1}^P \sum_{d=1}^Q [w(c, d) * \tilde{w}(c, d)]}{\sum_{c=1}^P \sum_{d=1}^Q w(c, d)} \quad (9.10)$$

where  $w$  and  $\tilde{w}$  are the embedded and extracted watermarks, respectively.

Fig. 9.16 shows the watermarked images which were subjected to a host of signal processing and desynchronization attacks. For the sake of representation, we have shown the results for the cover image “Female”. The attacks include rotation, scaling, translation, JPEG compression, noise addition and a combination of these attacks. Specifically, these have been mentioned against each of the attacked images. It can be clearly seen that all these images maintain the invisibility of the watermark. Further, the watermark extracted from them under different strength of attacks, including the ones shown in Fig. 9.16, have been provided in Table 9.4. It should also be noted that the watermarked images which were subjected to different attacks, as mentioned in Fig. 9.14 correspond to the attacks of moderate strength/degree.

For comparison, we use the BER and NC results obtained for orthogonal polar and Cartesian moments, QEMs and FrQEMs. Specifically, we compare our results

with the works based on QEM [84], QLFM [92], QRSCM [93], FrQEM [65] and QPHT [91]. The extracted binary watermarks for different kinds and strengths of attacks have been tabulated under Table 9.4. Table 9.5 and Table 9.6 list the BER and NC values corresponding to the watermarks retrieved from the attacked images and shown in Table I.

Table 9.4 Extracted Watermark under Different Attacks

Attacks	Strength	QEM [84]	QLFM [92]	QRSCM [93]	FrQEM [65]	QPHT [91]	Proposed
Rotation	15						
	35						
	45						
Scaling	0.75						
	1.5						
	2						
Translation	H3, V3						
	H6, V6						
Magnification	(1.75) (25%)						
	+(0.75) 90%)						
Rotation	+						
Compression	++						

	Proposed	QPHT [91]	FrQEM [65]	QRSCM [93]	QLFM [92]	QEM [84]	Strength	Attacks
							(1.75 90%)	Magnificati on
							+(25° 90%)	Rotation
							+80%	+Compressi on
							90%	+Compressi on
							0.03	Noise, Salt and Pepper
							0.03	Noise Gaussian
							3x3	Gaussian Filtering
							3x3	Median Filtering

Table 9.5 BER Of the Watermark Retrieved under Different Attacks

Attacks	Strength	QEM [84]	QLFM [92]	QRSCM [93]	FrQEM [65]	QPHT [91]	Proposed
Rotation	5	0.087	0.060	0.054	0.020	0.151	0.019
	15	0.070	0.047	0.047	0.019	0.158	0.019
	35	0.055	0.036	0.044	0.017	0.153	0.014
	45	0.054	0.045	0.045	0.015	0.151	0.018
Scaling	0.5	0.087	0.050	0.046	0.018	0.198	0.012
	0.75	0.078	0.046	0.051	0.016	0.137	0.014
	1.5	0.028	0.009	0.012	0.004	0.089	0.005
	2	0.032	0.007	0.020	0.003	0.058	0.001
Translation	H1, V1	0.054	0.019	0.010	0.007	0.081	0.004
	H3, V3	0.018	0.020	0.010	0.003	0.062	0.001
	H6, V6	0.047	0.021	0.020	0.004	0.063	0.002
	H9, V9	0.065	0.018	0.018	0.005	0.564	0.003
Rotation on Magnification Rotation on Compression Rotation on Magnification Rotation on Compression Rotation on Magnification Rotation on Compression	(1.75) (25°)	0.169	0.021	0.024	0.004	0.034	0.001
	+(0.75) 90%)	0.106	0.020	0.021	0.010	0.055	0.003
	+(1.75) 90%)	0.088	0.010	0.012	0.004	0.029	0.001
	+(25°) 90%	0.140	0.045	0.056	0.019	0.074	0.003
	+40%	0.054	0.073	0.015	0.006	0.156	0.004

Attacks	Strength	QEM [84]	QLFM [92]	QRSCM [93]	F+QEM [65]	QPHT [91]	Proposed
	50%	0.049	0.006	0.012	0.004	0.129	0.003
	80%	0.020	0.012	0.018	0.005	0.085	0.002
	90%	0.010	0.002	0.004	0.003	0.069	0.001
Noise, SaltNoise and Pepper	0.03	0.084	0.014	0.015	0.006	0.016	0.003
	0.03	0.072	0.010	0.018	0.003	0.029	0.001
Gaussian Filtering	3x3	0.100	0.012	0.014	0.004	0.016	0.001
Median Filtering	3x3	0.085	0.013	0.028	0.006	0.034	0.003

Table 9.6 NC of the watermark retrieved under different attacks

Attacks	Strength	QEM [84]	QLFM [92]	QRSCM [93]	F+QEM [65]	QPHT [91]	Proposed
Rotation	5	0.901			0.966	0.775	0.989
	15	0.914	0.940	0.940	0.975	0.794	0.991
	35	0.931	0.955	0.944	0.978	0.794	0.995

Proposed	QPHT [91]	F+QEM [65]	QRSCM [93]	QLFM [92]	QEM [84]	Strength	Attacks
0.998	0.794	0.975	0.943	0.943	0.932	45	
0.978	0.789	0.964			0.891	0.5	Scaling
0.995	0.814	0.979	0.937	0.942	0.904	0.75	
0.999	0.882	0.994	0.984	0.988	0.965	1.5	
0.999	0.925	0.995	0.974	0.990	0.960	2	
0.999	0.918	0.997			0.987	H1, V1	Translation
0.999	0.923	0.995	0.986	0.974	0.977	H3, V3	
0.998	0.922	0.994	0.974	0.973	0.941	H6, V6	
0.999	0.900	0.989			0.932	H9, V9	
0.997	0.958	0.994	0.969	0.973	(1.75) (25°)	0.767	Magnification on Rotation
0.999	0.931	0.986	0.973	0.974	+(0.75) 90%)	0.859	Reduction on Compression
0.999	0.964	0.994	0.984	0.986	+(1.75) 90%)	0.888	Magnification on Compression
0.999	0.910	0.975	0.930	0.943	+(25°) 90%	0.813	Rotation on Compression
0.999	0.854	0.987	0.965	0.986	+40%	0.962	+Compression
0.993	0.869	0.983	0.952	0.990	50%	0.970	

Attacks	Strength	QEM [84]	QLFM [92]	QRSCM [93]	FrQEM [65]	QPHT [91]	Proposed
	80%	0.974	0.984	0.976	0.992	0.883	0.989
	90%	0.986	0.996	0.994	0.995	0.910	0.997
Noise, Salt and Pepper	Noise	0.03	0.890	0.982	0.980	0.991	0.979
	Salt and Pepper	0.03	0.906	0.986	0.976	0.995	0.964
Gaussian Filtering	3x3	0.867	0.984	0.982	0.994	0.979	0.999
Median Filtering	3x3	0.895	0.983	0.965	0.991	0.958	0.999

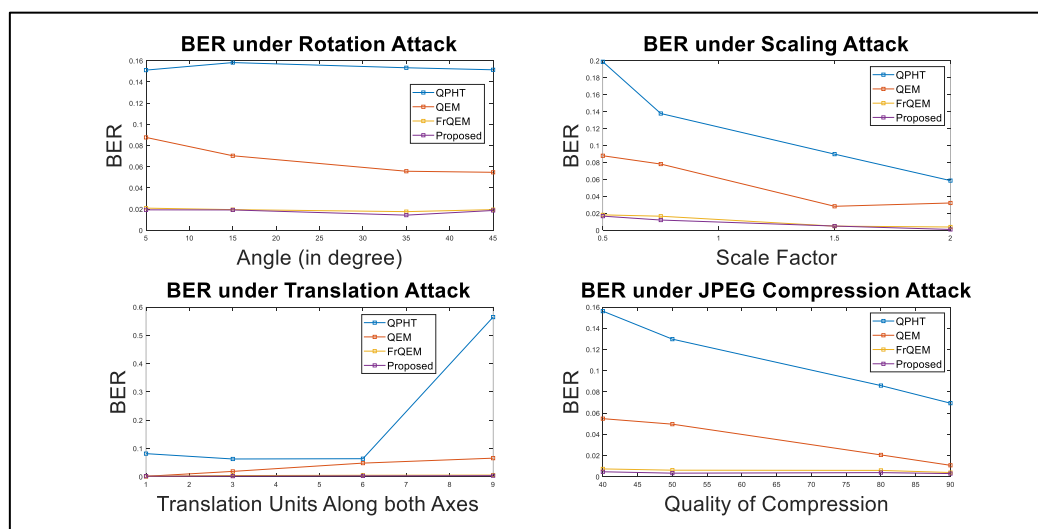


Figure 9.17: BER for Rotation, Scaling, Translation and JPEG compression attacks

From Table 9.4, it is clear that the quality of the watermark retrieved from the proposed scheme is much better in terms of visual appearance when compared to the other schemes. This is a testimony of the higher robustness of the embedded watermark and its greater resilience against a wide range of signal processing and desynchronization attacks.

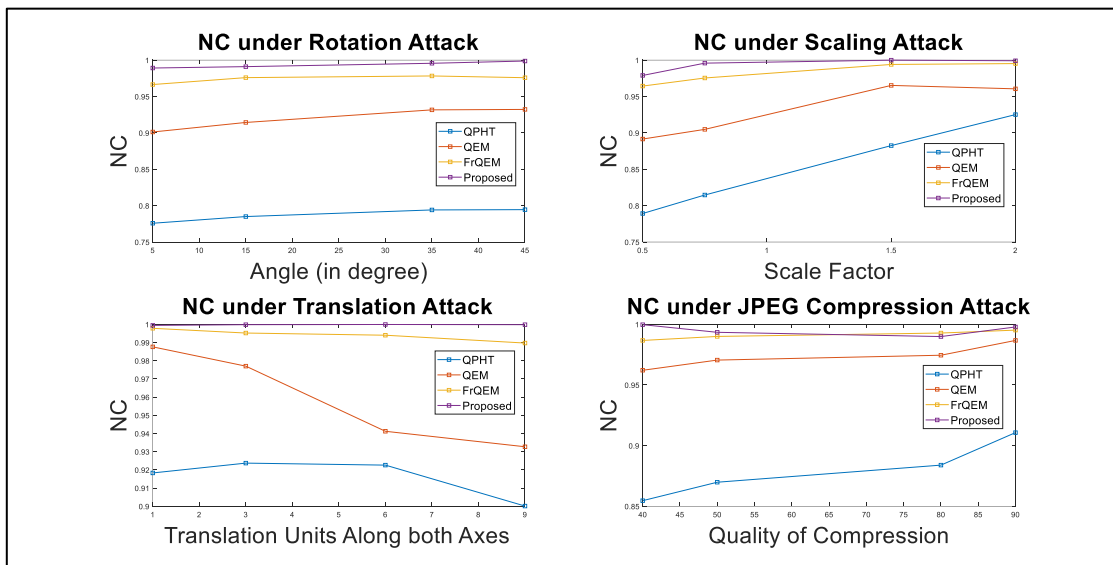


Figure 9.18: NC for Rotation, Scaling, Translation and JPEG compression attacks

From Table 9.5 and Table 9.6, we can see that the values of the BER are lower and that of NC are higher for a particular type and strength of attack executed on a given image, watermarked using the state-of-the-art techniques. This demonstrates the superiority in terms of robustness and stability of the embedded watermark. The proposed scheme therefore, is said to offer a strong resistance to a diverse set of signal processing and desynchronization attacks. The values of the BER and NC for Rotation, Scaling, Translation and JPEG compression attacks of varying strength and degree have also been plotted graphically in Fig. 9.17 and Fig. 9.18 to show the primacy of the proposed scheme



over the state-of-the-art schemes. It should be noted that the overall BER for the proposed scheme is lower than the state-of-the-art schemes. Also, the NC of the proposed scheme is higher than the state-of-the-art schemes for the givens set of signal processing and desynchronization attacks.

#### 9.4. IMAGE WATERMARKING USING GRAPH SIGNAL PROCESSING AND LOCAL DOMINANT FEATURES

The efficiency of the technique is assessed by the mean squared error (MSE), peak signal to noise ratio (PSNR) and the normalized cross-correlation (NC), which interrelated as follows

$$MSE = \frac{1}{OP} \sum_{u,v} (K(u,v) - L(u,v))^2 \quad (9.11)$$

where O and P are the length and breadth of the cover work K and recovered/transformed image L.

$$PSNR = 10 \log_{10} \left( \frac{255^2}{MSE} \right) \quad (9.12)$$

The above formula has been specified for 8-bit pixel representation.

$$NC = \frac{\sum_u \sum_v W \cdot W^*}{\sqrt{\sum_u \sum_v W^2 \sum_u \sum_v W^{*2}}} \quad (9.13)$$

where  $W$  and  $W^*$  represent the embedded and extracted watermarks respectively.

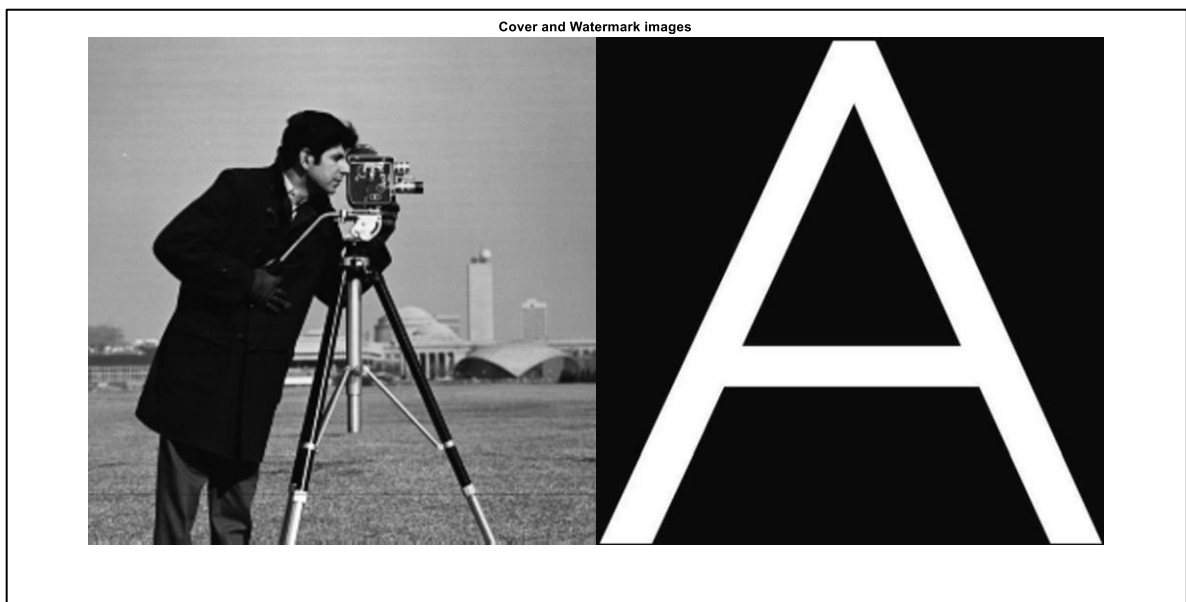


*Figure 9.19: Original Cover Work and Watermark*

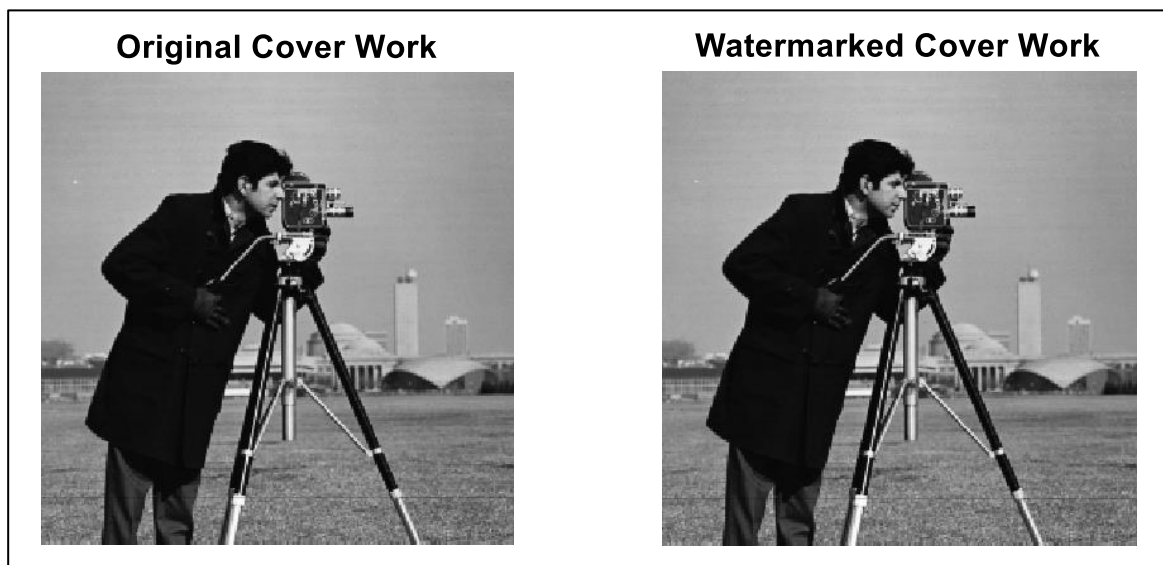


*Figure 9.20: Original vs Watermarked Cover Work*

We present below the comparison between the original cover and watermarked images and the watermark samples retrieved under different attacks of

maximum strength/degree. Table 9.7 provides proof for the imperceptibility and robustness of the embedded watermark via the PSNR and NC figures of merit.

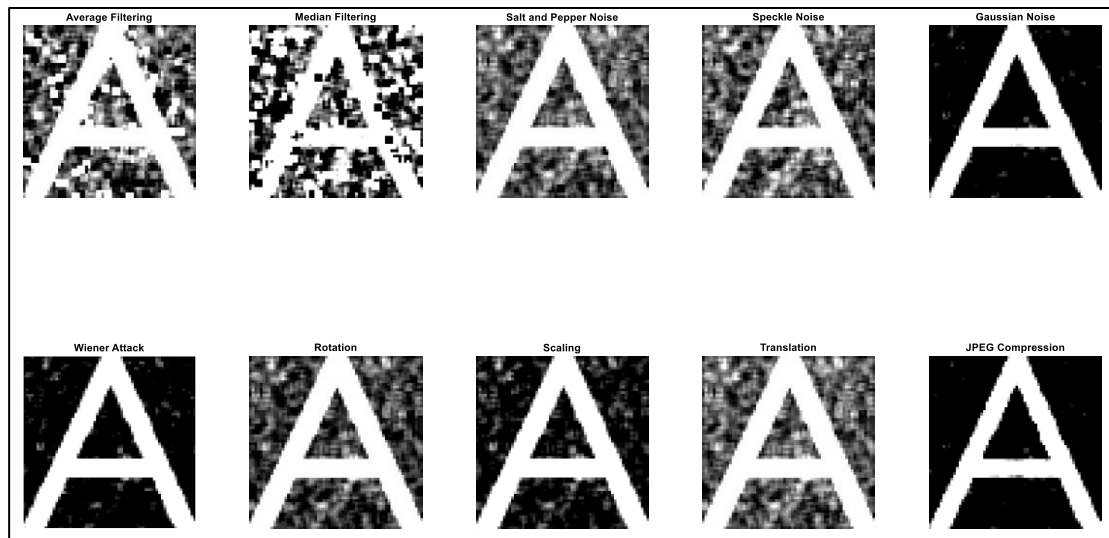


Figure 9.21: Watermark Retrieved under Different Attacks of Maximum Strength/Degree

Table 9.7: PSNR of Cover Image and Watermark and NC of Watermark

S.No.	Type of Attack	Strength of Attack/Degree	PSNR of Cover Image (dB)	PSNR of Watermark (dB)	Normalized Cross-Correlation of Watermark
1	Average Filtering	3x3	72.6538	40.2365	0.9013
		5x5	69.5841	39.6528	0.9024
		7x7	66.2354	98.7589	0.8956
		9x9	64.2879	37.2145	0.8856
2	Median Filtering	3x3	68.2354	39.5492	0.9124
		5x5	67.8912	39.4787	0.8946
		7x7	67.5466	38.2974	0.8975
		9x9	66.9877	38.6937	0.8912
3	Salt and Pepper Noise	0.005	72.3654	62.5687	0.9256
		0.01	72.8974	62.3297	0.9221
		0.02	72.6999	60.2583	0.9023
		0.05	73.5684	59.8946	0.9009
4	Speckle Noise	0.005	71.5689	70.2567	0.9263
		0.01	71.2415	70.4517	0.9214
		0.02	70.6598	70.6668	0.9119

5	Gaussian Noise	0.04	70.2634	69.3546	0.9096
		0.0001	72.6589	64.2332	0.9326
		0.0002	72.5445	64.5784	0.9216
		0.0005	72.2638	63.2987	0.9225
		0.001	71.6259	64.2387	0.9198
6	Wiener Attack	1.1	73.6523	39.4877	0.9987
		1.5	73.8977	39.1201	0.9963
		1.8	73.5688	38.6774	0.9982
		2.0	73.5124	38.5666	0.9912
7	Rotation	0.5	69.8456	40.6523	0.9423
		1	68.9566	40.6612	0.9356
		2	68.6771	39.9984	0.9247
		5	68.4598	39.7846	0.9267
8	Scaling	0.5	72.5688	71.6645	0.9356
		0.6	72.6254	71.8425	0.9354
		2	71.8574	70.6528	0.9237
		3	71.2694	70.2341	0.9264
9	Translation	H1,V1	68.2341	40.1245	0.9236
		H1,V3	68.5746	39.6847	0.9268
		H3,V1	68.0101	37.4655	0.9211
		H3,V3	67.6263	35.8911	0.9167
10	JPEG Compression	40	69.6789	38.6847	0.9845
		50	69.2345	39.0015	0.9876
		80	69.7171	38.5496	0.9990
		90	68.4572	38.5441	0.9941

It is evinced that the watermarking scheme is non-blind. However, it endures a large variety of signal processing and feature distortive attacks, as evidenced from Figure 9.21. Due to its invisible nature, it provides high levels of watermark imperceptibility. The security of is ensured via by the Arnold transform. The salient feature of this watermarking scheme is its power spectrum compatibility which enables it to effectively deal with MMSE type attacks. The proposed scheme offers good payload capacity it allows embedding of watermark nearly equal to the size of the cover media.

## **CHAPTER 10**

### **CONCLUSION**

Preservation of the authenticity of the data and ensuring the non-infringement intellectual rights of the owners and authorized users is of key importance in the generation, exchange and transmission of the data. With the attacks on the secured information becoming more advanced with the progress made by the technology, we need to effectively deal with problems of such kind, by ensuring that the content of the data being transmitted is minimally modified, if not left unchanged, on exposure to such attacks. Further, the identity of the owner and her intellectual rights should not be compromised.

Through the use of digital watermarking we embed secret data (watermark) in the cover work, through minimal modification of its content. This is key to maintaining the imperceptibility of the embedded watermark. Also, necessary levels of robustness and security can be attained under applicable trade-offs.

Implementation of the watermarking on 1-D, 2-D data and 3-D data was undertaken as the challenges encountered in the process and the developed countermeasures would prove instrumental in addressing similar issues where applications involve cover work with higher data volume and complexity.

We begin by performing the watermarking of the audio signal in the time-frequency domain using the linear canonical transform (LCT), by employing frequency dependent clustering. It was found that the watermark securely resisted a wide range of signal processing and audio feature distortive attacks and offered a good payload capacity up to 15% of the audio signal length. The research undertaken as part of this watermarking experiment has been published under the title “Audio Watermarking in Linear Canonical Transform Domain Using Frequency-Dependent Clustering” in *Cyber Intelligence and Information Retrieval*, 978-981-16-4283-8, 513403\_1\_En, (Chapter 15) (Refer Appendix A).

Next, we shifted our focus to 2-D and 3-D data, in the form of grayscale and colour RGB images, respectively. We deployed the Image Partitioning technique which is based on the use of psycho-visual redundancy in the image. Post watermark scrambling using Arnold Transform, it was inserted in the lowest frequency DWT sub-band. This bolstered the security, robustness as well as the imperceptibility of the proposed technique vis-a-vis existing schemes. The experimental results obtained as part of this research have been published under the title “A Secure Wavelet based Watermarking Approach using Psycho-Visual Redundancy in Image” in the conference proceedings of IEEE conference 2021 7th International Conference on Advanced Computing and Communication Systems (ICACCS) (Refer Appendix A).

For 3-D colour (RGB) images, we proposed 2 techniques. As many image moments suffer from limited reconstruction ability, errors during numerical approximation, low stability and diminished feature integrity, we described a novel two-tiered zero watermarking framework for color images using Fractional Order Generic Polar Complex Exponential Transform (FrGPCET). This was secured through the use of quasi-affine

transform and two-tiered methodology. The scheme was made stable and accurate through calculation of fractional order moments. Through incrementally iterative pseudo-random selection and Otsu thresholding, an augmented moment feature vector was formed which is in-turn used for embedding the watermark. The second tier featured the use of Discrete Cosine Transform and Huffman coding. Its primary objective was to reduce the visibility of the embedded watermark. Comparison with the state-of-the-art methodologies revealed that the proposed technique surpasses them in terms of watermark's imperceptibility and robustness to different attacks. Further, it was inherently secure, offered good payload capacity. Additionally, the experimental results obtained as part of this research have been submitted for publication to IEEE Access journal.

Our second approach was based on enhancing the similarity between the power spectra of the host and watermark images. This was done to mitigate the strength of the attacks based on estimation of the MMSE, thus leading to an energy efficient watermarking scheme offering contemporary imperceptibility and robustness against state-of-the-art watermarking techniques. The principles leveraged included inter alia graph signal processing, spectral graph wavelet, variational mode decomposition and local dominant orientation feature extraction. Each of them contributed towards the improvement of the watermarking characteristics, quantified in terms of imperceptibility, robustness, security, payload capacity and energy efficiency.

## REFERENCES

1. Q. Wu., M. Wu “A Novel Robust Audio Watermarking Algorithm by Modifying the Average Amplitude in Transform Domain”, *in Appl. Sci.* , vol. 8, issue 5, pp. 723 (2018)
2. A. Al-Haj. “An imperceptible and robust audio watermarking algorithm”, *EURASIP Journal on Audio, Speech, & Music Processing*. 2014, 37 (2014).
3. Global Music Report 2021. International Federation of Phonographic Industry (IFPI), [https://www.ifpi.org/wpcontent/uploads/2020/03/GMR2021\\_STATE\\_OF\\_THE\\_INDUSTRY.pdf](https://www.ifpi.org/wpcontent/uploads/2020/03/GMR2021_STATE_OF_THE_INDUSTRY.pdf)
4. Abbas Cheddad, Joan Condell, Kevin Curran, Paul Mc Kevitt, "Digital image steganography: Survey and analysis of current methods," *Signal Processing*, vol. 90 (3), pp. 727-752 (2010)
5. I.J.Cox, J. F. (1997). Secure spread spectrum watermarking for multimedia. *IEEE Transactions on Image Processing*, 6, 1673-1687.
6. D. Megías, J. Herrera, J. Minguillón, “Robust Frequency Domain Audio Watermarking: A Tuning Analysis”, *Lecture Notes in Computer Science*, vol 3304, pp. 244-258. Springer, Berlin, Heidelberg (2004)
7. A. A. Attari and A. A. B. Shirazi, "Robust and Transparent Audio Watermarking based on Spread Spectrum in Wavelet Domain," *2019 IEEE Jordan International Joint Conference on Electrical Engineering and Information Technology (JEEIT)*, 2019, pp. 366-370
8. N. Cvejic,, T. Seppanen, “Digital Audio Watermarking Techniques and Technologies: Applications and Benchmarks”, 1<sup>st</sup> edn. IGI Global, Hershey PA, USA (2007).
9. P.K. Dhar, T. Shimamura, “Blind Audio Watermarking in Transform Domain Based on Singular Value Decomposition and Exponential-Log Operations”, *Radioengineering* vol. 26, no. 2, pp. 552-561 (2011)
10. Zhang, H., A Time-Frequency Perspective on Audio Watermarking, <https://arxiv.org/abs/2002.03156>
11. Wei-Min Yang, Z. J. (2009). A watermarking Algorithm Based on Wavelet and Cosine Transform for Color Image. *International Workshop on Education Technology and Computer Science*, (pp. 899-903).
12. H. Guang, J. Huang, J. Y. Shi, J. Goh, V. Thing, “Twenty years of digital audio watermarking-a comprehensive review”, *Signal Process.*, vol. 128, pp. 222–242 (2016).



13. S.K. Narang, A. Ortega: 'Perfect reconstruction two-channel wavelet filter banks for graph structured data', in *IEEE Trans. Signal Process.*, vol. 60, issue 6, pp. 2786–2799, 2012
14. D.K. Hammond., P. Vandergheynst, R. Gribonval: 'Wavelets on graphs via spectral graph theory', in *Appl. Comput. Harmon. Anal.*, vol. 30, issue 2, pp. 129–150, 2011
15. S.K. Narang, A. Ortega: 'Compact support biorthogonal wavelet filter banks for arbitrary undirected graphs', in *IEEE Trans. Signal Process.*, vol. 60, issue 19, pp. 4673–4685, 2013
16. D.I. Shuman, S.K.,Narang, P. Frossard, *et al.*: 'The emerging field of signal processing on graphs: extending high-dimensional data analysis to networks and other irregular domains', in *IEEE Signal Process.*, vol. 30, issue 3, pp. 83–98, 2013
17. X. Zhang: 'Design of orthogonal graph wavelet filter banks'. In IEEE annual Conf. (IECON), pp. 889–894, October 2016
18. P. K. Dhar and I. Echizen, "Robust FFT Based Watermarking Scheme for Copyright Protection of Digital Audio Data," 2011 Seventh International Conference on Intelligent Information Hiding and Multimedia Signal Processing, 2011, pp. 181-184
19. J. Liu, Z. Lu and J. Pan, "A Robust Audio Watermarking Algorithm Based on DCT and Vector Quantization," 2008 Eighth International Conference on Intelligent Systems Design and Applications, 2008, pp. 541-544
20. J. Panda, K.R. Gera, A. Bhattacharya, "Non-Blind Audio Watermarking Scheme Based on Empirical Mode Decomposition", International Journal of Advanced Science, Engineering and Technology, vol. 3, no. 3, pp. 38-43 (2014)
21. R.Esgandari and Mehdi Khalili, "A robust image watermarking scheme based on discrete wavelet transforms", 2nd International Conference on Knowledge-Based Engineering and Innovation (KBEI), pp. 988-992, Nov 2015.
22. Q. Su, X. Liu, W. Yang, "A watermarking algorithm for color image based on YIQ color space and Integer Wavelet Transform," International Conference on Image Analysis and Signal Processing, Apr 2009.
23. Z. Rui-mei; W. Mei; H. Bo-ning; L. Hua, "Digital Image Watermarking Algorithm Based on Wavelet Transform", Third International Symposium on Intelligent Information Technology Application, Nov 2009.
24. W. Yang; Z. Jin, "A Watermarking Algorithm Based on Wavelet and Cosine Transform for Color Image", First International Workshop on Education Technology and Computer Science, pp. 899-903, Mar 2009.
25. C. -. Teh and R. T. Chin, "On image analysis by the methods of moments," in *IEEE Transactions on Pattern Analysis and Machine Intelligence*, vol. 10, no. 4, pp. 496-513, July 1988
26. G.A. Papakostas, "Improving the Recognition Performance of Moment Features by Selection", Stańczyk U., Jain L. (eds) *Feature Selection for Data and Pattern Recognition. Studies in Computational Intelligence*, vol. 584 (2015)
27. J. Kautsky and J. Flusser, "Blur Invariants Constructed From Arbitrary Moments," in *IEEE Transactions on Image Processing*, vol. 20, no. 12, pp. 3606-3611, Dec. 2011
28. M. Alghoniemy and A. H. Tewfik, "Image watermarking by moment invariants," *Proceedings 2000 International Conference on Image Processing (Cat. No.00CH37101)*, 2000, pp. 73-76 vol.2

29. G.A. Papakostas, Y.S. Boutalis, D.A. Karras, et al., "Efficient computation of Zernike and Pseudo-Zernike moments for pattern classification applications", *Pattern Recognit. Image Anal.*, vol. 20, pp. 56-64 (2010)
30. Khalid M. Hosny, "Exact Legendre moment computation for gray level images", *Pattern Recognition*, vol. 40, no. 12, pp. 3597-3605 (2007)
31. R. Mukundan, S. H. Ong and P. A. Lee, "Image analysis by Tchebichef moments," in *IEEE Transactions on Image Processing*, vol. 10, no. 9, pp. 1357-1364, Sept. 2001
32. Xiang-Yang Wang, Yi-Ping Yang, Hong-Ying Yang, "Invariant image watermarking using multi-scale Harris detector and wavelet moments", *Computers & Electrical Engineering*, vol. 36, no. 1, pp. 31-44 (2010)
33. E.D. Tsougenis, G.A. Papakostas, D.E. Koulouriotis, E.G. Karakasis, "Adaptive color image watermarking by the use of quaternion image moments", *Expert Systems with Applications*, vol. 41, no. 14, pp. 6408-6418 (2014)
34. George A. Papakostas, "Over 50 Years of Image Moments and Moment Invariants", *Moments and Moment Invariants - Theory and Applications*, vol. 1, Science Gate Publishing 2014
35. G.A. Papakostas, E.D. Tsougenis, D.E. Koulouriotis, "Moment-based local image watermarking via genetic optimization", *Applied Mathematics and Computation*, vol. 227, pp. 222-236 (2014)
36. J. Flusser, B. Zitova, and T. Suk, *Moments and Moment Invariants in Pattern Recognition*. John Wiley & Sons, 2009.
37. M. R. Teague, "Image analysis via the general theory of moments," *J. Opt. Soc. Am. A*, vol. 70, no. 8, pp. 920-30, Aug 1980.
38. T. Suk and J. Flusser, "Affine moment invariants of color images," in *Proc. Int. Conf. Comput. Anal. Images Patterns*, Sep. 2009, pp. 334-341.
39. Y. Xin, S. Liao, and M. Pawlak, "Circularly orthogonal moments for geometrically robust image watermarking," *Pattern Recognit.*, vol. 40, no. 12, pp. 3740-3752, Dec. 2007.
40. I. Djurovic, H. Stankovic, I. Pitas, "Digital watermarking in the fractional Fourier transformation domain", *Journal of Network and Computer Applications*, vol. 24, no. 2, pp. 167-173 (2001).
41. Q. Xiang and K. Qin, "The Linear Canonical Transform and Its Application to Time-Frequency Signal Analysis," *2009 International Conference on Information Engineering and Computer Science*, 2009, pp. 1-4
42. F. S. Oktem and H. M. Ozaktas, "Exact Relation Between Continuous and Discrete Linear Canonical Transforms," in *IEEE Signal Processing Letters*, vol. 16, no. 8, pp. 727-730
43. J.J. Healy, J.T. Sheridan, "Sampling and discretization of the linear canonical transform", *Signal Processing*, vol. 89, no. 4, pp. 641-648 (2009)
44. G.A. Papakostas, Y.S. Boutalis, D.A. Karras, B.G. Mertzios, "Pattern classification by using improved wavelet Compressed Zernike Moments", *Applied Mathematics and Computation*, vol. 212, no. 1, pp. 162-176 (2009)
45. G.A. Papakostas, Y.S. Boutalis, D.A. Karras, B.G. Mertzios, "A new class of Zernike moments for computer vision applications", *Information Sciences*, vol. 177, no. 13, pp. 2802-2819 (2007)
46. R. Mukundan, KR Ramakrishnan, *Moment functions in image analysis*. World Scientific Publishing, Singapore (1998)

47. P. . -T. Yap, R. Paramesran and Seng-Huat Ong, "Image analysis by Krawtchouk moments," in *IEEE Transactions on Image Processing*, vol. 12, no. 11, pp. 1367-1377, Nov. 2003
48. Hyung Shin Kim and Heung-Kyu Lee, "Invariant image watermark using Zernike moments," in *IEEE Transactions on Circuits and Systems for Video Technology*, vol. 13, no. 8, pp. 766-775, Aug. 2003
49. Yongqing Xin, Simon Liao, Mirosław Pawlak, Circularly orthogonal moments for geometrically robust image watermarking, *Pattern Recognition*, vol. 40, no. 12, pp. 3740-3752 (2007)
50. Cheng Deng, Xinbo Gao, Xuelong Li, Dacheng Tao, A local Tchebichef moments-based robust image watermarking, *Signal Processing*, vol. 89, no. 8, pp. 1531-1539 (2009)
51. G.A. Papakostas, E.D. Tsougenis, D.E. Koulouriotis, V.D. Tourassis, "On the robustness of Harris detector in image watermarking attacks", *Optics Communications*, vol. 284, no. 19, pp. 4394-4407 (2011)
52. Hong-Ying Yang, Xiang-Yang Wang, Pan-Pan Niu, and Ai-Long Wang., "Robust Color Image Watermarking Using Geometric Invariant Quaternion Polar Harmonic Transform", *ACM Trans. Multimedia Comput. Commun. Appl.*, vol. 11, no. 3, Article (2015)
53. V. Balntas, K. Lenc, A. Vedaldi, T. Tuytelaars, J. Matas, and K. Mikolajczyk, "H-Patches: A benchmark and evaluation of handcrafted and learned local descriptors," *IEEE Trans. Pattern Anal. Mach. Intell.*, vol. 42, no. 11, pp. 2825-2841
54. K. Mikolajczyk and C. Schmid, "A performance evaluation of local descriptors," *IEEE Trans. Pattern Anal. Mach. Intell.*, vol. 27, no. 10, pp. 1615-1630, Oct. 2005.
55. J. Yuan, Y. Wu, and M. Yang, "Discovery of collocation patterns: from visual words to visual phrases." in *Proc. IEEE Conf. Comput. Vis. Pattern Recognit.*, Jun. 2007, pp. 1-8.
56. M. K. Hu, "Visual pattern recognition by moment invariants," *IRE Trans. Inf. Theory*, vol. 8, no. 2, pp. 179-187, Feb. 1962.
57. Dong Xu and Hua Li, "3-D Surface Moment Invariants," 18th International Conference on Pattern Recognition (ICPR'06), 2006, pp. 173-176
58. T. V. Hoang, "Image representations for pattern recognition," Ph.D. dissertation, Dept. Comput. Sci., Nancy 2 Univ., Nancy, France, 2011.
59. H. Zhu, H. Shu, J. Zhou, L. Luo, and J. L. Coatrieux, "Image analysis by discrete orthogonal dual Hahn moments," *Pattern Recognit. Lett.*, vol. 28, no. 13, pp. 1688-1704, Oct. 2007.
60. H. Zhu, H. Shu, J. Liang, L. Luo, and J. L. Coatrieux, "Image analysis by discrete orthogonal Racah moments," *Signal Process.*, vol. 87, no. 4, pp. 687-708, Apr. 2007.
61. J. Shen, Orthogonal Gaussian-Hermite moments for image characterization, in *Proc. SPIE Intell. Rob. Comput. Vis.*, Sep 1997, pp. 224-233.
62. K. M. Hosny, "Image representation using accurate orthogonal Gegenbauer moments," *Pattern Recognit. Lett.*, vol. 32, no. 6, pp. 795-804, Apr. 2011.
63. H. Zhu, "Image representation using separable two-dimensional continuous and discrete orthogonal moments," *Pattern Recognit.*, vol. 45, no. 4, pp. 1540-1558, Apr. 2012.
64. C. Singh and J. Singh, "Multi-channel versus quaternion orthogonal rotation invariant moments for color image representation," *Digit. Signal Process.*, vol. 78, pp. 376392, Jul. 2018, 10.1016/j.dsp.2018.04.001.

65. X. Hongcai, X. Kang, Y. Chen, Y. Wang, "Rotation and scale invariant image watermarking based on polar harmonic transforms", *Optik*, vol. 183, pp. 401-414, Apr. 2019, 10.1016/j.ijleo.2019.02.001
66. K. M. Hosny and M. M. Darwish, "A kernel-based method for fast and accurate computation of PHT in polar coordinates," *J. Real-Time Image Process.*, vol. 16, no. 4, pp. 1235-1247, Jul. 2019, 10.1007/s11554-016-0622-y.
67. M. Unser, P. Thevenaz and L. Yaroslavsky, "Convolution-based interpolation for fast, high-quality rotation of images", *IEEE Transactions on Image Processing*, vol. 4, no. 10, pp. 1371-1381, Oct. 1995, 10.1109/83.465102.
68. C. Camacho-Bello, A. Padilla-Vivanco, C. Toxqui-Quitl, and J. J. Báez-Rojas, "Reconstruction of color biomedical images by means of quaternion generic Jacobi-Fourier moments in the framework of polar pixels," *J. Med. Imag.*, vol. 3, no. 1, Mar. 2016, 10.1117/1.jmi.3.1.014004
69. J. Flusser, B. Zitova, and T. Suk, *Numerical Analysis*, Boston, MA, USA: Cengage, 2009, pp. 193-224
70. B. Chen and G. W. Wornell, "Quantization index modulation: a class of provably good methods for digital watermarking and information embedding," *IEEE Transactions on Information Theory*, vol. 47, no. 4, pp. 1423-1443, May 2001, 10.1109/18.923725.
71. Alistair Moffat. "Huffman Coding", *ACM Comput. Surv.* vol. 52, no. 4, Article 85 (July 2020)
72. D.C. Wyld, J. Zizka,, D. Nagamalai (eds)., *Advances in Computer Science, Engineering & Applications. Advances in Intelligent Systems and Computing* (Springer, Berlin, Heidelberg, vol. 167, 2012
73. S. K. Narang and A. Ortega, "Compact Support Biorthogonal Wavelet Filterbanks for Arbitrary Undirected Graphs," in *IEEE Transactions on Signal Processing*, vol. 61, no. 19, pp. 4673-4685, Oct.1, 2013, doi: 10.1109/TSP.2013.2273197.
74. D.K. Hammond., P. Vandergheynst, R. Gribonval, *The spectral graph wavelet transform: Fundamental theory and fast computation.* In: Stanković L., Sejdić E. (eds) *Vertex-Frequency Analysis of Graph Signals. Signals and Communication Technology.* Springer, Cham. , 2019, [https://doi.org/10.1007/978-3-030-03574-7\\_3](https://doi.org/10.1007/978-3-030-03574-7_3)
75. N. Leonardi and D. Van De Ville, "Wavelet frames on graphs defined by fMRI functional connectivity," *2011 IEEE International Symposium on Biomedical Imaging: From Nano to Macro*, 2011, pp. 2136-2139, doi: 10.1109/ISBI.2011.5872835.
76. K. Dragomiretskiy, D. Zosso, *Two-dimensional Variational Mode Decomposition. Energy Minimization Methods*, in *Computer Vision and Pattern Recognition*. Springer International Publishing; pp. 197–208, Jan 2015.
77. F. Deprettere, *SVD and Signal Processing: Algorithms, Applications and Architectures*, Elsevier Science Pub. Co., 1988.
78. H. Takeda, S. Farsiu and P. Milanfar, "Kernel Regression for Image Processing and Reconstruction," in *IEEE Transactions on Image Processing*, vol. 16, no. 2, pp. 349-366, Feb. 2007, doi: 10.1109/TIP.2006.888330.
79. XiaoGuang Feng and P. Milanfar, "Multiscale principal components analysis for image local orientation estimation," *Conference Record of the Thirty-Sixth Asilomar Conference on Signals, Systems and Computers*, 2002., 2002, pp. 478-482 vol.1, doi: 10.1109/ACSSC.2002.1197228.

80. I. Djurovic, H. Stankovic, I. Pitas, "Digital watermarking in the fractional Fourier transformation domain", *Journal of Network and Computer Applications*, vol. 24, no. 2, pp. 167-173 (2001).
81. D.Vaishnavia, T.S.Subashini, "Robust and Invisible Image Watermarking in RGB Color space using SVD", *Procedia Computer Science*, vol. 46, pp. 1770-1777, 2015, 10.1016/j.procs.2015.02.130
82. X. Zhang, X. Li, Z. Tang, S. Zhang and S. Xie, "Noise Removal in Embedded Image with Bit Approximation," *IEEE Transactions on Knowledge and Data Engineering*, 10.1109/TKDE.2020.2992572.
83. J. -H. Xue and D. M. Titterington, "\$t\$ -Tests, \$F\$ -Tests and Otsu's Methods for Image Thresholding," in *IEEE Transactions on Image Processing*, vol. 20, no. 8, pp. 2392-2396, Aug. 2011, doi: 10.1109/TIP.2011.2114358.
84. X. Y. Wang, H. Y. Yang, P. P. Niu, and C. P. Wang, "Quaternion exponent moments based robust color image watermarking," *J. Comput. Res. Dev.*, vol. 53, no. 3, pp. 651-665, 2016.
85. C. Tang and H. Hang, "A feature-based robust digital image watermarking scheme", *IEEE Transactions on Signal Processing*, vol. 51, no. 4, pp. 950-959, April 2003, 10.1109/TSP.2003.809367.
86. A. Piva, F. Bartolinin, V. Cappellini and M. Barni, "Exploiting the cross-correlation of RGB-channels for robust watermarking of color images," *Proceedings 1999 International Conference on Image Processing (Cat. 99CH36348)*, 1999, pp. 306-310 vol.1, doi: 10.1109/ICIP.1999.821619.
87. M. Barni, F. Bartolini and A. Piva, "Multichannel watermarking of color images," in *IEEE Transactions on Circuits and Systems for Video Technology*, vol. 12, no. 3, pp. 142-156, March 2002, doi: 10.1109/76.993436.
88. N. Ahmidi and R. Safabakhsh, "A novel DCT-based approach for secure color image watermarking," *International Conference on Information Technology: Coding and Computing*, 2004. *Proceedings. ITCC 2004.*, 2004, pp. 709-713 Vol.2, doi: 10.1109/ITCC.2004.1286738.
89. S. D. Lin, Shih-Chieh Shie and Han Yi Guo, "Improving the robustness of DCT-based image watermarking against JPEG compression," *2005 Digest of Technical Papers. International Conference on Consumer Electronics, 2005. ICCE.*, 2005, pp. 343-344, doi: 10.1109/ICCE.2005.1429858.
90. Q. Su, G. Wang, S. Jia, X. Zhang, Q. Liu and X. Liu, " Embedding color image watermark in color image based on two-level DCT," in *Signal, Image and Video Processing*, vol. 9, no. 3, pp. 991-1007, 2015
91. K. M. Hosny, M. M. Darwish and M. M. Fouda, "Robust Color Images Watermarking Using New Fractional-Order Exponent Moments," in *IEEE Access*, vol. 9, pp. 47425-47435, 2021, 10.1109/ACCESS.2021.3068211
92. K. M. Hosny and M. M. Darwish, "Robust color image watermarking using invariant quaternion Legendre-Fourier moments," *Multimedia Tools Appl.*, vol. 77, no. 19, pp. 24727\_24750, Oct. 2018.
93. K. M. Hosny and M. M. Darwish, "Resilient color image watermarking using accurate quaternion radial substituted Chebyshev moments," *ACM Trans. Multimedia Comput., Commun., Appl.*, vol. 15, no. 2, pp. 24727-24750, 2019.

## APPENDIX A (LIST OF PUBLICATIONS)

### DETAILS OF PUBLICATIONS

Below is the list of published research article in SCOPUS indexed conference proceedings along with the proofs of publications

1. Audio Watermarking in Linear Canonical Transform Domain Using Frequency-Dependent Clustering in *Cyber Intelligence and Information Retrieval*, 978-981-16-4283-8, 513403\_1\_En, (Chapter 15), 10.1007/978-981-16-4284-5\_15 (**SPRINGER**)
2. A Secure Wavelet based Watermarking Approach using Psycho-Visual Redundancy in Image, in *IEEE conference 2021 7th International Conference on Advanced Computing and Communication Systems (ICACCS)*, 10.1109/ICACCS51430.2021.9442032 (**IEEE XPLORE**)

# Audio Watermarking in Linear Canonical Transform Domain using Frequency Dependent Clustering

Ashish Sinha<sup>1</sup>✉ and Jeebananda Panda<sup>2</sup>

<sup>1,2</sup> Delhi Technological University, Delhi, India  
ashishsinha\_2k20spd02@dtu.ac.in, jpanda@dce.ac.in

**Abstract.** Audio watermarking is considered as a challenging domain owing to the requirement of imperceptibility post watermarking, while keeping the robustness intact [1]. This paper proposes an effective methodology for watermarking of the audio signal using Linear Canonical Transform (LCT), which has found its use in a multitude of signal processing applications, due to its flexibility [2]. The proposed work uses a watermark sequence of complex numbers which is suitably embedded into the transformed audio signal using frequency dependent clustering. The watermark detection is blind and performed reversibly. It is found that the watermark is extremely resilient against a wide range of signal processing and feature distortive attacks. The technique is also secure, imperceptible, stable and offers sufficient payload capacity of nearly 15% of the audio signal length.

**Keywords:** Audio Watermarking, Transform Domain, Frequency Dependent Clustering, Linear Canonical Transform.

## 1 Introduction

Recent strides made in the field of digital media and related technologies have spurred an unprecedented growth and have also led to mis-utilization of data and copyright infringements, thus imperilling intellectual property rights and causing monumental financial losses [3,4]. Copyright infringement to exploit the work of artists and make undue profits has been recognized as a grave concern in the music industry [5]. As a counteractive measure, audio watermarking has been broached upon in this paper.

The scheme chiefly entails hiding the watermark information (owner/distributor identity, file manipulation/ transactions information etc.) into the original audio signal, in an imperceptible manner and without affecting the fundamental characteristics of the audio signal [6].

An effective and efficient watermarking scheme, in general, is characterized by robustness, security, imperceptibility and high payload capacity [6]. Imperceptibility is vital as it has been observed that embedding the watermark often leads to perceptible distortions. Further, watermarking schemes with blind extraction are preferred for their higher efficiency and security. Techniques for watermarking of audio signals are

# A Secure Wavelet based Watermarking Approach using Psycho-Visual Redundancy in Image

Ashish Sinha

Master of Technology Student  
Delhi Technological University

Delhi, India

[ashishsinha\\_2k20spd02@dtu.ac.in](mailto:ashishsinha_2k20spd02@dtu.ac.in)

Jeebananda Panda

Professor: Department of ECE  
Delhi Technological University

Delhi, India

[jpanda@dce.ac.in](mailto:jpanda@dce.ac.in)

**Abstract**— The principal requirements of any digital watermarking algorithm are imperceptibility, robustness, security and capacity of the watermark [2,9]. Imperceptibility and robustness are inherently conflicting in nature. Over numerous trials of digital watermarking of multimedia, it has been found that embedding a watermark with high strength also decreases its obscurity and makes the watermark more prone to detection. On the other hand, a watermark embedded with a low strength improves the imperceptibility but causes degradation of robustness against signal processing, geometric and feature-distortive attacks. This paper proposes a secure approach for watermarking using the Image Partitioning approach, which exploits the psycho-visual redundancy in the image to embed the watermark. Using the chaotic scrambling based Arnold Transform, watermark is first scrambled and then embedded in the sub-band of the image obtained using the Discrete Wavelet Transform and characterized by the lowest frequency. This improves the security as well as enhances the imperceptibility of the watermark, without significant deviation in visual appearance of the watermarked image from the cover image. Further, frequency domain embedding leads to better robustness and stability. The method is used to perform watermarking of grayscale images and performs well when subjected to common distortions, geometric, order-statistic filtering and signal processing attacks. This was determined by calculating the Peak Signal to Noise Ratio of the watermarked cover image and the retrieved watermarks and the Normalized Cross-Correlation of the embedded and extracted watermarks.

**Keywords**— *Digital Watermarking, Psycho-Visual Redundancy, Image Partitioning, Discrete Wavelet Transform, Arnold Transform, Chaotic Scrambling, Spatial Compression, Order-Statistic Filtering.*

## I. INTRODUCTION

The use of digital technologies and associated media and products has grown exponentially in the recent past, fueled by the advent of economical and more accessible technologies. This has also led to an unprecedented level of proliferation of digital data, driven by the expanding outreach of the Internet. Such a wide-scale growth has presented new challenges as to the security and ownership of the intellectual properties of the digital media, for the purposes of copyright protection, verification and authentication [5]. On account of unrecognizable differences between the original and the counterfeit digital media, there is an urgent need to prevent

unauthorized duplication of the media as well as to distinguish between its original and illegitimate copy. Therefore, in this parlance, the protection of intellectual property assumes importance. Digital watermarking is a technique deployed to achieve this objective for a variety of digital media formats [2].

Digital watermarking scheme is used to embed a digital instrument of ownership in the digital media, known as the watermark [10]. This watermark may take the form of an image of a copyright notice, the identity of the owner and/or its authorized users or a secret message, and is decipherable only by the authorized personnel. It is also instrumental in determining the ownership of the work. The media is converted to a suitable format for insertion of the watermark, and is known as the cover signal. The process of insertion of the watermark is called embedding and the transformed signal post embedding of the watermark is regarded as the watermarked signal. Extraction or detection involves the process of retrieval of the embedded watermark. These two therefore constitute the fundamental steps in the watermarking process [5].

In general, digital watermarking may be classified into different types, based on the nature of the cover signal, watermark insertion process and the embedded watermark [5]. Based on the appearance of the watermarked signal, the watermarking scheme may be classified into visible and invisible types. Treating robustness as a criterion for categorization, the watermarking schemes may be divided into robust (those resistant to different attacks), semi-fragile (resistant only to a narrow range of attacks) and fragile (destroyed in the event of attack strength being equal to or higher than a pre-determined strength, which is usually kept low to detect even the slightest of the attacks on the watermarked signal). Based on the requirement of the cover signal for extraction of watermark, the watermarking methods may be divided into blind (does not require the cover signal), semi-blind (requires the cover signal in some form) and non-blind (requires the cover signal). Further, watermark embedding may be done in spatial or transform domain, the latter being preferred due to the stability and robustness of watermarks to a variety of attacks [9]. All the above different types of watermarking methods are suitably deployed based on the requirements of the particular application and the level



**APPENDIX B (PLAGIARISM REPORT)**

**PLEASE SEE OVERLEAF**

PAPER NAME

**Major Project Thesis - Ashish Sinha - 2K  
20SPD02.docx**

AUTHOR

**Ashish Sinha**

WORD COUNT

**22046 Words**

CHARACTER COUNT

**127285 Characters**

PAGE COUNT

**134 Pages**

FILE SIZE

**11.7MB**

SUBMISSION DATE

**May 26, 2022 12:27 PM GMT+5:30**

REPORT DATE

**May 26, 2022 12:30 PM GMT+5:30**

### ● 16% Overall Similarity

The combined total of all matches, including overlapping sources, for each database.

- 6% Internet database
- Crossref database
- 5% Submitted Works database
- 14% Publications database
- Crossref Posted Content database

### ● Excluded from Similarity Report

- Bibliographic material
- Cited material
- Quoted material
- Small Matches (Less than 8 words)

● **16% Overall Similarity**

Top sources found in the following databases:

- 6% Internet database
- Crossref database
- 5% Submitted Works database
- 14% Publications database
- Crossref Posted Content database

TOP SOURCES

The sources with the highest number of matches within the submission. Overlapping sources will not be displayed.

1	<b>Ashish Sinha, Jeebananda Panda. "A Secure Wavelet based Watermar...</b>	2%
	Crossref	
2	<b>Ashish Sinha, Jeebananda Panda. "Chapter 15 Audio Watermarking in ...</b>	2%
	Crossref	
3	<b>deepai.org</b>	<1%
	Internet	
4	<b>Parminder Kaur, Husanbir Singh Pannu, Avleen Kaur Malhi. "Comprehe...</b>	<1%
	Crossref	
5	<b>Shuren Qi, Yushu Zhang, Chao Wang, Jiantao Zhou, Xiaochun Cao. "A S...</b>	<1%
	Crossref	
6	<b>Shikha Chaudhary, Saroj Hiranwal, Chandra Prakash Gupta. "Spectral G...</b>	<1%
	Crossref	
7	<b>ee.umanitoba.ca</b>	<1%
	Internet	
8	<b>dspace.vutbr.cz</b>	<1%
	Internet	